MASTERARBEIT / MASTER’S THESIS

Titel der Masterarbeit / Title of the Master‘s Thesis

„Fault-controlled hydrocarbon reservoir distribution in the Vienna Basin“

verfasst von / submitted by

Augusto Barbosa Coelho Guimaraes, BSc

angestrebter akademischer Grad / in partial fulfilment of the requirements for the degree of

Master of Sciences (MSc)

Wien, 2023 / Vienna, 2023

Studienkennzahl lt. Studienblatt / degree programme code as it appears on the student record sheet:	A 066 815
Studienrichtung lt. Studienblatt / degree programme as it appears on the student record sheet:	Masterstudium Erdwissenschaften UG2002
Betreut von / Supervisor:	Univ. Prof. Mag. Dr. Bernhard Grasemann
Mitbetreut von / Co-Supervisor	Dr. Katerina Schöpfer

Acknowledgements

I am very happy to have been given credit by **Bernhard Grasemann**, who recommended me among all other students for this project in cooperation with "Österreichische Mineralölverwaltung Aktiengesellschaft" (OMV), where I was amazingly well received by **Volker Schuller**. Volker created this project and due to his cooperation with Bernhard and the University of Vienna, gave me the opportunity to deepen and apply my knowledge acquired through Bachelors and Masters outside university. I would expressly extend my thanks to OMV for providing me the data.

In the first meetings **Michael Kettermann** and **András Zámolyi** were also present. Michael was always there to explain all discussed topics over and over again. Not only did Michael go through the topics, but he also gave lots of geological inputs to the master thesis and encouraged me to keep going. András, like Michael, was always there for me during the duration of my master thesis. From the beginning until the end, András helped me a lot not only with problems regarding Petrel, but provided me with all the necessary data, and gave lots of geological input and feedback.

I have to admit that at first, it was very difficult to have three main supervisors, Volker, Michael and András, and to coop with all the new input from them, being actually lost at some points. However, I can consider myself fortunate to have all three of them, each of them providing in their own way support, feedback and encouragement.

During the whole thesis I also had support from **Katerina Schöpfer**; at the beginning, especially regarding Petrel and providing essential feedback about what is expected in a master thesis, either in the written part or in the images. More to the end, she gave me ideas on how improve the content of the thesis and motivated and encouraged me to cross the finish line. "How does it feel that you can already see the end?" was one of these motivational sentences.

I would also like to thank all my professors that accompanied me during my bachelor (at University of Brasilia, Brazil and University of Vienna, Austria) and masters (University of Vienna) sharing their knowledge about earth sciences. I could go to any professor from both institutions anytime to ask for help when something related to earth sciences was not clear. I would like to express my gratitude to three professors, **Martin Schöpfer**, **Oscar Bellon** and **Rainer Abart**. Martin was my supervisor during my Bachelor thesis and was my first contact with the University of Vienna (at that time I was not a student at University of Vienna) and allowed me to go on a field trip with his class to Silbersee. Oscar brought a "Brazilian atmosphere" to the university because I could talk with him in Portuguese. Abart was, at some point, "Studienprogrammleiter" of Earth Sciences and wrote a recommendation letter on my behalf regarding my legal situation in Austria. Without it I do not know for certain, if I could finish my masters or even my bachelors here in Vienna.

I would also like to thank all my colleagues that accompanied me during this time. Either by studying for an exam, going for a beer; having deep talks or even talking nonsense. All these experiences not only made me grow professionally, but also personally and created a lighter atmosphere along my study. Studying itself is far from over, since each day you learn something new and who knows what life is going to bring. Some of these colleagues became dear friends and together with new ones that are coming in the future to face new obstacles with me. Just to name a few friends that this time of studies brought me: **Guilherme**, **Grazi**, **Iago**, **Regina**, **Peter**, **Mario**, **Monika**, **Jennifer**, **Lukas** and **Julian**.

I would like to dedicate this thesis to my **family** and **Milica** for all the support, encouragement and for making it possible for me to finish my studies (until now) abroad. Milica and my family accompanied, encouraged and motivated me through all the studies in Austria, from the remote UNIGIS course to the end of my masters. There are actually no words to describe how I feel about everything they have done for me. And I would like to tell my uncle **Edison**, wherever he is now (past away in the pandemic), that there is (hopefully) another Earth Scientist in the family from this moment on.

Abstract

The Vienna Basin is a polygenetic basin, which evolved from a piggy back basin to a thin skinned pull apart basin (Royden, 1985; Strauss et al., 2006), located between the Alps and the Carpathians. In the Vienna Basin, oil and gas discoveries date back to the beginning of the 20th century (Hamilton et al., 2000) and have played an important role in the exploration ever since. The hydrocarbon exploration is not uniform through the Vienna Basin, but is limited to places, which are structurally or stratigraphically suitable to retain oil and/or gas accumulations. Stratigraphic and structural traps together with a good reservoir rock can store hydrocarbons (temporarily, when taken from geological time perspective) and inhibit migration to other places. The reservoirs that contain hydrocarbon accumulations and from which hydrocarbons can be extracted are known as production units. In this study, from the initial 270 production units (active in 2020) 42 production units were found suitable for analyses, i.e., the unit must be fault controlled. The main goal of this study is to find if there are more production units located in the hanging wall or in the footwall of large-scale faults in the Vienna Basin. Subsequently, it is determined, if there is a pattern between the analyzed parameters. In case the pattern is found, a development of an algorithm and training of a model via machine learning (Verbraeken et al., 2021) could predict the probability of finding and help implementing new production units. In order to answer these questions, detailed information about the production units in this study (seismic data, geospatial data and well top data) was provided by OMV ("Österreichische Mineralölverwaltung Aktiengesellschaft"). The production units were predominantly found to be located in the hanging wall of faults (when comparing absolute numbers), but the volume of hydrocarbon content was not analyzed. The dominance of production units in the hanging wall is independent from the spatial distribution and depth of the production units. Wells were drilled based on hydrocarbon indicators depending on the technology available at the time of the drilling (e.g. gravimetry, nearby hydrocarbon founds, 3D seismic). Therefore, a statistically meaningful and equally distributed sampling of hanging wall and footwall traps is not guaranteed. In this study, depth vs. throw diagrams was the main method used for analyzing the production units. The second task of finding a pattern, as well as creating an algorithm capable of predicting the discovery of new oil/gas fields was not finally developed due to low number of production units with suitable parameters. The occurrence of parallel faults can lead to confusion on which side of which fault the production unit is located, e.g. borehole Pirawarth 18 is located in footwall of one of the two parallel faults and at the same time is located in the hanging wall of the other fault. Therefore, a clear definition of the fault location was made. Based on this study, large-scale fault lenses should be studied in detail since they could act as a migration pathway for hydrocarbons (Lindanger et al., 2007). Additionally, studies of the relationship between faults of the same and different hierarchic levels should be applied in future studies and complemented with a detailed mapping of the previously uninterpreted small-scale faults. Lastly, implementation of length vs. throw diagrams (Reeve et al., 2015), not widely applied in the Vienna Basin until now, would lead to a better understanding of fault relationships in the basin.

Zusammenfassung

Das Wiener Becken ist ein polygenetisches Becken, das sich von einem Huckepack-Becken zu einem dünnhäutigen, Pull-Apart Becken entwickelt hat (Royden, 1985; Strauss et al., 2006), welches zwischen den Alpen und den Karpaten liegt. Im Wiener Becken wurden Öl- und Gasfunde ab Beginn des 20. Jahrhunderts entdeckt (Hamilton et al., 2000) und spielen seitdem eine wichtige Rolle bei der Exploration von Kohlenwasserstoff. Die Kohlenwasserstoffexploration erfolgt nicht einheitlich im gesamten Wiener Becken, sondern ist auf Orte beschränkt, die strukturell oder stratigraphisch für die Speicherung von Öl- und/oder Gasansammlungen geeignet sind. Stratigraphische und strukturelle Fallen können zusammen mit dem Vorhandensein eines guten Speichergesteins Kohlenwasserstoffe speichern (vorübergehend, wenn man sie aus geologischer Sicht betrachtet) und die Migration an andere Orte verhindern. Die Lagerstätten, die Kohlenwasserstoffansammlungen enthalten und aus denen Kohlenwasserstoffe gefördert werden können, werden als Produktionseinheiten bezeichnet. In dieser Studie wurden von den ursprünglich 270 Produktionseinheiten (aktiv im Jahr 2020) 42 Produktionseinheiten als für die Analyse geeignet befunden, d. h. die Einheit muss störungsgebunden sein. Das Hauptziel dieser Studie besteht darin, herauszufinden, ob sich im Hangenden oder im Liegenden, von großflächigen Störungen im Wiener Becken, die Mehrheit dieser Produktionseinheiten befindet. Anschließend wird festgestellt, ob ein Muster zwischen den analysierten Parametern besteht. Falls ein Muster gefunden wird, könnte die Entwicklung eines Algorithmus und dessen Training eines Modells mittels maschinellem Lernen (Verbraeken et al., 2021) den Erfolgswahrscheinlichkeiten vorhersagen um neue Produktionseinheiten zu finden und zu implementieren. Um diese Fragen zu beantworten, wurden von der OMV (Österreichische Mineralölverwaltung Aktiengesellschaft) detaillierte Informationen zu den Produktionseinheiten in dieser Studie (seismische Daten, Geodaten und Bohrungsdaten) bereitgestellt. Die Produktionseinheiten befanden sich überwiegend im Hangenden von Störungen (beim Vergleich absoluter Zahlen), das Volumen des Kohlenwasserstoffgehalts wurde jedoch nicht analysiert. Die Dominanz der Produktionseinheiten im Hangenden von Störungen ist unabhängig von der räumlichen Verteilung und Tiefe der Produktionseinheiten. Die Bohrlöcher wurden auf der Grundlage von Kohlenwasserstoffindikatoren gebohrt, abhängig von der zum Zeitpunkt der Bohrung verfügbaren Technologie (z. B. Gravimetrie, nahegelegene Kohlenwasserstofffunde, 3D-Seismik). Durch diesen Umstand ist eine statistische und gleichmäßig Verteilung der berücksichtigten Produktionseinheiten und Fallen in Bezug auf ihre Lage in der Hangend- und Liegendscholle nicht gewährleistet. In der vorliegenden Studie wurden hauptsächlich Tiefen-Versatz-Diagramme zur Analyse der Produktionseinheiten verwendet. Die zweite Aufgabe, ein Muster zu finden und einen Algorithmus zu erstellen, der die Entdeckung neuer Öl-/Gasfelder vorhersagen könnte, wurde aufgrund der geringen Anzahl von Produktionseinheiten mit zielführenden Parametern nicht endgültig entwickelt. Des Weiteren ist für Produktionseinheiten, die zwischen zwei parallel verlaufenden Störungen gelegen sind, eine eindeutige Zuordnung des Speichergesteins in das liegende bzw. hangende einer Störung nicht eindeutig. Für die in Bohrung Pirawarth 18 angetroffene Produktionseinheit, die zwischen zwei parallelen Störungen angetroffen wurde, wurde in der vorliegenden Studie eine klare Definition der Lage in Bezug auf die Störungen durchgeführt, um eine Zuordnung zu ermöglichen. Basierend auf der vorliegenden Studie empfiehlt es sich, großräumige Störungslinsen im Detail zu untersuchen, da diese als Migrationswege für Kohlenwasserstoff dienen könnten (Lindanger et al., 2007). Darüber hinaus sollten Untersuchungen zur Beziehung zwischen Störungen derselben und unterschiedlicher Hierarchieebenen in zukünftigen Studien angewendet und durch eine detaillierte Kartierung der bisher nicht interpretierten kleinräumigen Störungen ergänzt werden. Schließlich würde die Implementierung von Längen-Versatz-Diagrammen (Reeve et al., 2015), die im Wiener Becken bisher nicht weit verbreitet sind, zu einem besseren Verständnis der Beziehungen zwischen den Störungen im Becken führen.

Contents

1. Introduction

The aim of this thesis is to analyze active production units (often in this thesis used abbreviation: PU), which are fault-controlled and are located in the northern part of the Vienna Basin (Figure 1). The Vienna Basin is located in central Europe, at the junction of three countries: Austria, the Slovak Republic and the Czech Republic (Figure 2). The Vienna basin is a thin-skinned pull apart basin (Royden, 1985) with an SW-NE oriented rhombohedral shape with dimensions of 200km length and 40km width. The basin occupies the space at the transition between the Alps and the Western Carpathian Mountains (Figure 1).

The production units are defined here as hydrocarbon reservoirs with the same hydrodynamic regime and being active in the year 2020. The database used in this study include all boreholes that extracted hydrocarbon north of the Danube during 2020 and were kindly provided by OMV Vienna.

An existing literature on global hydrocarbon exploration shows an ongoing debate about which side of a fault (hanging wall or footwall) is more promising regarding hydrocarbon discoveries. The general presumption is that it is worthier to explore footwall plays for hydrocarbons rather than hanging walls (e.g. Hardman and Booth, 1991).

Interestingly, and in contrast to the above-mentioned general assumption, majority of production units in the Vienna Basin occur in the hanging wall cut-off. Great volumes of oil and gas are extracted every year from fault bound traps located in hanging wall plays. Recent research of Kularathna et al., 2020 showed that structures in the hanging wall are also capable of storing great hydrocarbon volumes, pointing to the fact that it is also worthy of exploring this side of the fault.

Under this pretense, the first aim of this study is to check occurrences of production units in the Vienna Basin in relation to faults, and to discuss reasons that might have caused this situation.

The second aim is to determine controlling factors that made some hanging wall plays more productive than others and if there is a trend or pattern when comparing different parameters. These parameters were extracted from borehole logs and seismic data provided by OMV and from published data. In case a trend is identified through correlation of various parameters, an algorithm can be developed to enable the prediction of finding hydrocarbon plays (oil and gas) in specific fault-bound structures.

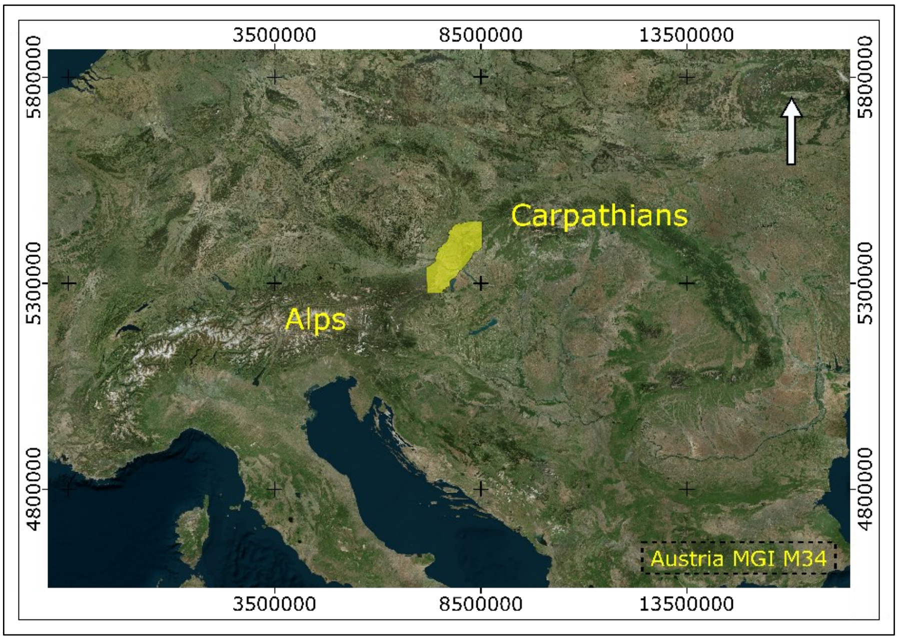

Figure 1: Vienna Basin at transition between Alps and Carpathians (modified from QGIS basemap, "bing aerial").

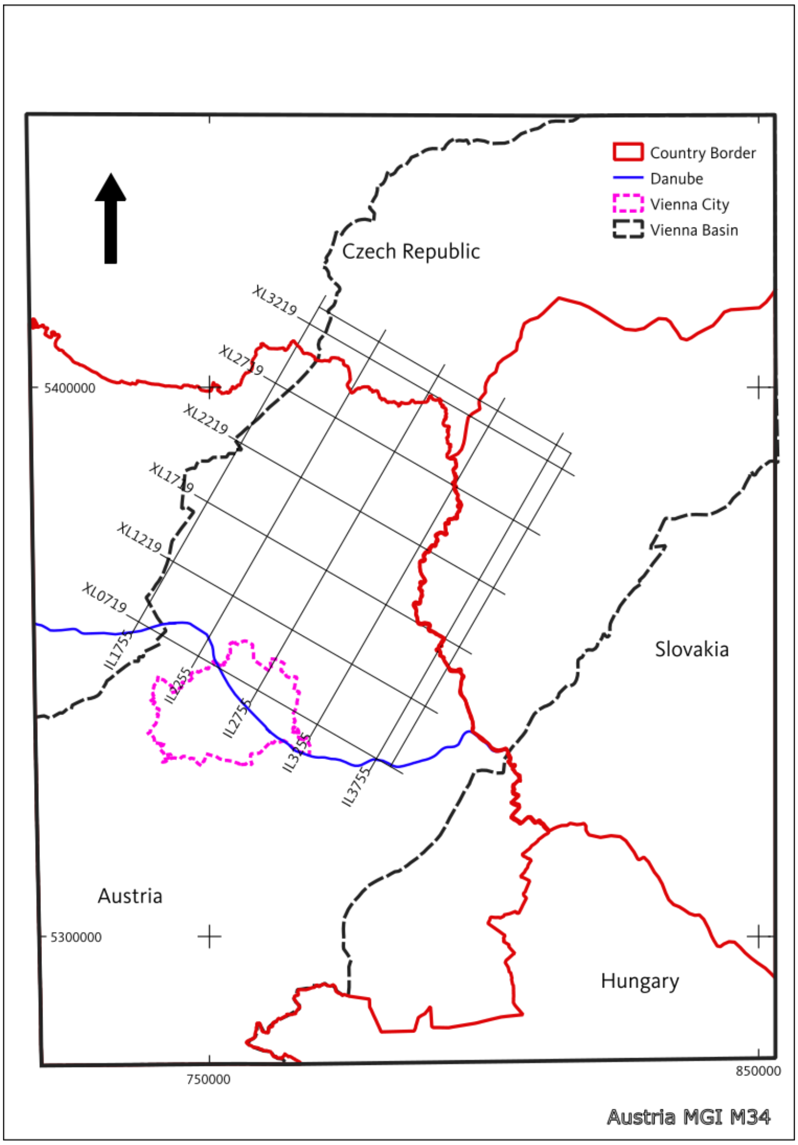

Figure 2: Location of the Vienna Basin (dashed black line) in Austria, partly extending into Czech Republic and Slovakia. Adopted Vienna Basin extension from Wessely, 2006. Map generated in QGIS software.

2. Geological setting and basin evolution

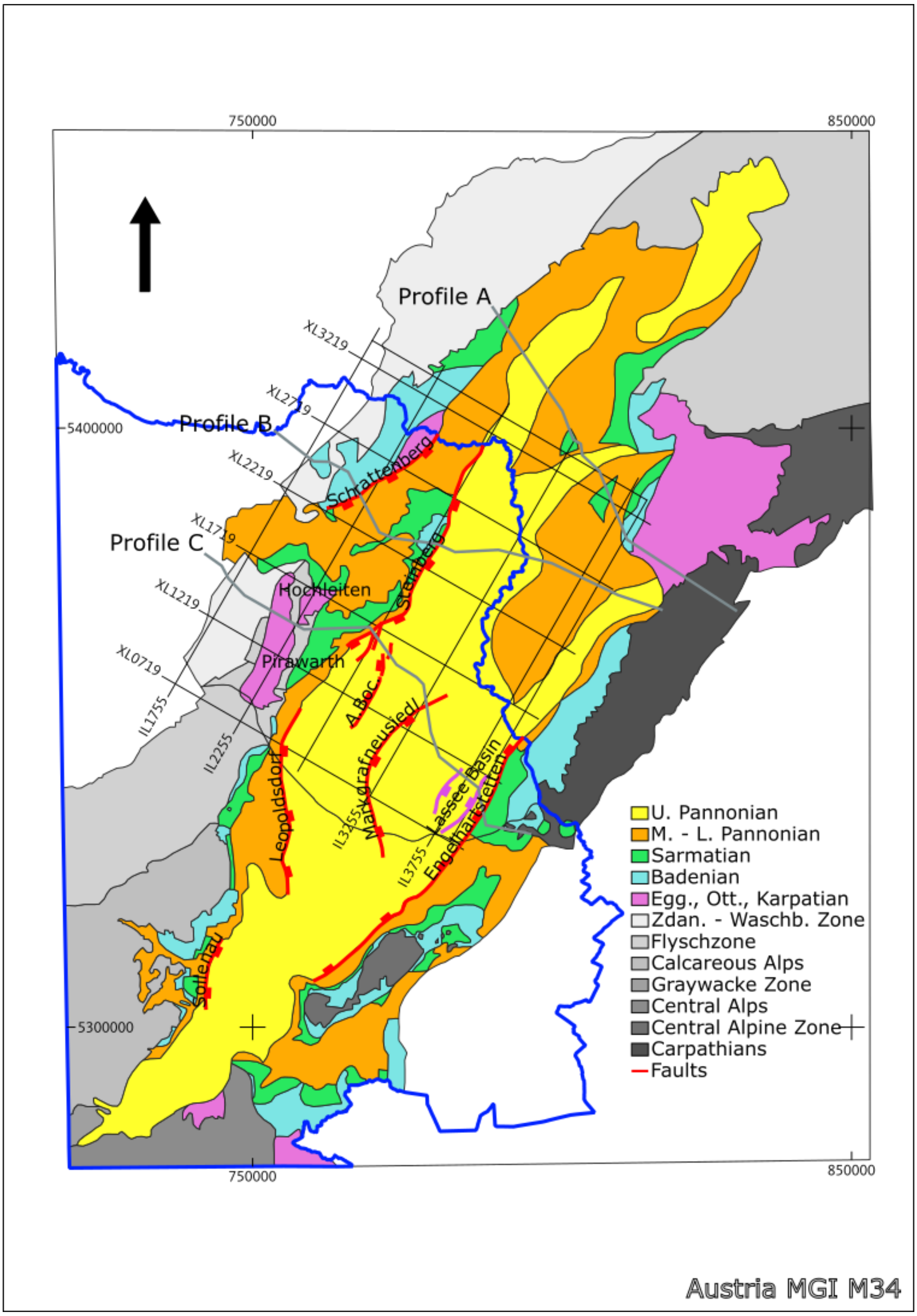

Figure 3: Geology of the Vienna Basin (geological map modified from Wessely, 2006 and location of profiles from Arzmüller et al., 2006).

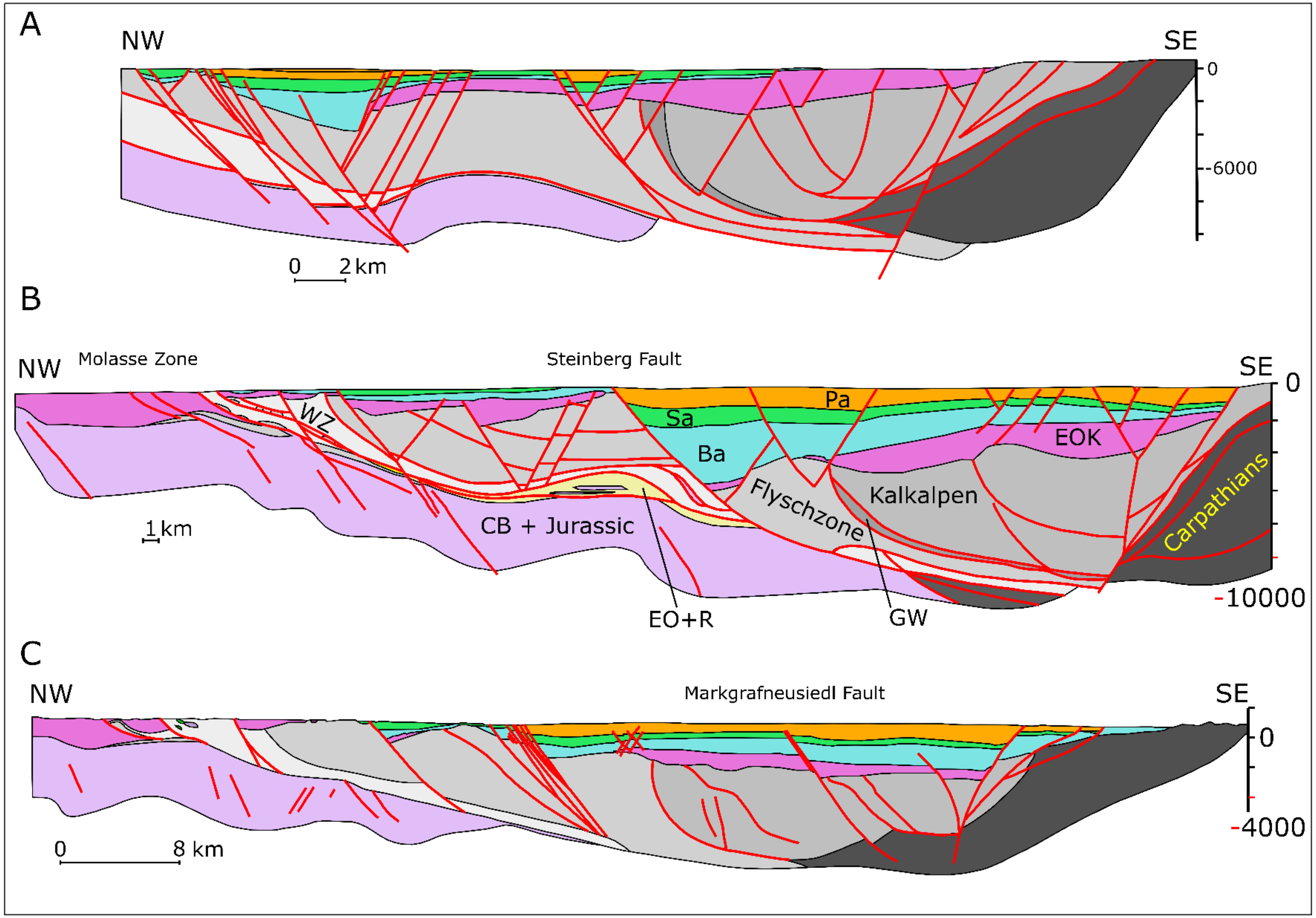

Figure 4: Profiles through the Vienna Basin. Exact locations can be seen in Figure 3 (simplified and modified from Arzmüller et al., 2006). Abbreviations: CB-Crystalline Basement, EO+R-Eocene Oligocene + Relicts, WZ-Waschberg Zdanice Zone, GW-Graywacke Zone, EOK-Eggenburgian Ottnangian Karpatian, Ba-Badenian, Sa-Sarmatian, Pa-Pannonian.

2.1 Geological setting

The tectonic-stratigraphic evolution of the Vienna Basin, Austria is very complex (Figures 3 and 4) since it formed during several tectonic phases (Figure 5a, b) under different fault regimes (strike-slip, normal and reverse). During individual stages of basin evolution, different regimes were predominant and controlled the shape of the basin and thicknesses of basin deposits. Due to these differences the Vienna Basin is considered to represent a polygenetic basin (Decker 1996, Wessely 2006). It was formerly a piggy back basin and evolved to a thin skinned pull apart basin (Royden, 1985; Lankreijer et al., 1995; Strauss et al., 2006; Kováč et al., 2007).

Wessely (2006) divided the evolution of the Vienna Basin in the three parts: pre-Vienna Basin (Figure 5a-I-II), the proto Vienna Basin, representing the first stages of the formation of the Vienna Basin (Figure 5a-III) and the today existing neo-Vienna Basin (Figure 5a-IV). The individual stages of basin formation are described briefly in the following section.

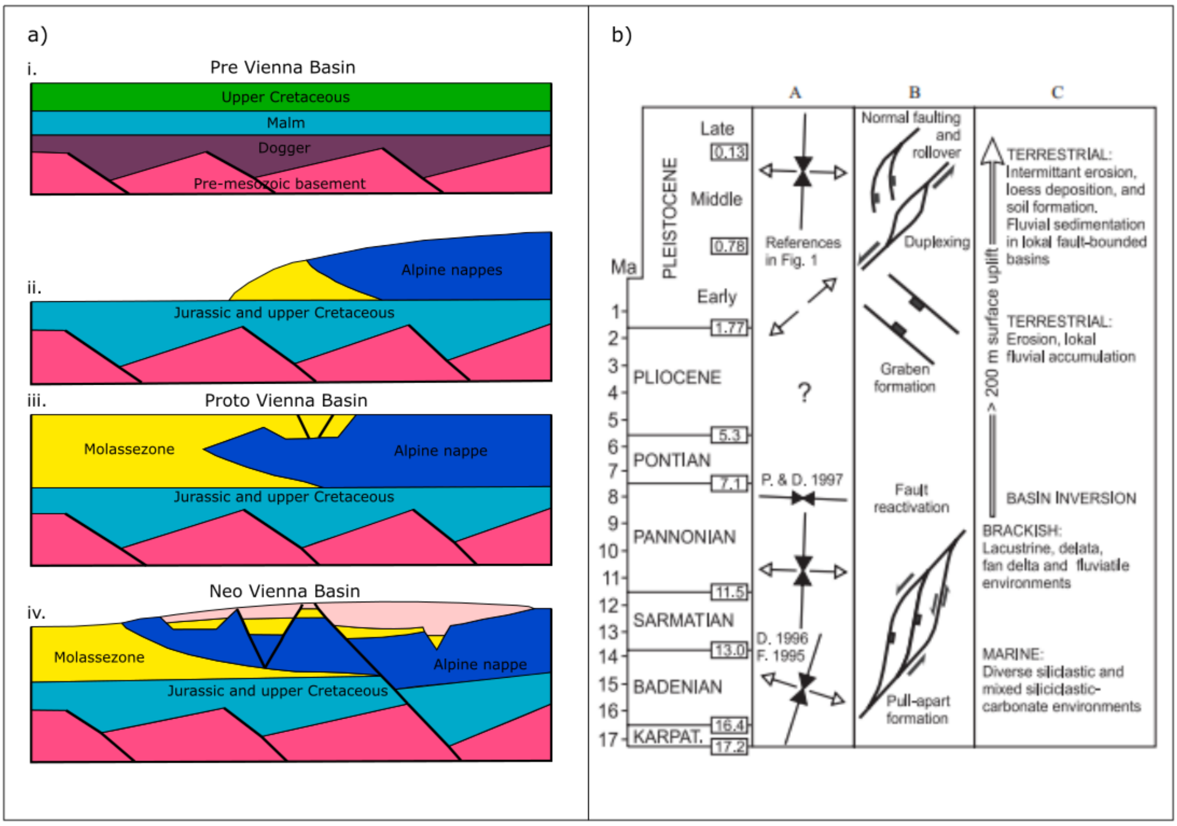

Figure 5: Evolution of the Vienna Basin and the direction of the stress field through time. Figure A after Wessely (2006), Figure B is taken from Decker (1996).

Prior to the formation of the Vienna Basin, which is schematically shown in Figure 5a-i, a rift system opened in the Jurassic (Dogger) that accommodated deposition of Jurassic and Cretaceous sediments over the "European" basement under a passive continental margin Figure 5a-i (Arzmüller et al., 2006, Wessely 2006).

During the Paleogene, a thrusting occurred, and the alpine nappe was thrusted over the sedimentary rocks that were deposited during the Jurassic and Cretaceous on the European continental shelf (Figure 5a-ii). The thrusting was due to regional compression and the proto Vienna Basin formed due to local extension on the back of the over thrusting block, “piggy back” (Figure 5a-iii). The over thrusted alpine nappes and molasse also served as basement for the Miocene sediment layers (Figure 5a-iii).

During the Paleogene, a thrusting system started and the Alpine-Carpathian nappes was thrusted over the sedimentary rocks that were deposited during the Jurassic, Upper Cretaceous and early Tertiary Molasse (Arzmüller et al., 2006). The sediments deposited during these periods (in this order, from oldest to youngest) were deposited on the European continental shelf Figure 5a-ii.

The north-northwest oriented thrusting (Lee and Wagreich, 2017) resulted from a regional compressional setting and it is under a local extension on the back of the over thrusting block (“piggy back”) that the first stages of the Vienna Basin was formed (proto Vienna Basin). As can be seen in Figure 5a-iii, the over thrusted alpine nappes and molasse also serve as basement for the Miocene sediment layers (Figure 4b).

From the Proto Vienna Basin stage (Figure 5a-iii) to the Neo Vienna Basin stage (Figure 5a-iv) the thrusting of the Alpine-Carpathian nappe ceased (Figure 5a-iv) in the late Karpatian (Decker, 1996) and the geometry changed from piggy back basin into a rhombic pull apart basin, with NE-SW compression and NW-SE extension (Figure 5b), due to lateral extrusion (Decker, 1996; Peresson and Decker, 1997; Strauss et al., 2006). This process of horizontal extension was, however, limited to the northern part of the Vienna Basin (Arzmüller et al., 2006), where synsedimentary structures can be seen along seismic profiles. East of the Steinberg Fault (normal fault), synsedimentary depositions with considerable offsets within Early Miocene deposits can be encountered (Arzmüller et al., 2006; Ladwein et al., 1991).

The Karpatian/Badenian boundary is marked by a major regressive event (Strauss et al., 2006). This regression can be seen in documented nearshore settings (Rögl et al., 2002). With this regression, the SW-NE oriented Matzen Flysch Ridge separated the marine in the north from nonmarine environments in the south (Arzmüller et al., 2006; Lee and Wagreich, 2017; Rögl et al., 2002).

During the Sarmatian and Pannonian most of the sedimentation in the Vienna Basin occurred without major interruptions within marine environment (Arzmüller et al., 2006; Lee and Wagreich, 2017). The salinity started to decrease already in the Sarmatian (Wagreich and Schmid, 2002) turning into more lacustrine environment in the Pannonian (Strauss et al., 2006).

At the end of the Pannonian the basin changed to a terrestrial environment (Strauss et al., 2006), due to uplift as a result from a basin inversion (Figure 5b). Responsible for this changing in movement was slab detachment and isostatic rebound in the aftermath of continental convergence (Lee and Wagreich, 2017).

At some point, the thrusting in the Alps ceased, the proto Vienna Basin became inactive and a major extensional phase began (Figure 5a-iv). However, the thrusting was still active in the Carpathians further east. This process changed the paleographic stress field and the evolution of the Vienna Basin acted correspondingly (Beidinger and Decker, 2011). In the Badenian, a more detailed approach on the micro fauna made it possible to divide rocks stratigraphically during the Badenian into zones (Wessely, 2006).

During the evolution of the Vienna Basin, the main stress field changed during time (column A in Figure 5.b). These stress field variations resulted in the generation of different structures (column B in Figure 5.b), delimited by new faults and having as result, the reactivation or ceasing the motion along pre-existing faults.

The generation of new faults, reactivation or movement ceasing of already existing faults would have direct impact on the volumes of sediment deposition, since close to active faults, the accommodation is bigger, which would proportionate that the thickness of the layers is bigger when compared to areas where no faults are present or inactive. The relative sea level in the Central Paratethys is another conditioner since it will impact directly if one specific layer is going to be deposited or eroded.

All these processes: fault generation, activation, ceasing and relative sea level will affect the magnitude of the layer. Due to the diverse space related evolution of the Vienna Basin, either because the creation of new faults or reactivation of pre-existing faults and space specific deposition conditions and erosion during time resulted on a varying thickness along the basin. This thickness variation (Figure 6) along the Vienna Basin is hereby represented by: 1st Lower Pannonian, 5th Sarmatian and 5th Badenian because these were the most documented stratigraphic units in the provided database.

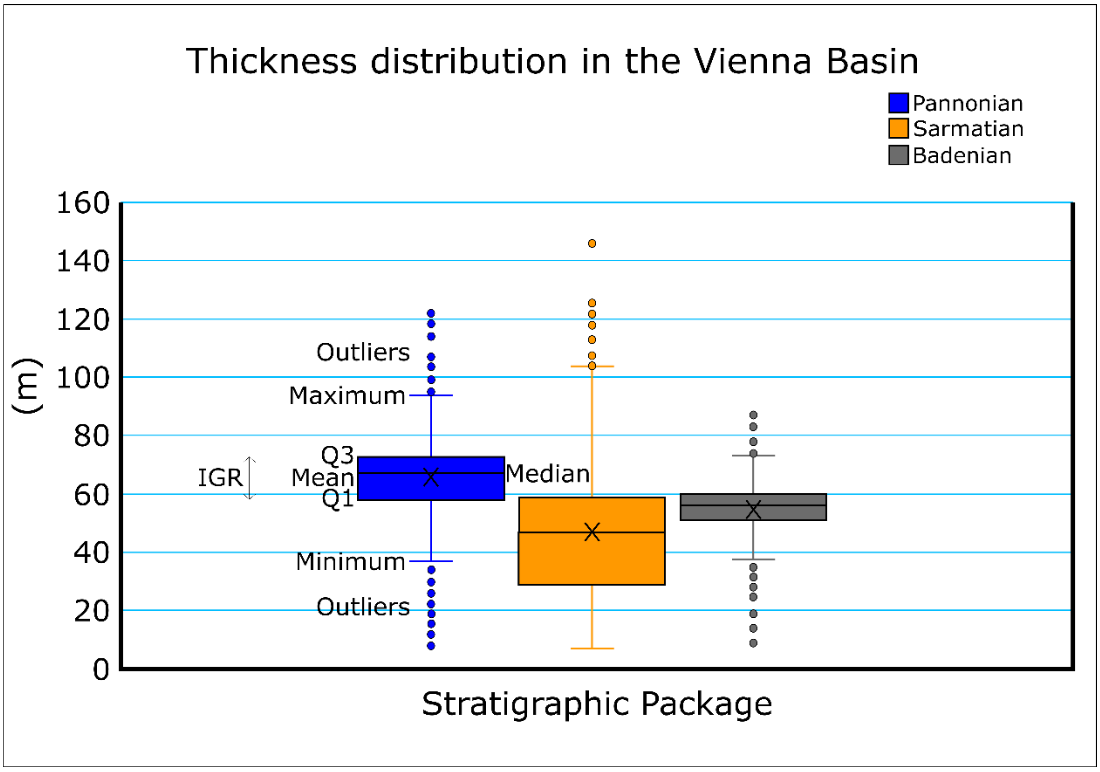

Figure 6: Variation on thickness of layers of Pannonian, Sarmatian and Badenian through the Vienna Basin. Q3: Quartile 3, Q1: Quartile 1, IGR: Interquartile range, x marks the mean for all values. For explanation of the building of the diagram see section 6.4.1.

2.2 Exploration history of the Vienna Basin

The Vienna Basin has been studied for a long time. From Austrian perspective, the first documentations date back to the beginning of the 19th century (Wessely, 2006). The interest was mainly focused on describing the fossil record in the basin and creating profiles through the basin. Due to technical limitation, this documentation occurred mostly on the surface or at shallower depths (shallow wells, surface mapping), yet this almost “2- dimensional” approach would have led to the discovery of oil and gas around 1930 (Hamilton et al., 2000).

Recovered fossils enabled to reconstruct the conditions that those organisms lived in (e.g., salinity, temperature, depth) and to date the sedimentary rocks that contained the fossils. Together with mapping of shallow structures, it was possible to start reconstructing the basin’s evolution (Wessely, 2006).

The drilling for oil and gas commenced later and helped to uncover fossils located in deeper layers as the drilled material was brought to surface in order to be analyzed and studied. The drilling ultimately led to better understanding of tectono-sedimentary evolution of the Vienna Basin. The advances in drilling (e.g., maximum drilling depth and evolution of cumulative drilling capacity) can be seen in Figure 7.

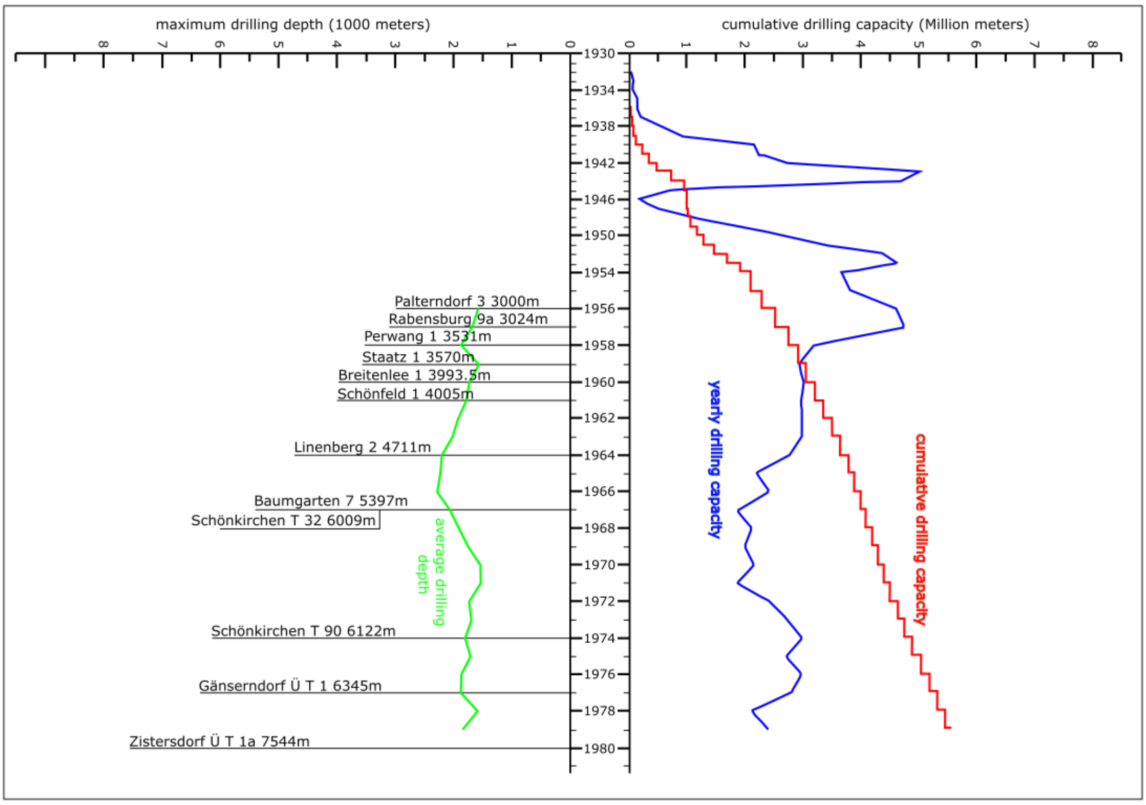

Figure 7: Left - Graphic showing reached depth milestone over the years from 1930 until 1980 in the Vienna Basin. Right – how many million meters on drills length (modified from Hamilton et al.(2000).

Among the new techniques that came within the 20th century the seismic imaging contributed greatly to finding new production units, since it allowed direct visualization below the surface. Therefore, possible structures that could act as hydrocarbon traps (structural and stratigraphic) could be localized and mapped. This new technology, along with those that were used before, brought an important advance in the oil industry. Before the finding of seismic method, the discovery of oil and gas relied mostly on gravimetric instruments and field research with the main goal of analyzing structural features in outcrops. Studying the impermeability of a fault at certain depth or at the surface and projecting where this fault is located based on dip and dip direction contributed to hydrocarbon exploration.

3. Faults

Faults are surfaces or narrow bands, where displacement can be observed with predomination of brittle deformation mechanisms (Fossen, 2016). Depending on the tectonic regime for a given area at specific time, specific fault systems can develop, due to different magnitude and orientation of the main forces generated by tectonism.

There are mainly three of these regimes (normal fault regime, strike slip regime and reverse fault regime). The difference between them are the orientations of the main forces and how the lithosphere responds to these forces. In Figure 8 these three regimes are displayed (Anderson stress classification) with the main stress components.

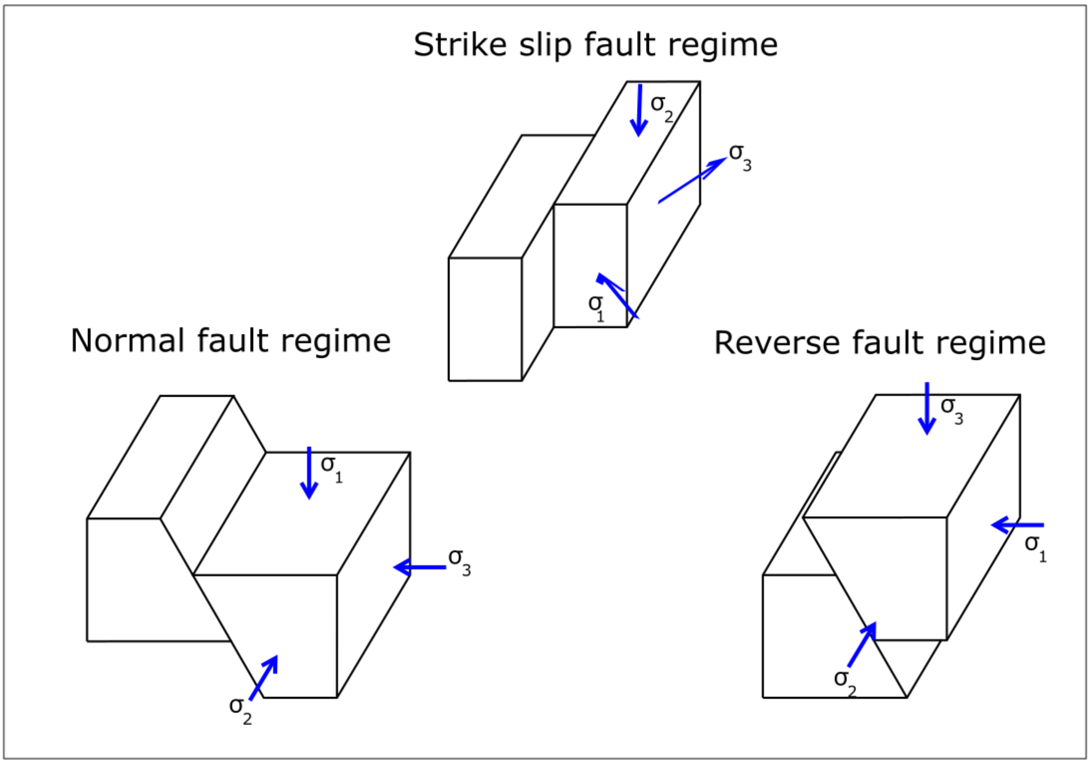

Figure 8: Different faults as an answer to tectonic forces (modified from Fossen, 2016).

Another point, regarding faults, is that having the predomination of one of these regimes does not eliminate the existence of faults from the other two regimes. For example, in strike slip predominating regimes, depending on the orientation of the main forces and bending of the strike slip fault, local normal faults (transtensional) and reverse faults (transpressional) can be present (Figure 9). Typical structures generated in these are the positive flower structure and negative flower structure (Figure 9), which are already documented in the Vienna Basin (Beidinger and Decker, 2011; Hinsch et al., 2005a, 2005b).

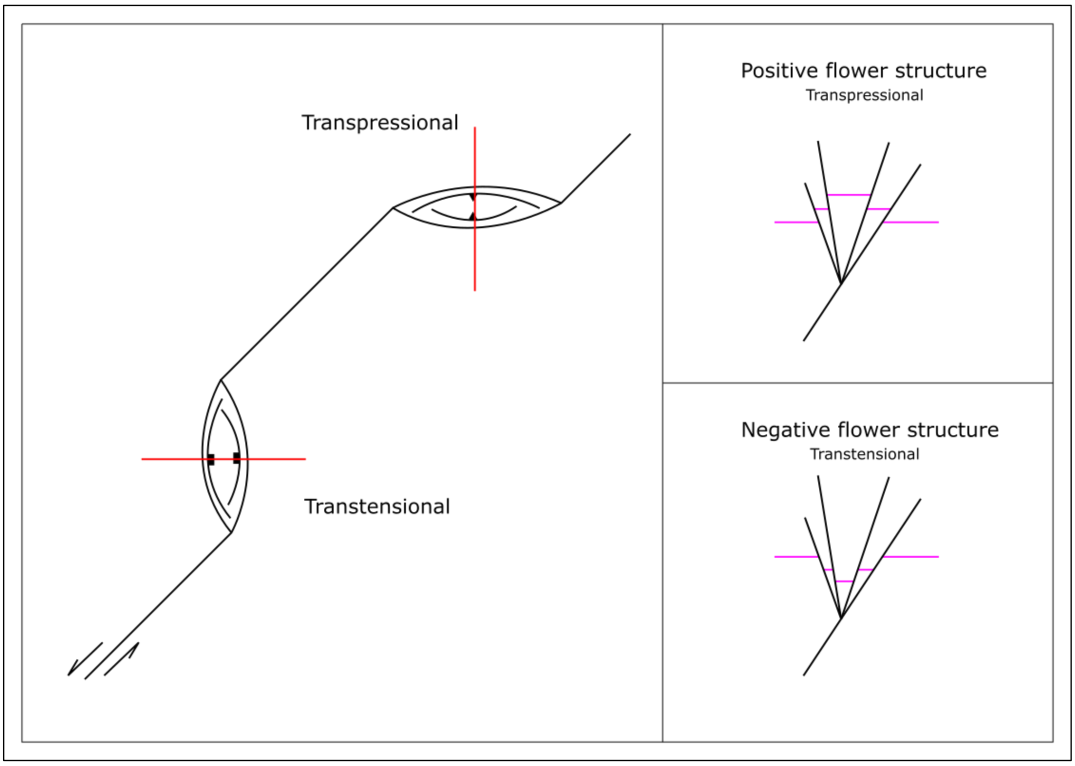

Figure 9: Predomination of strike slip fault regime, with local normal faults (transtensional) and reverse normal faults (transpressional) (modified from Fossen, 2016).

Faults that originated before, responding to tectonism, can stay inactive for many Ma before being reactivated since they could act as weak zones. However, the faults have to be analyzed since it can come to a strengthening (more stress deviation needed to generate movement) along the fault (Vitale and Mazzoli, 2008; Chen et al., 2023).

The movement along the fault can occur continuously through many Ma, moving some mm/year, or having eventual events that displace the rocks along the fault. One way to quantify this movement along faults is to map the stratigraphic units provided through well tops and looking what happens to the thickness of the reflectors close to the fault and farther away. In case the fault was active during deposition, a thinning away of the fault is expected since the accommodation close to the fault is bigger. Consequently, more sedimentation can take place at these depocenters with higher accommodation (Villamil, 1999; Morton et al., 2009; Lee and Wagreich, 2017).

In order to understand and interpret correctly the geological history of an area we have to analyse field data, observe microstructures in thin sections under the microscope, if existing seismic profiles, sedimentological features, stratigraphy, structural geology and also aerial image can be studied. After analyzing all the available data, all of them should point to the same interpretation. A textbook example in the Vienna Basin can be found on the northern side of the Danube where the Lassee Basin shows active tectonic feature (Figure 10) (Decker et al., 2005; Beidinger and Decker, 2011).

Topographic high is controlled by faults. However, if we analyze the sedimentological record and have seismic profiles we can see that only the basins between the terraces are actually fault controlled and faults can be seen in the subsurface (Beidinger and Decker, 2011). The others are controlled by erosion (in Figure 10 fault-controlled sides are represented by F and erosion-controlled by ER, most likely by the paleogeography of the Danube and the March River).

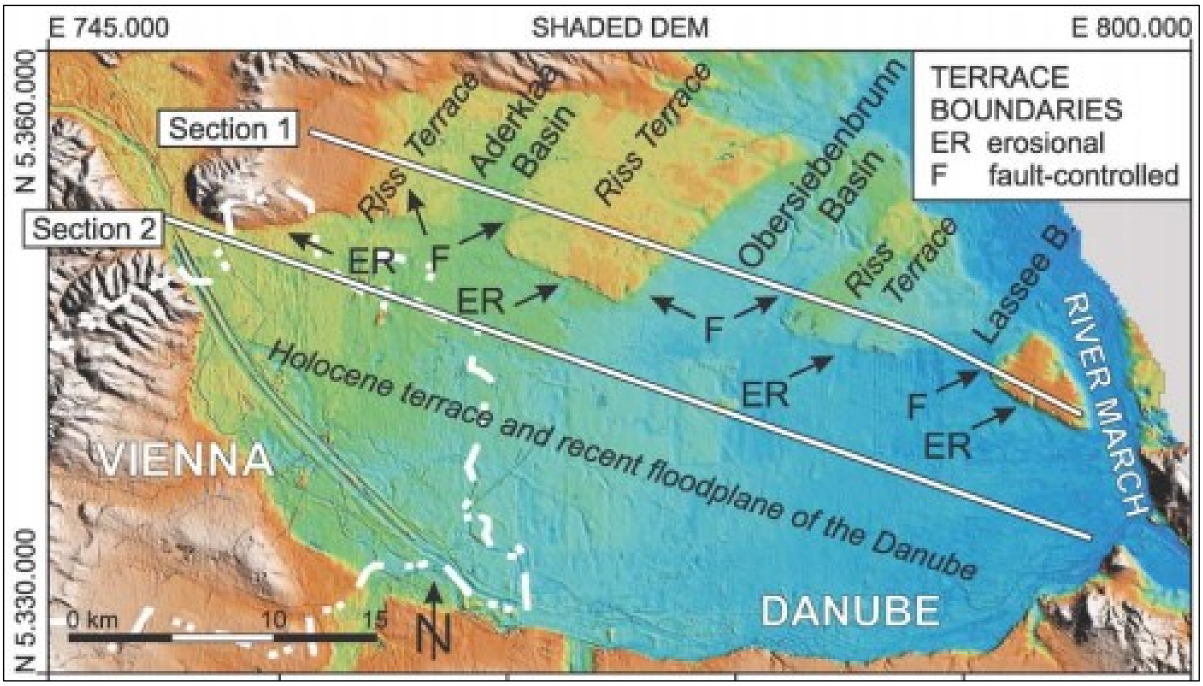

Figure 10: Shaded DEM of local smaller basins and surrounding within the Vienna Basin (Quaternary Aderklaa-, Obersiebenbrunn- and Lassee Basin) and adjacent areas (Decker et al., 2005). The terraces are separated by linear NE-trending faults, represented by "F" and the erosional generated cliffs by "ER" (Decker et al., 2005).

Besides the work of Decker et al. (2005), there are many other publications that support the idea that the Vienna Basin is still active (Hinsch et al., 2005a; Decker et al., 2005; Strauss et al., 2006; Beidinger and Decker, 2011; Lee and Wagreich, 2017). Another point is to analyze the current tectonic generated stress within the soil and map the recent earthquakes happening dispersed within the basin along major faults.

One important point for fault bounded hydrocarbon play is that for trapping hydrocarbons, the fault has to be already present in order to trap hydrocarbons. The fault can still have its highest displacement afterwards; however, the fault needs to have had enough movement to produce high enough shale gouge ratio (SGR) values to seal the trap. In case, the fault is not present or have not so much movement (small SGR values), the hydrocarbon will not be trapped and migrate to another possible trap.

3.1 Normal faults

In this master thesis we will focus on normal faults and oblique dip slip fault, since these are the main fault system in the Vienna Basin. Dip slip faults happen in extensional setting and a more realistic approach of normal faults is brought in Figure 11, where the highest displacement is expected to be in the middle of the fault (most likely to be also the oldest part of the fault) and in the direction towards the fault tips the displacement is expected to be smaller or even not show any offset at all.

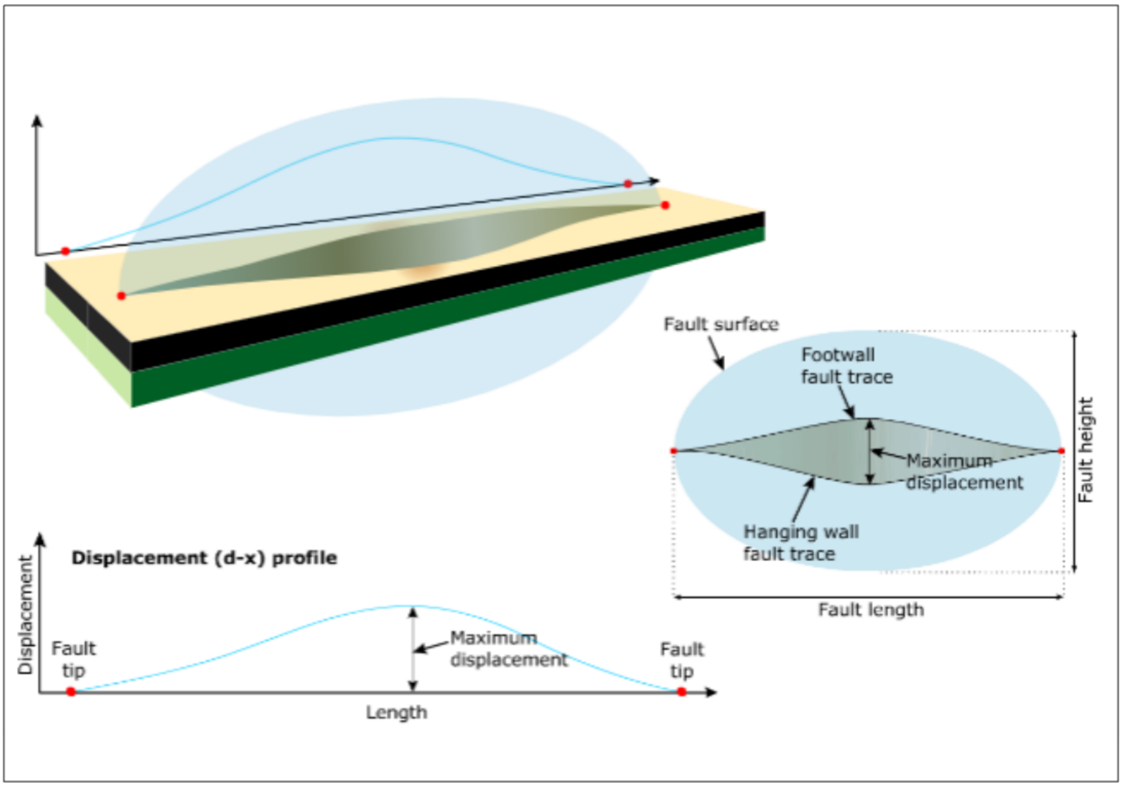

Figure 11: Representation of normal faults, with parameters regarding normal faults and displacement along the length of the fault (extracted from Fossen, 2016).

3.2 Oblique Normal Fault

This kind of fault is originated when the extensional force is oblique to the strike direction of the fault. Therefore, this force can be divided into two components. The first will be in the direction of σ_3 in normal faults and the second will be parallel to σ_3 in pure strike slip faults (Figure 8). As a consequence of this the first component will be acting as a normal fault where the hanging wall will have a pure dip slip displacement (vertical throw), while the other component will act as a purely strike slip fault and the displacement horizontal. Combining these two displacements, we are going to have a vertical and horizontal displacement (Figure 12).

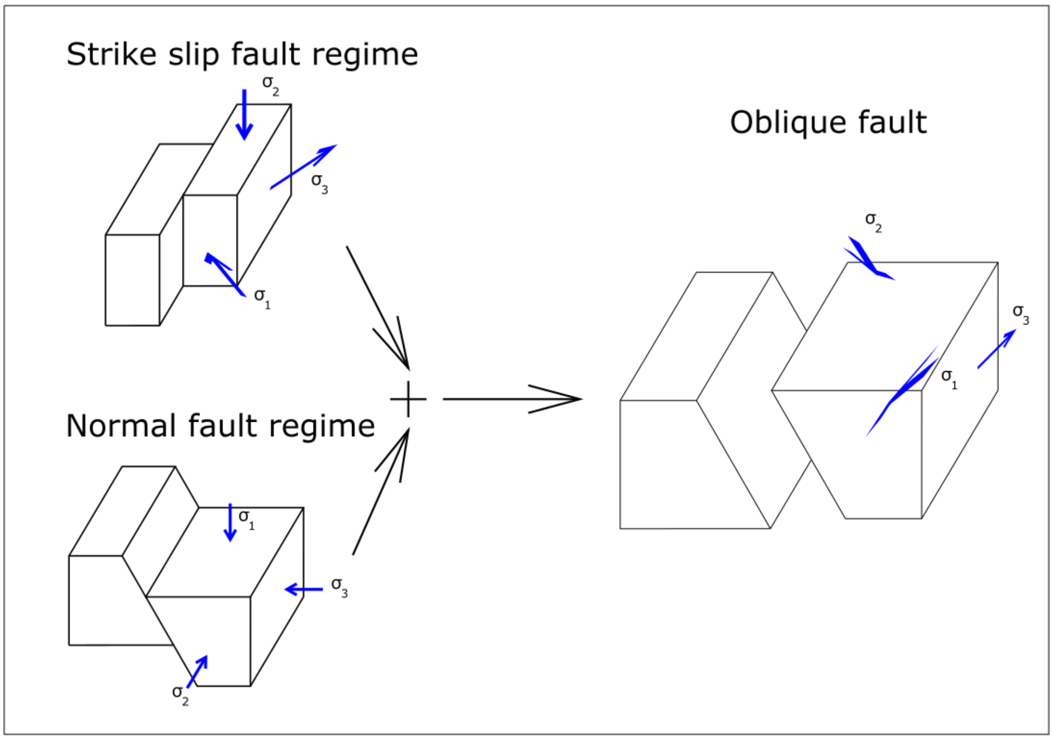

Figure 12: Anderson's stress classification combined to form oblique fault. Based on Anderson's stress classification.

3.3 Relay Ramps

It seems that for some of the production units within the Vienna Basin, relay ramps are structures where hydrocarbons can be found. Therefore, we will give these structures also some importance.

In the space between two normal faults that are parallel to each other a relay ramp can be formed. These two faults do not have to be of same age, however, there has to be a time in which both are active. Peacock and Sanders (1994) classified relay ramps according to its development stage into four stages (Figure 13):

1. The two main faults are isolated and do not interact.
2. These two main faults propagate to one another and there is an overlapping zone between the two faults. In this overlapping the interaction between these two faults occurs. The displacement of the bedding is accommodated by rotation, giving origin to the relay ramp.
3. Smaller faults linking these two main faults start to connect the two major faults and break the connectivity along the ramp.
4. The last stage is when the one or the two smaller faults completely destroy the ramp and connects the major faults. In case one of the smaller faults develops more than the other one the ramp can still be connected either to the hanging wall or footwall and separated from the other one. Or it can get completely isolated (higher throw) in case both minor faults develop and connect the major faults.

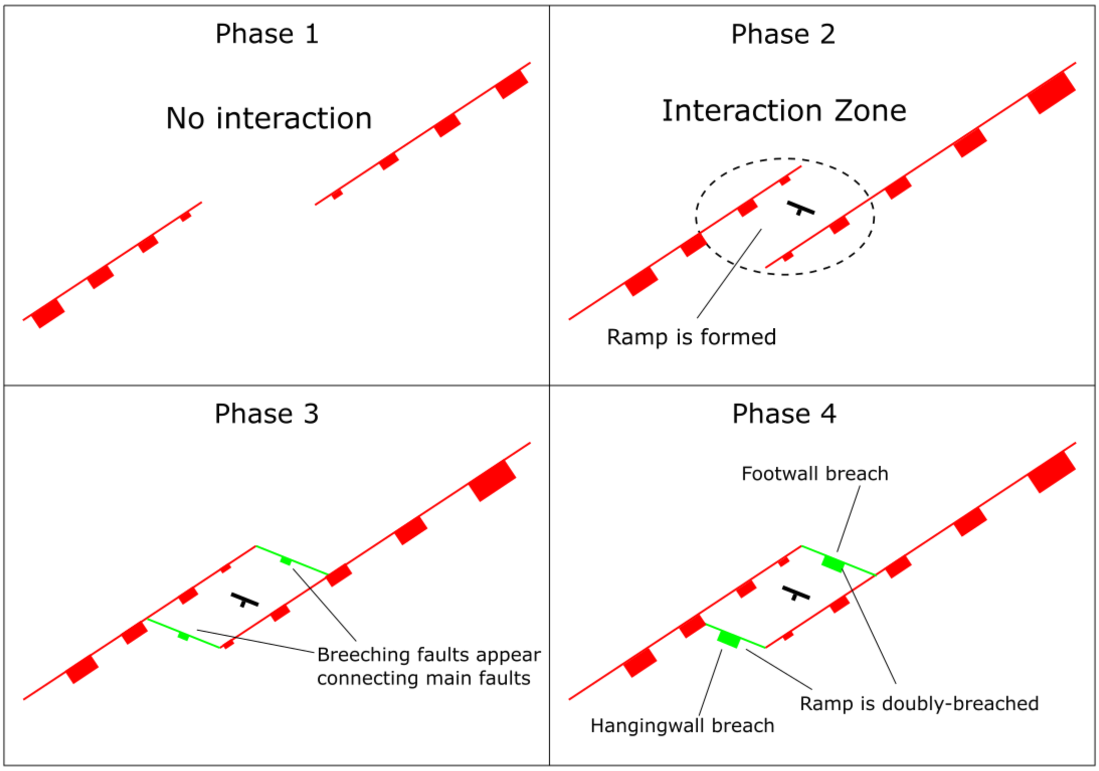

Figure 13: Evolution of relay ramp (Peacock and Sanders, 1994).

Depending on what evolution stage the relay ramp is currently in, the ramps can act as a passageway (across the fault) for fluid migration between the hanging wall and the footwall. These would happen in phase 2 and in phase 3 (considering the faults in phase 4 isolate the ramp), later depending on the displacement on the minor fault represented in green in Figure 13.

The ramp in phase 4 can act as a trap, when there is enough displacement to trap the hydrocarbons. In this case, not only the upper green fault has to have high enough SGR value but also the two main faults at this area (three-way fault). Here the phase 4 is represented by both minor faults (footwall breach and hanging wall breach) showing higher offset which would completely isolate the cut off ramp, but it can also be just one of them. Local folding (anticlines and/or synclines) can develop in these ramps which can also act as hydrocarbon reservoirs.

3.4 Fault throw vs depths diagrams

In the Result section, number of throw vs depths diagrams are shown and discussed for different faults in the Vienna Basin included in this study. In order to understand those correctly, we explain how to read throw vs depth diagrams shown in Figure 14. The diagrams include theoretical pattern of different types of faults.

Generally, faults are limited in space and have one center where the fault starts to displace rocks. This point tends to be the oldest and therefore also with continuous movement along this fault tends accumulate the highest throw values. From this point going either laterally (map) or into depth (cross section) the throw tends to decrease and these relations are shown in schematic Figure 14 for different faults.

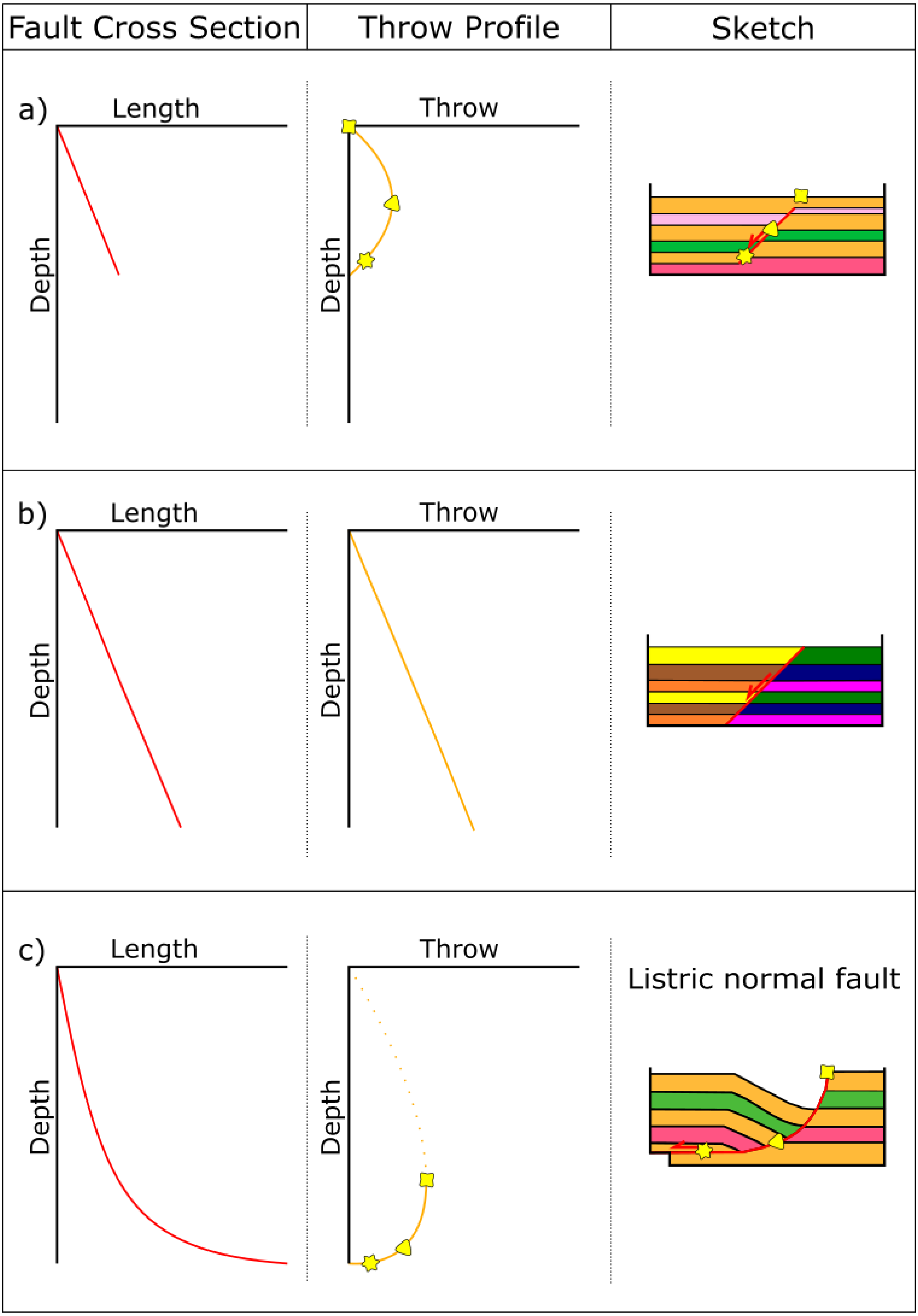

Figure 14: Theoretical geometries of fault as shown in depth vs throw diagrams when comparing different type of faults.

The throw vs depth diagram in Figure 14a shows a normal fault with small displacement. In this case, the largest throw is in middle of the fault (marked by yellow triangle). At the upper fault tip near the surface (square) and at the lower fault tip (star), the throw is smaller.

When analyzing faults, their size has to be considered in order to choose a better map extent and have better understanding of the feature. The needed map extent for small geological features can be small while larger features need larger areas. Example is shown in Figure 14b, where the fault throw is much larger than the map extent.

Assuming that the big fault mentioned above is a listric fault and we choose a cross section extend where we can see the whole fault (Figure 14c) we would also be able to see where the faults gets horizontal (detachment level, Spahić et al., 2011). The throw vs depth diagram shows that the throw is largest for the first orange layer (square) and for deeper layers the throw gets smaller.

3.5 Shale Gouge Ratio

Juxtaposition between two segments of one layer that can act as a reservoir to another sealing layer (e.g. shale) on the other side of the fault is called juxtaposition seal. This situation can occur and is one of the sealing mechanisms along faults. However, this does not happen every time and one reservoir layer can stay in juxtaposition with another potential hydrocarbon bearing layer (Figure 15). The brown production unit on the hanging wall is separated through the fault to the yellow production unit on the footwall. Decisive to note is that they are distinct Pus isolated by the fault. Therefore, the pressure applied by each one of them into the surroundings is different. If the fault was not sealing, hydrocarbons would cross from the production unit with more pressure to the production unit with lower pressure in order to turn the pressures equal (Fitzpatrick, 2017; Dembicki Jr, 2017; Axaopoulos and Tzanes, 2021). The point where shale gouge ratio and other algorithms become important is to determine what faults are flow independent.

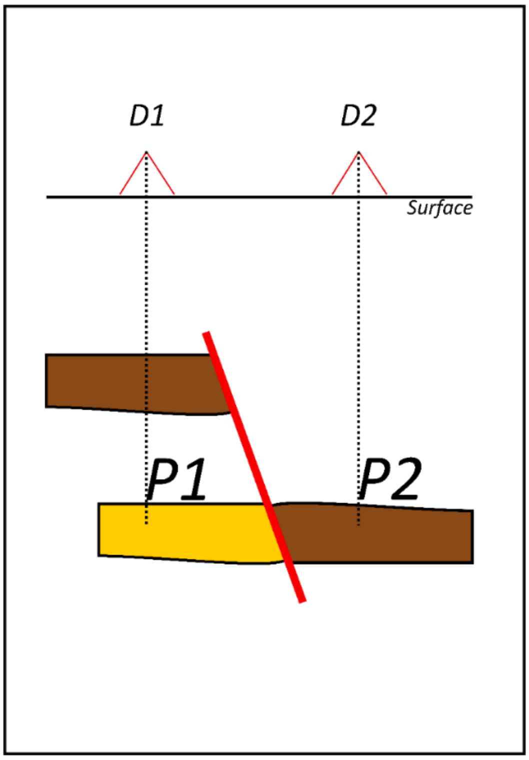

Figure 15: Two distinct prodution units separeted by a fault.

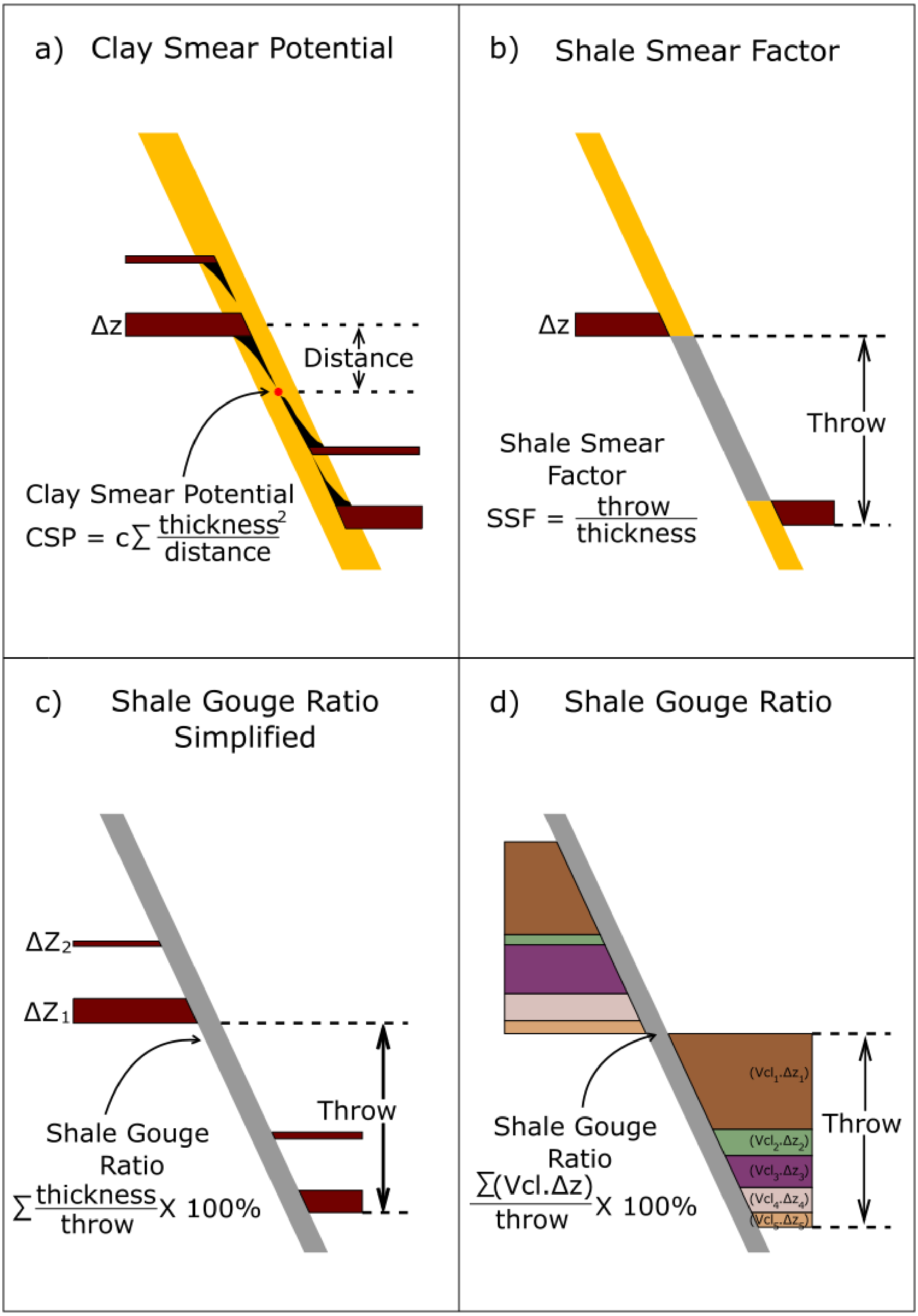

Figure 16: Algorithms trying to predict if fault are impermeable (modified from Vrolijk et al., 2016).

There has been many studies trying to predict if a fault is sealing or not. And it is under this pretense that many algorithmic approaches relating to the impermeability of the clay smear in the faults have been developed over the years. In this thesis, we are going to work with shale gouge ratio (SGR), however it is also important to know that there are other models, two of them will be briefly presented as well as two calculation methods for Shale Gouge Ratio (Figure 16).

The SGR threshold value of 15-20% was adopted in this thesis to distinguish if a fault is leaking or sealing was taken from the literature (Harris et al., 2002; Yielding et al., 2010). For SGR Values over 20% the fault is considered flow impendent. The diagram in Figure 17 was provided by OMV and it was calculated and generated with the formula presented in Figure 16d. For this, the shale content in many depths were determined along the respective borehole. We can see such SGR Diagram (Figure 17) below (for one borehole in the Matzen area) where if one 40m magnitude layer is displaced by its magnitude the SGR values are already over the threshold value (red area).

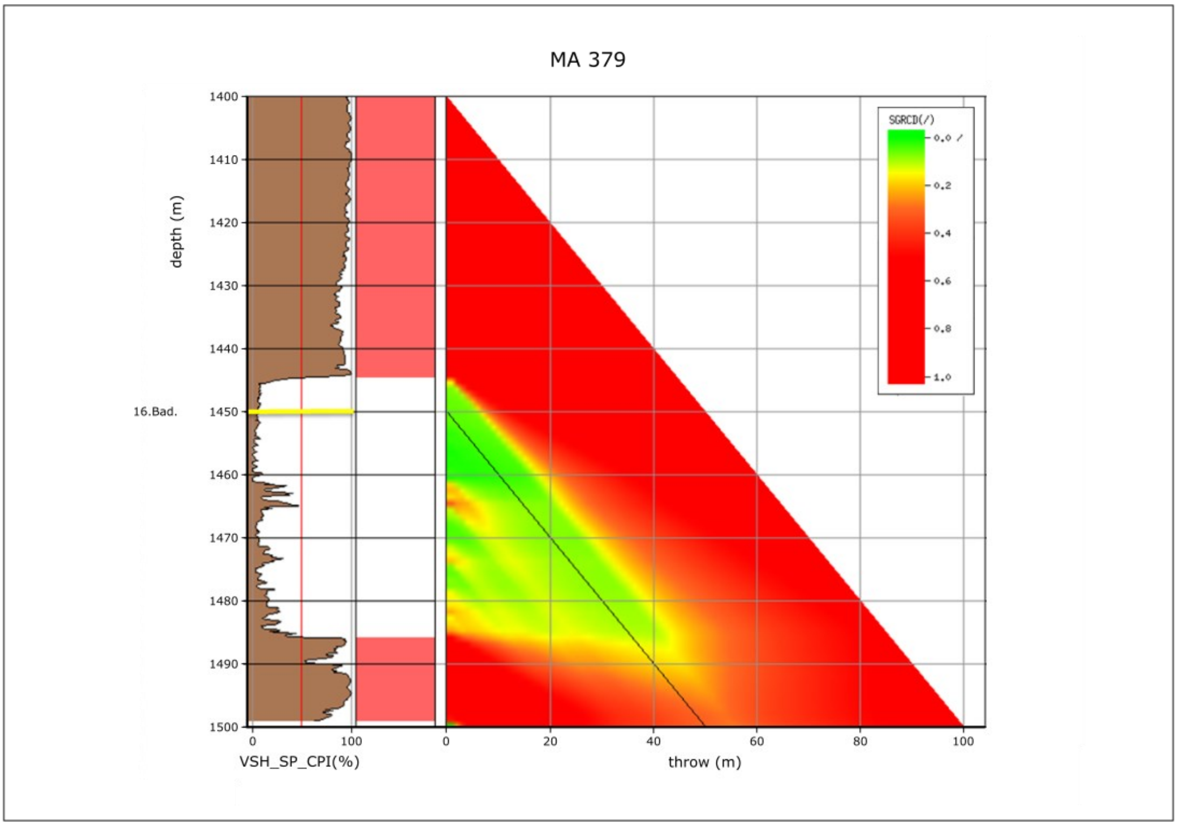

Figure 17: Typical shale gouge ratio Diagram for one borehole in the Matzen area (OMV internal report).

4. Hydrocarbons

4.1 Hydrocarbon origins

To test the hypothesis of impermeable faults, the origin and timing of hydrocarbon migration has to be studied. Hydrocarbons are formed under certain temperature and pressure conditions, known as oil and gas windows. The first relates to the depth, in which oil forms and the latter to the depth, in which gas forms. The depth is, however, not the only important factor for hydrocarbon formation, but also the total organic content of the source rock is considered during evaluation of the production.

A source rock originates from sediments with great amount of organic matter incorporated at the time of deposition and rock formation. The organic matter has to be later preserved during diagenesis, the right temperature and pressure conditions has to be met and also the right period of time for this reaction to occur in order to be transformed into hydrocarbons. In the Vienna Basin, the main source rock originated in the upper Jurassic sediments, namely the marlstones in the Mikulov Formation and the marly limestones in the Falkenstein Formation (Rupprecht et al., 2017).

4.2 Hydrocarbons Migration

Hydrocarbons migrate from the source rock to the reservoir and accumulates in traps, either structural or stratigraphic. This process is known as hydrocarbon migration. For the purpose of this study, geological structures that could act as a trap must be evaluated, in order to determine if they are dry or contain hydrocarbon. In the latter case an existence of source rock in older stratigraphic units is essential. The structure/trap can also be dry, either due to (i) earlier or no migration related to the formation of the structure or (ii) absence of the source rock.

In simplicity, hydrocarbon migration can occur either stratigraphically (membrane seal or hydraulic seal) or along/across faults. Individual migration mechanisms are briefly mentioned in the following paragraphs:

Membrane seal (also known as capillary seal) is based on the pressure that the water contained in the cap rock’s pores can support (Figure 18a). In case the buoyant pressure exceeds the maximum pressure threshold from the cap rock, the water present in the cap rock start to be expelled and the hydrocarbons takes its place and works its way up (Yielding et al., 1997; Vrolijk et al., 2016) and can be stored in younger stratigraphic units, generating in many cases shallower production units.

On the other hand, at the hydraulic seal failure, also as a consequence of higher hydrocarbon pressure, however, the ascending of fluid does not occur through the pores, but by fracturing of the cap rock, directly related to the thickness of the cap rock (Watts, 1987), and consequently, moving to shallower stratigraphic units. This does not happen continuously but by periodic events when the hydrocarbons’ pressure exceeds the supported pressure of the cap rock. After the migration and pressure relief the fractures in the cap rock “close” and the cap rock remains “closed” until the next migration event occurs when the hydrocarbons’ pressure exceeds the one from the already fractured cap rock.

Migration can also occur along/across a fault and the same principle as for membrane seal applies here (Figure 18b). This time, however, with the pressure from the hydrocarbon against the threshold supported by the fault. The larger fault throw, the thicker fault rock is expected (Childs et al., 2009) and therefore can potentially support greater hydrocarbon column (Figure 18b). In order to verify, if the sealing of the fault is the key factor controlling the presence of the hydrocarbons, the timing of hydrocarbon migration has to be clarified. Migration of hydrocarbons into the fault related trap can occur before or after fault reactivation (Cong et al., 2020).

From the exploration perspective, two of the ideal trap conditions is if this fault is able to store all volume of produced volume of hydrocarbons and also have a cap rock that can support the vertical pressure generated by the hydrocarbons themselves. However, in reality, these two premises do not always happen. Either the volume of a trap is not big enough and hydrocarbons are going leave the reservoir through the spilling point (the lowest part of the structure) or the cap rock cannot support the whole pressure either in the peak of the structure or on a point where it leaks hydrocarbons (also called spilling points). Thus, hydrocarbons eventually leave the trap and move to another trap closer to the surface.

These two mechanisms explain (at least partly) how oil and gas can migrate vertically to shallower stratigraphic units, however, since oil is heavier than gas, we tend to presume that gas would be found at shallower depths while oil appears deeper in the column. In other words, for shallow production units it is easier to find gas in shallower traps and moving deeper to find at some point only oil. However, as described in (Watts, 1987), at deeper depths it is easier to trap gas than oil.

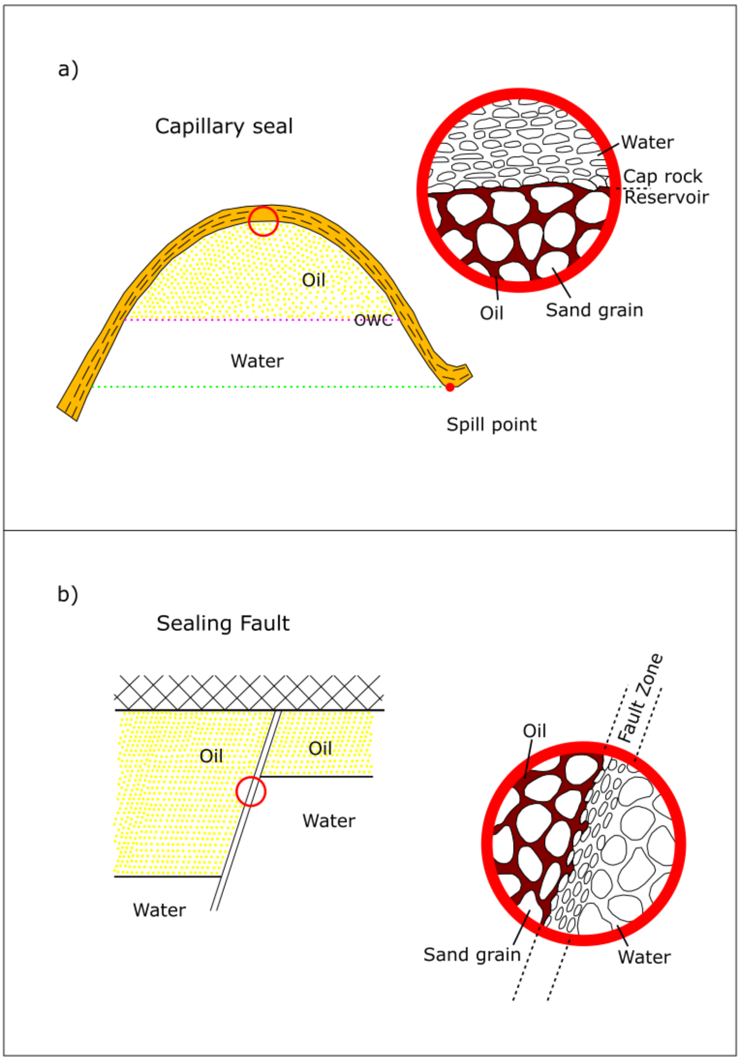

Figure 18: Showing in microscale how hydrcarbons can be trapped, both cases show situations where the pressure threshold of the cap rock (a) or fault (b) are not reached (modified from Watts, 1987).

4.3 Significance of oil-water-contact (OWC)

It is known that fluids that are not compatible (density and polarity), will not mix (heterogeneous mixture) and therefore two phases will be present (Holleman-Wiberg, 1976). The lighter phase will move to the top and the denser phase stays below the lighter phase. Gas, oil and water (from lightest to heaviest) have different densities and polarity, resulting in a heterogenic phase system.

The surfaces or zones that divide these phases are known as contacts and are also named accordingly: (i) OWC for oil water contact; (ii) GWC for gas water contact and (iii) GOC for gas oil contact. In the following paragraph, OWC is described and explained in detail. The same applies for GWC and GOC.

Firstly, Figure 19 shows two scenarios, when only hanging wall is considered. The interaction between the trap geometry and the depth of the OWC will determine if the production unit is fault related or not. Secondly, Figure 20 displays four different situations of OWC, where also footwall and a fault's throw are taken into consideration. In the latter case, all production units are fault-related.

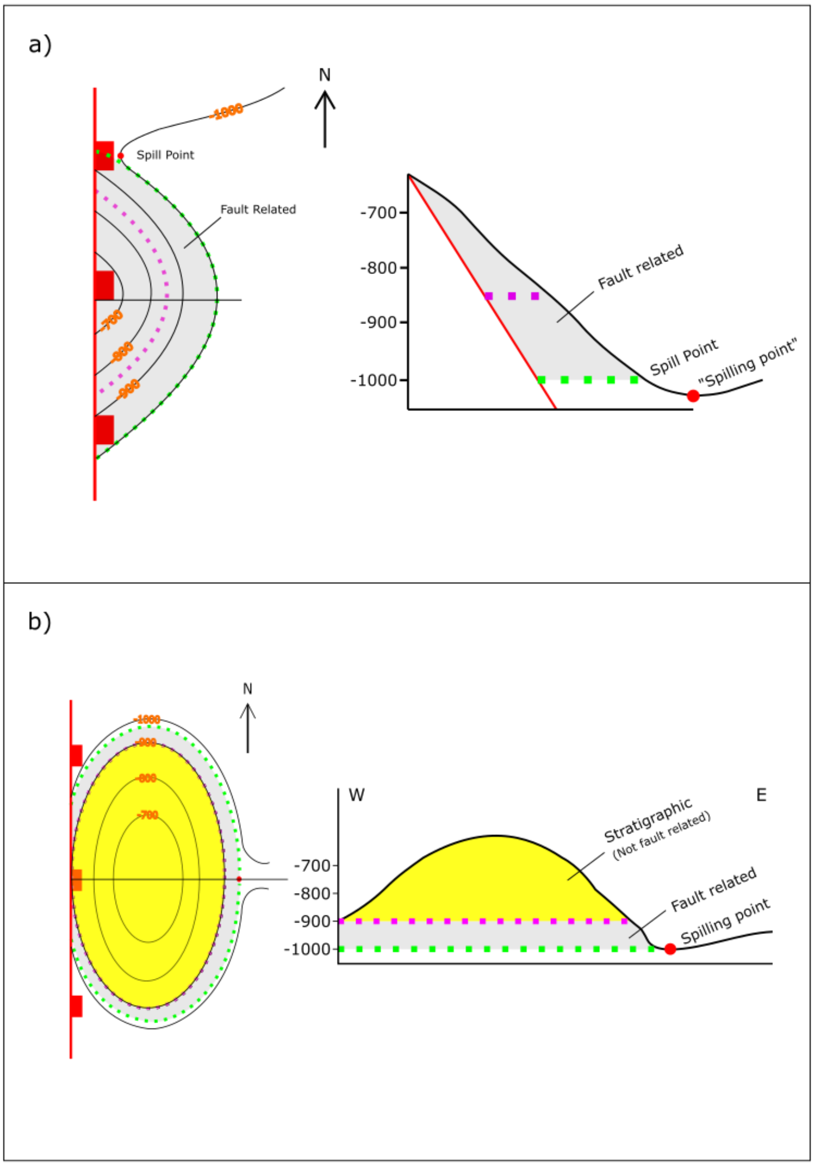

Figure 19: Two possible geometries of fault bounded traps.

Depending on the geometry of the production unit, OWC will provide a clue if a fault is sealing or not, exemplified here by two different geometries shown in Figure 19. In Figure 19a, the map view on the left shows that almost all the surface contour lines are being cut by the fault. The contour line with the value -1000 m is delimited by the fault on the western side, while on the northern side it forms an arch moving away from the fault. This point is defined as a spill point. Hydrocarbons can fill this structure to this depth, before leaking to another structure. The depth of 1000 m in Figure 19a will also be the deepest possible value for the OWC in the structure (shown as green dashed line). The profile shows that the spill point could be even deeper than 1000 m, however, as the structure's actual spill point is shallower (shown as red point further north on the contour line), the spill point along the profile will not be reached. The violet dashed line (Figure 19a, b) represents the OWC depth for situation, where the structure is not completely filled by hydrocarbons. For this geometry (Figure 19a), the oil water contact would always be below the point where the fault cuts the structure. In case that fault impedes flow, the production unit is going to be fault related.

Unlike in the first described geometry, where all possible OWC depths values are above the green dashed line (and therefore fault related), Figure 19b displays different scenario. The depth, in which the structure touches the fault is represented by the violet dashed line (Figure 19b). All OWC values above this line will not be fault related, but stratigraphically controlled. Like in Figure 19a, here also, the green dashed line is representing the greatest depth value for OWC. So, for the trap geometry shown in Figure 19b, the only cases where the production units would be fault related are those, where the OWC lies between the violet and green dashed lines.

4.4 Description of trap geometries

The best way to predict if fault is sealing or not, would be to study contact between fluids (OWC, GWC, GOC). Different structural situations, where at least two boreholes were drilled are shown in Figure 20a-c. Here, wells were drilled at both sides of the fault. This allows for good stratigraphic correlation across the fault and to determine the depth of OWC. A case, where no well was drilled in the footwall is shown in Figure 20d)

If hydrocarbons can be found on both sides of the fault (Figure 20a-b), it needs to be evaluated if it is only one production unit (fluids cross non-sealing fault) or two different production units (fluids do not cross fault, fault is sealing). One way to answer this question would be to see if the OWC resides at the same depth (Figure 15). Fluids have tendency to flow from high to low pressure places and to achieve equilibrium (Fitzpatrick, 2017; Dembicki Jr, 2017; Axaopoulos and Tzanes, 2021). This can occur if the fault is not sealing, and it can be assumed that there is only one production unit (Figure 20a). The exception for this case, would be, if two different production units have coincidently their OWC at same depth. However, the pressure would probably be different in each unit since there was no fluids exchange.

The second scenario is shown in Figure 20b. There, the fault is impeding flow from one side to the other. Consequently, the OWC would not be the same level (different depth) and the pressure would be different.

The next situation, where it has been drilled on both sides of the fault, but hydrocarbons were found only in the hanging wall is shown in Figure 20c). Here the assumption used in previous cases from the first situation about OWC and pressure do not apply. However, it raises question, why the structure is "dry" on the other side. To answer this question, plausible explanations are presented below:

- Dry structures could point to the fact that no charge has taken place.

- Charge happened, but for some reason the hydrocarbons migrated somewhere else. A simple explanation for this would be that the fault is not sealing and the reservoir is juxtaposed to another layer with reservoir potential.
- The fault is not sealing.
- The sealing properties of a fault could have changed trough time. A fault at the beginning of its formation (small displacement) tends to permit cross-fault fluid flow, while faults with higher displacement will be inclined to impede flow (Yielding et al., 1997).

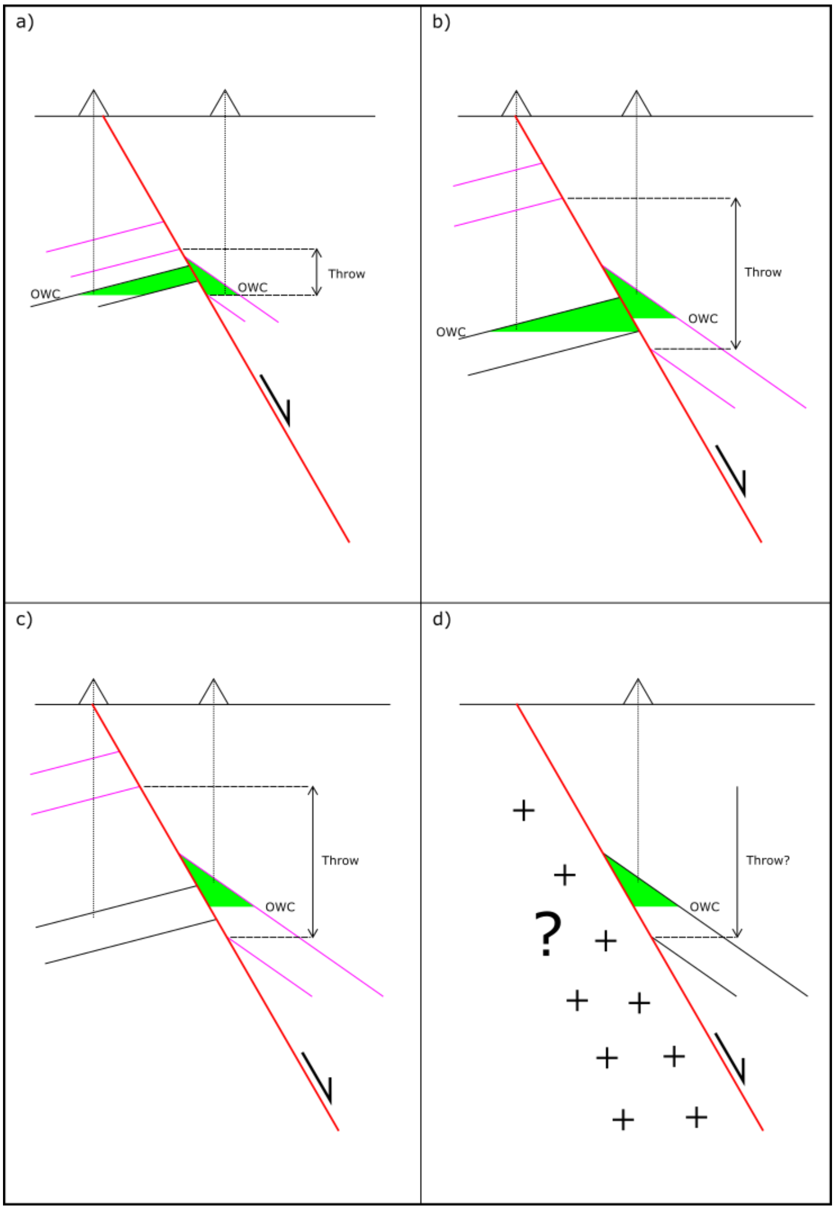

Figure 20: OWC in different situations. a-c) Boreholes at each side of the fault. a) OWC at same depth at both sides, therefore, fault is not sealing. b) OWC depth different at each side of the fault, therefore fault sealing and two distinct production units. c) Only the hanging wall contains hydrocarbons, the footwall, despite present structure, is dry. d) Production unit only at the hanging wall. There are no structures present at the footwall, for this reason there no drill was made at the footwall.

After all, the sequence and timing when everything happens (formation, migration, charging, fault sealing) could also be the explanation for a dry structure (in the footwall in case shown in Figure 20c).

The last situation shown in Figure 20d, where only one well was drilled (here in the hanging wall), would occur if only one side produces hydrocarbons and/or due to lack of possible hydrocarbon retaining structure on the other side of the fault (Figure 20d). These situations are the most complicated since there is almost no information about stratigraphy in the undrilled side of the fault and so it is difficult to extract information regarding e.g., fault throw, OWC.

5. Methodology (Definitions and Parameters)

This chapter contains information about data used in the study and includes definition of parameters, which were assessed to determine how many from the available 270 production units in the Vienna Basin are fault related. At the beginning of the project, OMV provided a list of producing reservoirs in 2020, in which each producing reservoir received a unique identifier. However, some production units had to be removed from this study due to number of reasons. These are presented in the next chapter in detail.

Evaluated parameters are listed in Tables 1 and 2. This chapter also explains how these parameters were obtained or calculated in detail. Table 1 contains additional data either provided directly by OMV or calculated data, which were acquired from original OMV data. Table 2 contains mainly data obtained by seismic interpretation directly in Petrel project and are presented in Chapter 6.

Table 1: Provided and calculated data

Reservoir identifier
5.1 Hydrocarbons
5.2 Borehole ID
5.3 Stratigraphic Unit
5.4 Depth Top Borehole
5.5 Fault

Table 2: Petrel extracted data

6.1 Thickness
6.2 Cap Rock Thickness
6.3 Ratio Cap Rock Thickness x Thickness
6.4 Thickness Factor
6.5 Highest Trap Point
6.6 Throw
6.7 Help drill
6.8 Position
6.9 Fault related preview
6.10 Fault related calculations

5.1 Hydrocarbons

Hydrocarbons within working trap are chains of molecules of organic matter and are exclusively composed of carbon and hydrogen atoms. However, some elements might also be present, e.g. oxygen and sulphur (Grotzinger and Jordan, 2017), when this is the case, special conditions have to be taken into consideration when fractionizing the oil (separating the lighter oil components from the heavier).

While gas includes the smaller chains, in oil the longer ones are predominant (Grotzinger and Jordan, 2017). However, both have the same origin, living organisms, specially plankton and plants, that died and have been buried below many layers of sediments (Vandenbroucke and Largeau, 2007; Grotzinger and Jordan, 2017). This organic matter, if special temperature and pressure conditions are met will start decomposing and forming oil, gas or both (Grotzinger and Jordan, 2017). The product that will be formed will depend on the original organic material (Vandenbroucke and Largeau, 2007). The duration that these rocks and especially the organic matter has been exposed to these conditions gives the maturation state (Sverdrup and Ragnarsdóttir, 2014).

This parameter gives information on what was found in the reservoir. Even if oil and gas are found in one production unit they cannot be extracted at the same point from the same borehole. Each product needs different completions.

5.2 Borehole ID

For each production unit a “BoreholeID” was added. In order to have better possibility of extracting information from layer below our production units the deepest reaching borehole was selected and its ID was added to the table.

5.3 Stratigraphic Unit

As shown in the geological setting section (Figure 6), the thickness of specific layers changed through the Vienna Basin. This will depend mostly on which faults were active at a specific time or over longer time in order to interpret location of depocenters. Local hiatuses (periods where no deposition take place in one area) or erosion can also reflect on the sedimentation history.

Each borehole contains information on the depth of each stratigraphic unit and each hydrocarbon reservoir (well tops) or wireline log interpretation. The nowadays accepted age and bio zonal division of the eastern Paratethys are based on planktonic foraminifera, nannoplankton and land mammals (Wessely, 2006). The depth of the production unit is important since it can influence chemical properties of oil and gas (Rupprecht et al., 2019). Additionally, the depth of a stratigraphic unit derived from the positions of well tops in a footwall and a hanging wall across a fault is a key parameter to determine a fault throw.

The depth from which oil or gas are extracted does not necessarily have to be simultaneously the highest point of a structure containing hydrocarbons. In Figure 21a, the borehole (violet circle) is located along profile 1 and it is shown that the highest point of the trap touching the fault is actually located along profile 2.

Information about stratigraphic unit was extracted from the reservoir identifier, which is in the format:

$$XX - YZZ - TT$$

XX represents a continuous number for the field, in which hydrocarbons are extracted. Y stands for the central Paratethys stage (Table 3, e.g., 0 for Pannonian and 6 for Cretaceous. ZZ represents the horizon within the stage. TT is a continuous number for the production unit within a field.

A production unit that is in the 5th Sarmatian would have the following reservoir identification XX-105-TT. It is also important to mention that the stratigraphic unit division is based on well log correlation, seismic mapping and on the analysis of fossils in each layer (Wessely, 2006).

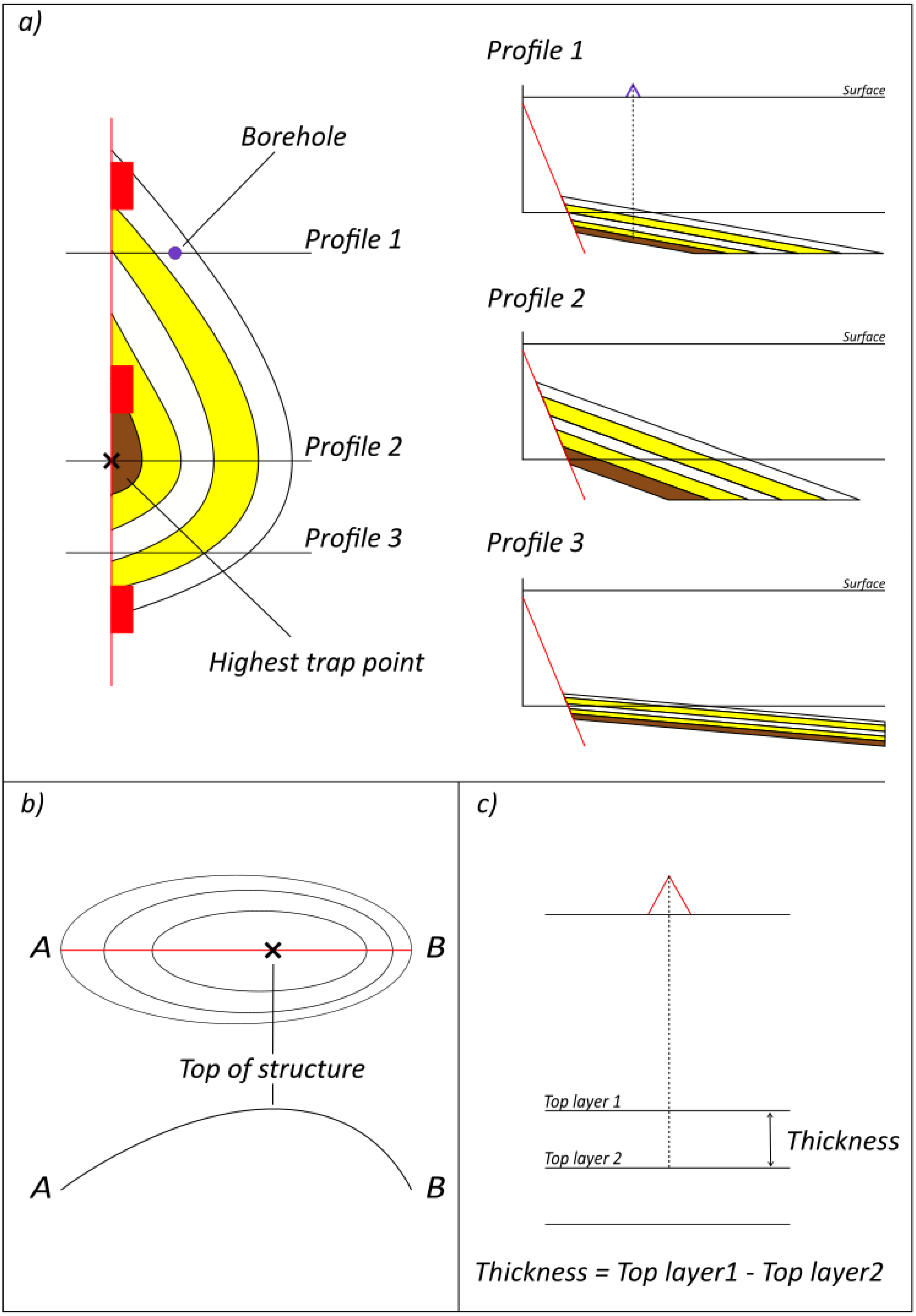

Figure 21: Schematic method to calculate parameters; a) Highest trap point, b) Geometry with top of structure, c) Thickness.

Table 3: Overview of the numbering of producing horizons.

Code	Geochronological layer
000	Pannonian
100	Sarmatian
200	Badenian
300	Karpatian
400	Ottnangian
500	Eggenburgian
600	Cretaceous
700	Triassic

5.4 Depth Top Borehole

Once the stratigraphic unit for each production unit was established, the corresponding depth for each production unit's top was extracted from OMV's database. In some cases, there was no depth information for the stratigraphic unit, and it was decided to look for another borehole in this production unit or even a borehole from an adjacent production unit in order to retrieve this information. In case the data came from another borehole, we correlated the seismic reflector in between the two boreholes, taking faults into account. In similar process the highest trap point and throw were obtained in sections 6.5 and 6.6.

5.5 Fault

The "Fault" column in Table 1 contains information on which fault could be acting as the seal for that specific production unit.

6. Results

Chapter 6 outlines how the parameters were calculated using schematic approach and real examples. The data presented below in Tables 4 and 5 were obtained either from the provided OMV dataset or extracted from Petrel.

6.1 Thickness

The main point, where the thickness is going to be important, is when we want to know the minimum displacement necessary to avoid juxtaposition (Figure 22). Further, thickness, together with the geometry and where the spilling point is located, controls how much oil can be trapped.

The thickness of a hydrocarbon reservoir (Figure 21c) is important as it gives an estimation of the volume of oil or gas that could be extracted. Additional factors as the shape of production unit (e.g., dome or having horizontal layers), the size of a trap, the sealing capacity of the fault and the cap rock big enough to store the volume on hydrocarbon have to be considered. In this study, where the structures mostly have a shallower dip than a fault itself, the OWC or spill point of the production unit will be important parameters.

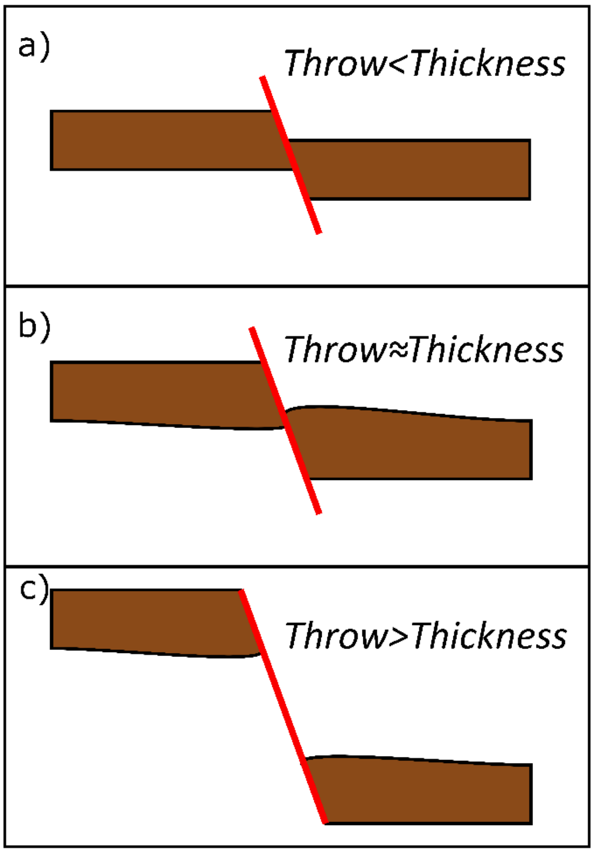

Figure 22: Three examples of relation between thickness of the production unit and fault throw.

The lithology bellow 7ASH shown in Figure 23 is interpreted as sandstone with its top defined in the well log. However, the bottom of the same sandstone unit is not specified as a horizon in the log and is for this reason estimated based on GR and SP logs.

Table 4: Extracted/calculated parameters for the analyzed fault bound production units (without production units along Steinberg Fault).

Sondenkurz	Hydrocarbon	Position	Fault	Stratigraphy	Thickness (m)	Throw (m)	Top Borehole (m)	Highest trap point (m)	Thickness/ Throw	Cap rock thickness (m)
HO O 2a	oil & gas	hw	SE00_Pirawarth	6 Sarmatian	20,96	845	-969,45	-900	0,024804734	22,01
NS 11	gas	hw	SE03_Altlichtwart	20 Sarmatian	15,82	1815,94	-1704,37	-1683,79	0,008711742	15,41
RAB W 4	oil & gas	hw	NW01_Steinberg_anthitetic	16 Sarmatian	25,21	220	-855,49	-847	0,114590909	15,49
RAB 15	gas	fw	W03_Rabensbug	20 Sarmatian	24,08	156	-1486,94	-1488	0,154358974	12,8
SPA S 1	gas	fw	MA_S_004	3 Sarmatian	-	52,08	-665,74	-645	Not defined	-
SPA 20	oil & gas	fw	MA_S_003	3 Sarmatian	-	101,4	-610,67	-605	Not defined	-
MA 5	oil & gas	fw	MA_N_002	5 Sarmatian	-	79,28	-567,09	-551,82	Not defined	-
P 102	gas	fw	TAL_S_002	5 Sarmatian	-	19,66	-583,59	-562,85	Not defined	-
OLL 5	gas	fw	TAL_S_002	7 Sarmatian	-	49,71	-662,48	-652,95	Not defined	-
TAL 10	gas	fw	TAL_S_002	8 Sarmatian	-	23,39	-756,29	-736,39	Not defined	-
PIR U 8	oil & gas	hw	SE01_Pirawarth	5 Sarmatian	7,31	319	-610,82	-555	0,022915361	14,07
HL 5	oil & gas	hw	SE01_Pirawarth	10 Sarmatian	2,47	378	-743,54	-712	0,006534392	11,12
HL 13	oil	hw	SE01_Pirawarth	12 Sarmatian	-	402	-788,65	-779	Not defined	-
PIR 17	oil & gas	fw	SE00_Pirawarth	5 Sarmatian	8,42	62	-556,59	-550	0,135806452	34,54
PIR 48	oil & gas	hw	SE00_Pirawarth	5 Sarmatian	7,49	62	-658,99	-615	0,120806452	39,6
PIR 18	oil & gas	hw	SE01_Pirawarth	7 Sarmatian	25,85	222	-703,37	-	0,116441441	5,92
PIR 18	oil & gas	fw	SE00_Pirawarth	7 Sarmatian	25,85	78	-703,37	-586	0,331410256	-
PIR 60	oil & gas	hw	SE00_Pirawarth	7 Sarmatian	11,68	78	-722,85	-664	0,14974359	8,61
PIR 11	oil & gas	hw	SE01_Pirawarth	13 Sarmatian	10,16	206	-869,55	-828	0,049320388	13,83
PIR 22	oil & gas	hw	SE00_Pirawarth	14 Sarmatian	5,8	87	-919,20	-895	0,066666667	-
PIR 73	oil & gas	hw	SE00_Pirawarth	3 Badenian	10,11	140	-1002,48	-1000	0,072214286	6,23
ZW 31	gas	hw	-	0 Karpatian	-	191	-1687,76	-	Not defined	-
MARK 2	gas	hw	SW01_MagaNeu	3 Sarmatian	-	366	-963,86	-951	Not defined	-

Table 5: Extracted/calculated parameters for the analyzed fault bound production units along Steinberg Fault.

Sondenkurz	Hydrocarbon	Position	Fault	Stratigraphy	Thickness (m)	Throw (m)	Top Borehole (m)	Highest trap point (m)	Thickness/Throw	Cap_rock thickness (m)
GOE 47	oil	hw	SteinbergFault	11 Sarmatian	-	1168,35	-1093,75	-1034	Not defined	-
GOE 41	oil	hw	SteinbergFault	12 Sarmatian	-	1215,04	-1098,90	-1082	Not defined	-
PLAT S 1	oil & gas	hw	SteinbergFault	8 Sarmatian	-	672,58	-547,45	-539,91	Not defined	-
VS 31	oil	hw	VanSickle	9 Sarmatian	6,31	620,18	-620,34	-492,96	0,010174465	14,65
VS 2	oil	hw	VanSickle	10 Sarmatian	-	623,47	-556,39	-498,75	Not defined	-
VS 30	oil	hw	VanSickle	12 Sarmatian	18,1	808,81	-767,11	-678,4	0,022378556	7,32
DOB 2a	oil	hw	SteinbergFault	18 Badenian	-	1845,04	-1832,69	-1714,38	Not defined	25,73
HO O 1	oil & gas	hw	Steinberg_Abzw.	3 Sarmatian	25,19	147	-811,11	-797	0,171360544	14,91
HO 41	oil & gas	hw	Steinberg	9 Sarmatian	13,37	1405,96	-1298,24	-1276,93	0,009509517	23,78
ERD 23	oil & gas	hw	SteinbergFault	6 Badenian	-	1739,19	-1666,42	-1609	Not defined	-
ERD 4	oil & gas	hw	SteinbergFault	10 Badenian	10,74	2017,85	-1889,55	-1887	0,005322497	26,93
ERD 5	oil & gas	hw	SteinbergFault	12 Badenian	11,66	2074,09	-1953,87	-1942,92	0,005621743	10,33
NS 10a	oil & gas	hw	SteinbergFault	1 Sarmatian	4,96	1018,45	-907,21	-887,53	0,004870146	3,54
ALI 18	oil	hw	SteinbergFault	21 Badenian	-	1658,82	-1572,61	-1527,28	Not defined	-
MUE S 3	gas	hw	SteinbergFault	5 Sarmatian	11,34	575,83	-434,82	-443,91	0,019693312	12,66
MUE S 1	oil & gas	hw	SteinbergFault	14 Badenian	21,67	1341,17	-1215,09	-1207,6	0,016157534	1,57
MUE 71	oil & gas	hw	SteinbergFault	19 Badenian	-	1397,25	-1335,31	-1265,47	Not defined	-
MUE S 2a	oil & gas	hw	SteinbergFault	19 Badenian	12,62	1504,24	-1379,87	-1371,64	0,008389619	3,23
BE S 7	oil	hw	SteinbergFault	24 Badenian	12,82	1599,37	-1499,67	-1467,99	0,008015656	-

As we are working with depth values, these values are shown in the Tables 4 and 5 as negative numbers. In order to determine the stratigraphic units' thickness (Equation 1) and immediately get a positive number, the depth of the top of the stratigraphic unit (Top layer 2) beneath the one containing the hydrocarbons (production unit) was subtracted from the top of the reservoir (Top layer 1).

$$Thickness = Top\ layer\ 1 - Top\ layer\ 2 \quad \textit{Equation 1}$$

Real example

To demonstrate how to calculate a thickness of a reservoir unit, we took the Spontaneous Potential (SP) and Gamma Ray (GR) logs from borehole PIR18 in the Pirawarth area (Figure 23). We can see that the top of the 7th Sarmatian (7ASH shown in purple), corresponding also to the top of our reservoir (sandstone), is located at a depth of around 703m and that the base of the sandstone unit should be around 728m.

The GR curves contains some smaller peaks, indicating an increase in gamma ray response. These peaks are due to a grain size and mineralogical change along the borehole. Two bigger spikes around 718m are interpreted as clay layers interbedded with thin sandstone layer. However, as they do not show substantial thickness, it is unlikely that these clay layers have enough lateral continuation to separate completely the sandstone intervals in depth of 703m-715m and 720m-728m. Therefore, the reservoir thickness for borehole PIR18 was established to be 25m.

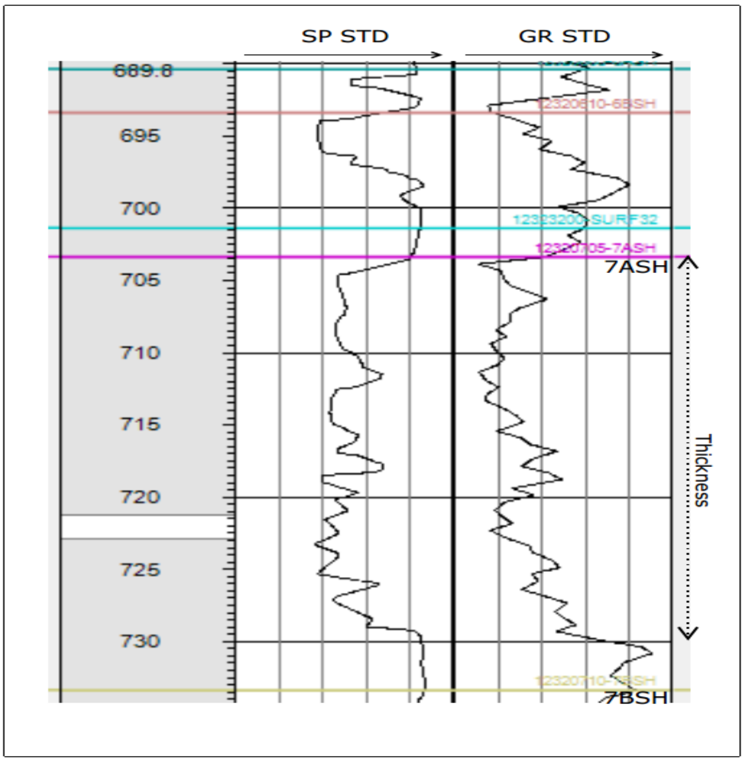

Figure 23: PIR18 thickness for 7th Sarmatian. The figure displays segment of SP and GR log curves.

6.2 Cap Rock Thickness

Cap rock thickness was calculated the same way as the thickness. In this case, however, we subtracted the top of the reservoir from the top of the overlying cap rock (Equation2).

$$\text{Cap Rock T.} = \text{ Bottom of the overlying stratigraphic l.} - \text{ Top reservoir layer}$$ Equation 2

6.3 Ratio: Production Unit Thickness / Cap Rock Thickness

To calculate the ratio, cap rock's thickness was divided through the thickness of the reservoir. As mentioned in the introduction, one of the aims of this thesis is to analyze those production units that are trapped by faults. Under these circumstances, fluids would not be able to migrate across or along the fault, since the fault is sealing, due to the high SGR values along the fault. In this scenario, which was discussed already for the Vienna Basin and recently published (Misch et al., 2022), the fluids have to ascend vertically from layer to layer. A similar process can be seen, in some cases, in seismic profiles (Figure 24) and is known as "chimneys" (Singh et al., 2016). In order for the ascending of fluids to happen, the pressure of the fluid would have to exceed the maximum threshold that the cap rock can support (Yielding et al., 1997). Subsequently, the cap rock will fracture, allowing the fluid to reach shallower layers. For this reason, one way to do this would be compare the cap rocks and reservoir's magnitude.

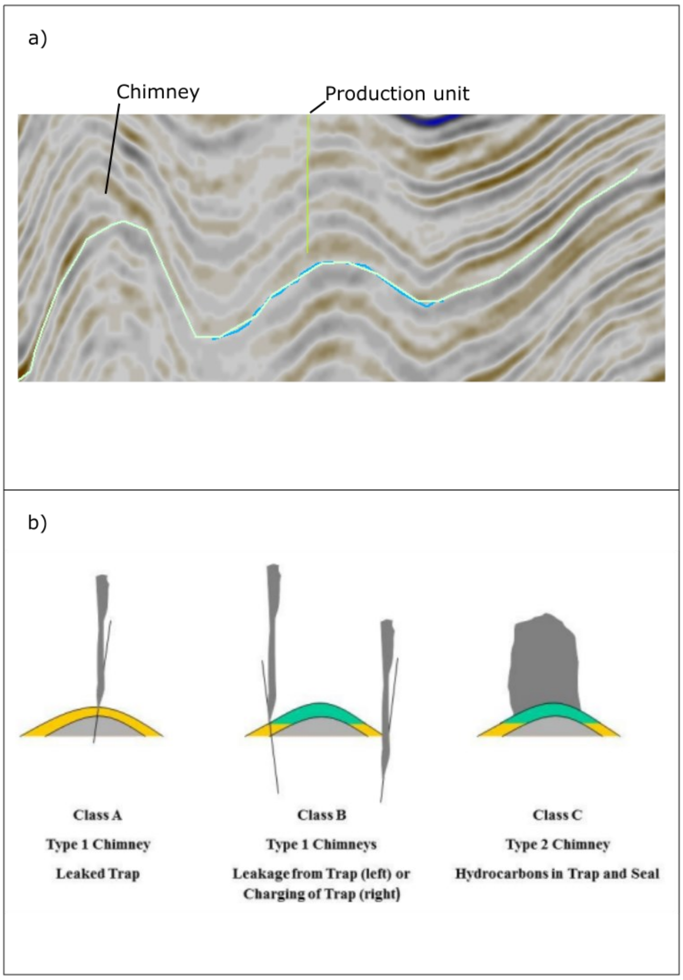

Figure 24: Seismic line showing chimney that might indicate leaking in the production unit.

6.4 Thickness Factor

Due to the fact that the basin's evolution is heterogeneous geographically and in time from sedimentary and structural perspective, stratigraphic thickness may be extremely variable through the entire basin. Some of these thickness variations can be results of numerous factors, which are discussed below:

- Heterogenic basin opening causes that in some areas the sediment input and accumulation had started much sooner than in other areas. Consequently, in these areas older sedimentary rocks would be found.
- One layer could have already been completely or partly eroded.
- Sediment provenience and sedimentation rates are not the same throughout the entire basin (Hölzel et al., 2008).
- Syn-sedimentary faulting also changes the layer thickness magnitude across the fault. Regarding active normal faults, the layers are usually thicker on the hanging wall than on the footwall. For example, the thickness of the sedimentary layers deposited between the Sarmatian and Pannonian along the Steinberg fault are in the order of hundreds of meters in the footwall and is in the order of thousands of meters in the hanging wall (Wessely, 2006). While moving away from the fault on the hanging wall side, layers exhibit syn-sedimentary thinning (Figure 25).

Considering all these aspects, a factor, which would provide us with more consistent thickness' values through the entire basin was added.

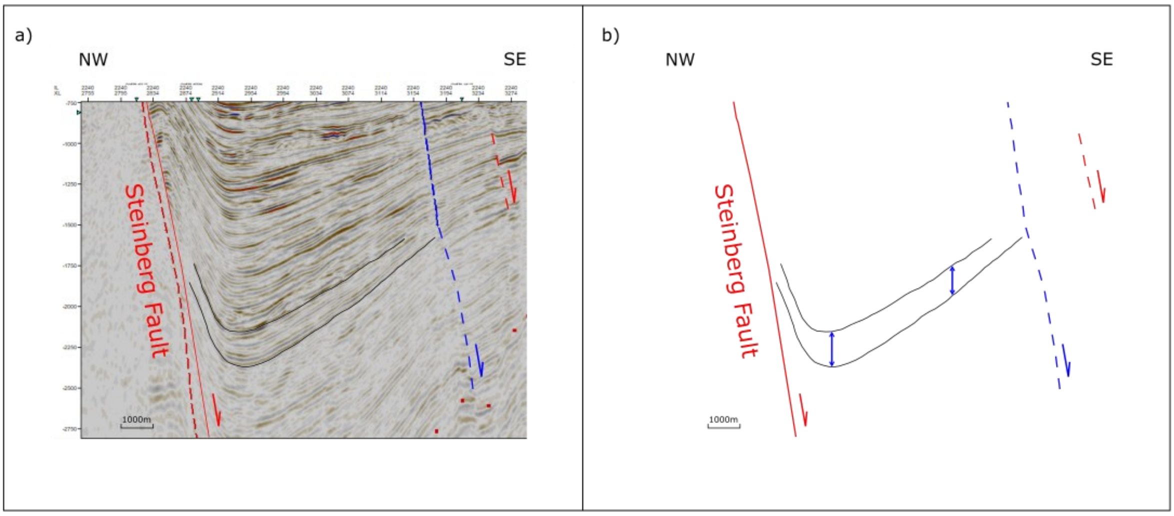

Figure 25: Example of a syn-sedimentary activity of the Steinberg Fault, evidenced by thickenning of the strata toward the fault.

6.4.1 Calculating the factor

The factor was calculated statistically by using boxplots, which is a statistical method to represent data and their range. The construction of boxplots and factor calculation is presented below (Figure 26).

Boxplots:

I. All values are put in ascending order.
II. The median, which divides the values in two equal groups (one half is below the median and the other above it), is established.

a. Number of values is odd: the value which divides the numbers in two equal groups is the median.
b. Number of values is even: the mean value of the numbers in the middle is the median.

III. The "median" (quartiles) for each group is calculated. While Q1 will delimit the line where 25% of all values are below it and 75% above it, Q3 will represent exactly the opposite.

IV. The interquartile range is calculated by Q3-Q1.

V. The minimum and maximum values are calculated by the following equations (Equation 3 and Equation 4):

$$Maximum = Q3 - 1{,}5 * (Q3 - Q1)$$ *Equation 3*

$$Minimum = Q1 - 1{,}5 * (Q3 - Q1)$$ *Equation 4*

VI. The values below the minimum or above the maximum are outliers.

Factor:

a. Firstly, verifying which stratigraphic unit has more input across the Vienna Basin, among the provided data.
b. Secondly, which underlying stratigraphic unit has more input.
c. The stratigraphic unit chosen was the one where the difference was lowest. Just for the probability of having more data for the thickness.
d. Calculating the factor by division (Equation 5).

$$F = Median/Minimum$$ *Equation 5*

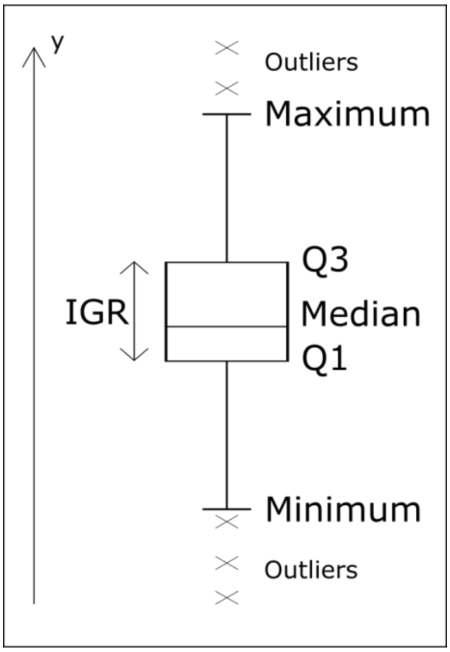

Figure 26: Showing a construction of a boxplot.

6.5 Highest trap point

The term "top of the structure" is avoided in the whole thesis, as this term has ambiguous meaning. For example, when considering a stratigraphic trap (not fault related) in shape of a dome (Figure 21b), the highest point for this structure would be its peak, here presented by a cross. On the other hand, and much more relevant in this thesis, the term would be the highest point where the intersection between the production unit and the fault plane occurs (also marked with a cross) (Figure 21a). This definition makes the reading of the throw values easier when using petrel. To avoid the ambiguity, the term will be substituted by 'highest trap point' (HTP). The HTP will help in cases where there is a dome structure and the fault cuts the structure at another position than its highest point (Figure 21a).

The depth of the reservoir in the borehole data do not necessarily represent the highest point of the trap (Figure 21a). Therefore, the highest trap point was determined by mapping the seismic reflector corresponding to the borehole's depth in Petrel. Exactly this situation can be seen in Figure 21a, where hydrocarbons are extracted by the borehole (violet point) from the reservoir presented by the brown layer. On the profiles 1-3 in Figure 21a is shown that despite the fact that the borehole produces oil or gas, it is not happening at the highest trap point. It can also be seen from the profiles that it would be at the cross at the map along profile 2. Consequently, the depth in which the top of the brown layer strikes the fault in profile 2 (Figure 21a) was inserted to Tables 4 and 5 under the 'Highest trap point'. The process, along with the real example on how it was calculated is presented in section 6.6. Another function for mapping the reflector is to get the structure of the production unit. Two of these structures, as real examples, are shown in Figure 27.

6.6 Throw

As shown in section 3.4, many quantitative parameters have already been developed to predict if a fault is capable of impeding flow.

The magnitude of the fault vertical displacement (throw) is going to be a key parameter, as it enables to predict if the layer containing hydrocarbons is in juxtaposition to its counterpart across the fault (Figure 22). In other words, depending on the thickness of a layer, the throw will also need a minimal threshold value to avoid juxtaposition to its counterpart at the other fault's side. Three situations are presented in Figure 22 and are outlined below.

The first shows a situation, in which the throw is less than the thickness of the layer (Figure 22a). The layer still is in juxtaposition, which will allow fault crossing flow. This will be immediately from hanging wall to footwall, but in the opposite direction it will depend on the OWC.

The second scenario, in which the throw is about the same as the thickness of the layer is shown in Figure 22b. In this case, the fault separating hanging wall and footwall could have a high enough SGR to impede flow (Yielding et al., 1997). However, it is common for faulted layers to have some deformation or small vertical extension (Figure 22b) closer to the fault (Hölzel et al., 2008; Spahić et al., 2013). Like in the first case, they could also be in juxtaposition.

The last scenario is presented in Figure 22c and comprehends situations where the throw is much larger than the layer thickness. In these cases, specially, there should not be flow between hanging wall and footwall. It is believed, due to high throw values within the Vienna Basin, and therefore also high SGR values, that many of the faults in the basin impede flow. Consequently, if oil, gas or both are found on both sides, hanging wall and footwall, this would mean that the fields have different OWC/GWC. Therefore, they could be ordered to two distinct production units.

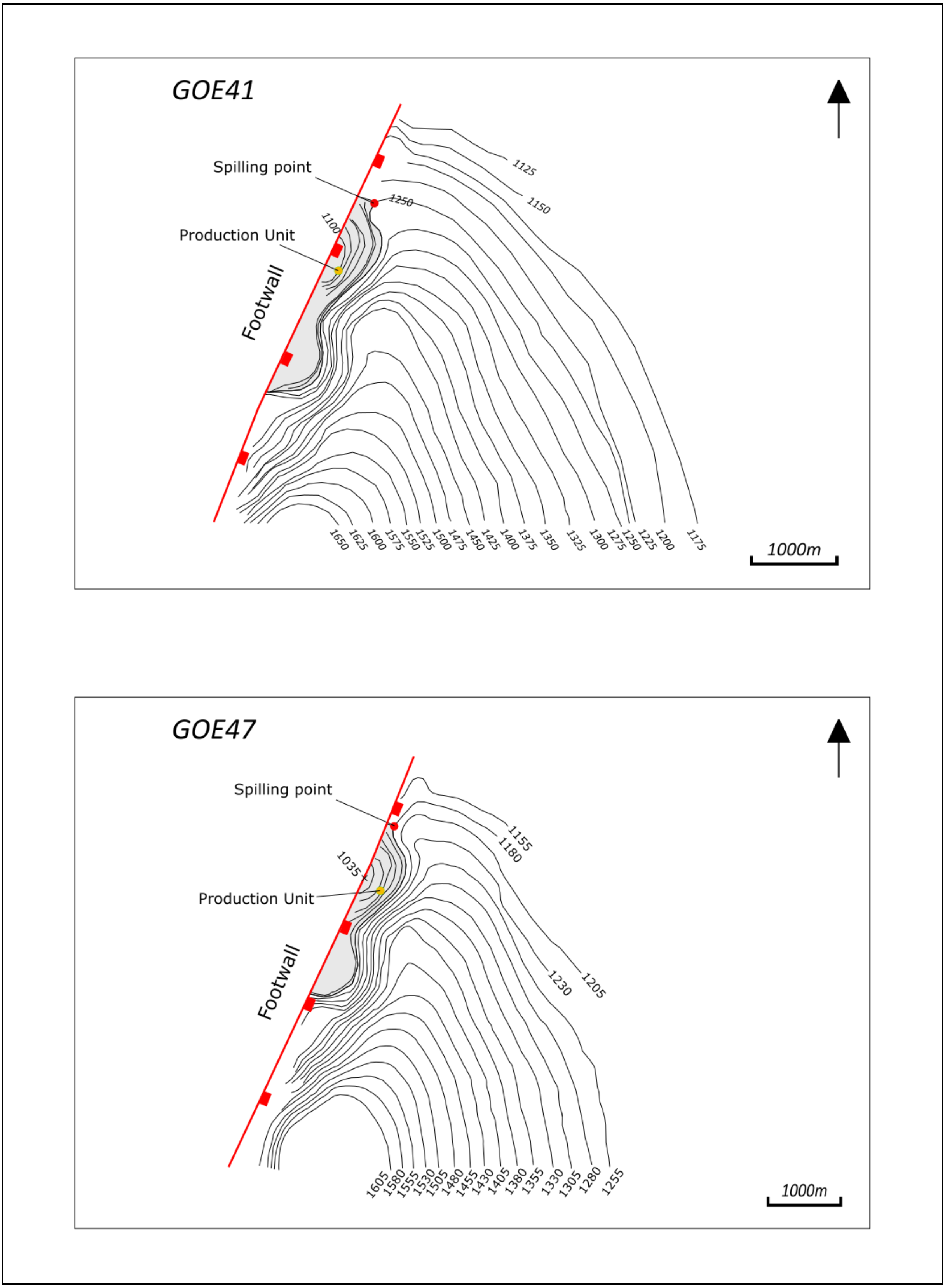

Figure 27: Examples of real geometry of 2 production units. Grey shaded area is the production unit.

To avoid any misunderstanding, juxtaposition, in order to occur, does not necessarily need to be with the same layer (all situations presented in Figure 22 with the brown layer). Juxtaposition can also happen, as shown in Figure 15 when one reservoir (P2 in brown in hanging wall) is next to another stratigraphic unit (P1 in yellow) which could also act as a reservoir. This is where the parameters discussed in section 3.4 come in.

The complete workflow how to calculate the throw value is shown on the example in Figure 21a is presented below:

i. Identify the deepest borehole for the production unit (violet borehole), which is in this case at the hanging wall.
ii. Creating a composite line (orthogonal to the faults strike direction), which acts as profile and includes the borehole (profile 1).
iii. Scrolling this composite line through the seismic cube, until the **highest trap point** has been achieved (profile 2).

The next few steps refer to Figure 28a while the last step to Figure 28b:

iv. Saving this profile, so we can refer to it at the other side of the fault afterwards (expanding profile 2 across the footwall).
v. Look for a borehole on the footwall that contains depth information for the same stratigraphic unit containing the hydrocarbons (green point).
vi. Once the layers' depth is known, create an auxiliary profile (help profile).
vii. Correlate the reflector (top of brown layer) along the auxiliary profile until the intersection point with profile 2 is reached (orange point in help profile).
viii. Correlate the reflector containing the orange point on profile 2 up to the fault.
ix. Calculate the depth's difference of the top of the brown layer at the fault on the footwall and the hanging wall.

Real example

Applying the same process for a real case in the Vienna Basin, only the workflow and concluding image of the whole process is going to be presented here. The other images showing all stages of the process are going to be shown in the Appendix A.

The borehole used for this purpose is borehole HL5 from Hochleiten and is represented as the pink point on Figure 29.

- The next step would be to construct a cross section containing the borehole and at the same time cutting the fault (green surface) orthogonally (parallel to profile 1, yellow line).
- Secondly, we had to run this NW-SE cross section to NE and SW in order to determine the highest trap point for the production unit. In this case, the yellow line represented by profile 1.
- We found one borehole containing the 10th Sarmatian on the footwall (HL50, red point) and followed the reflector corresponding to this stratigraphic unit to another borehole (HL74, yellow point) and traced a line connecting between the two boreholes (profile 2).
- Now it is time for us to bring the drawn stratigraphic unit along profile 2 to the profile in which we are going to measure the throw (profile 1). For this we again followed the reflector along profile 3.
- After following on profile 3 we automatically have the point where our stratigraphic unit cuts profile 1 and drawing it all the way to the fault on the footwall.
- Back to profile 1, we now have mapped at the hanging wall our production unit and on the footwall the equivalent stratigraphic unit.
- The last step is to calculate the vertical offset (throw) along profile 1 (Figure 30).

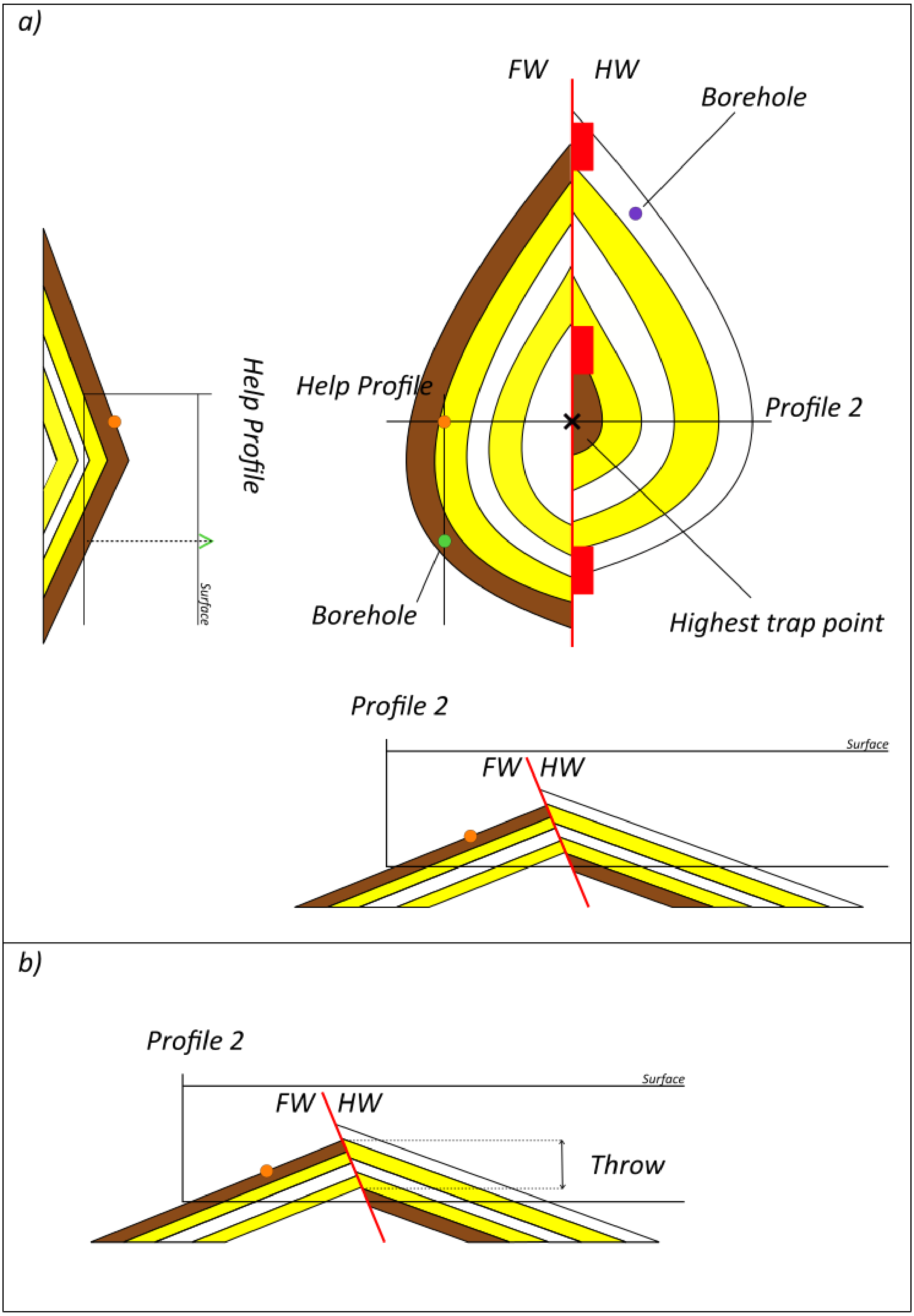

Figure 28: Schematic method to calculate throw.

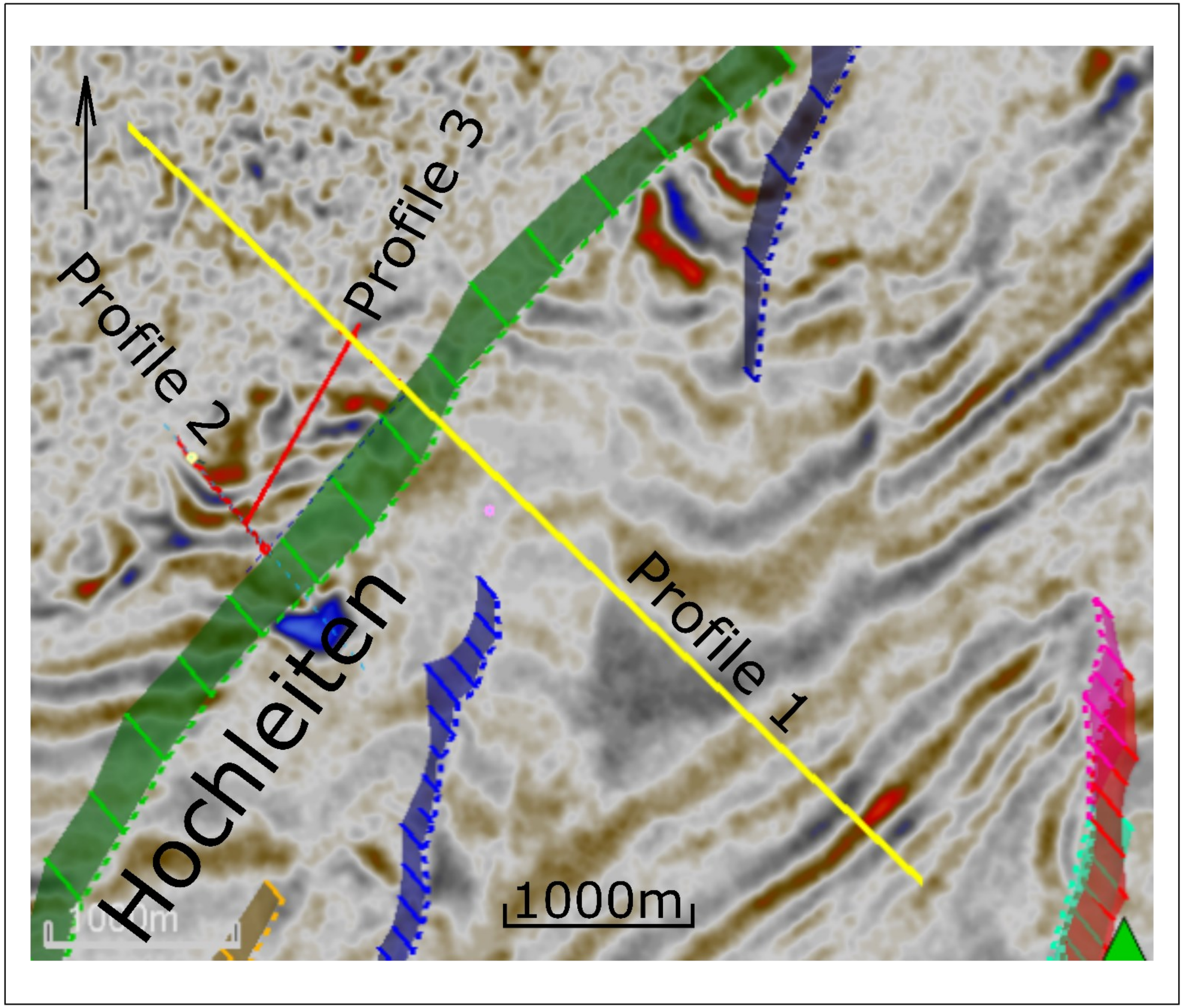

Figure 29: Constructing profiles in order to achieve real throw.

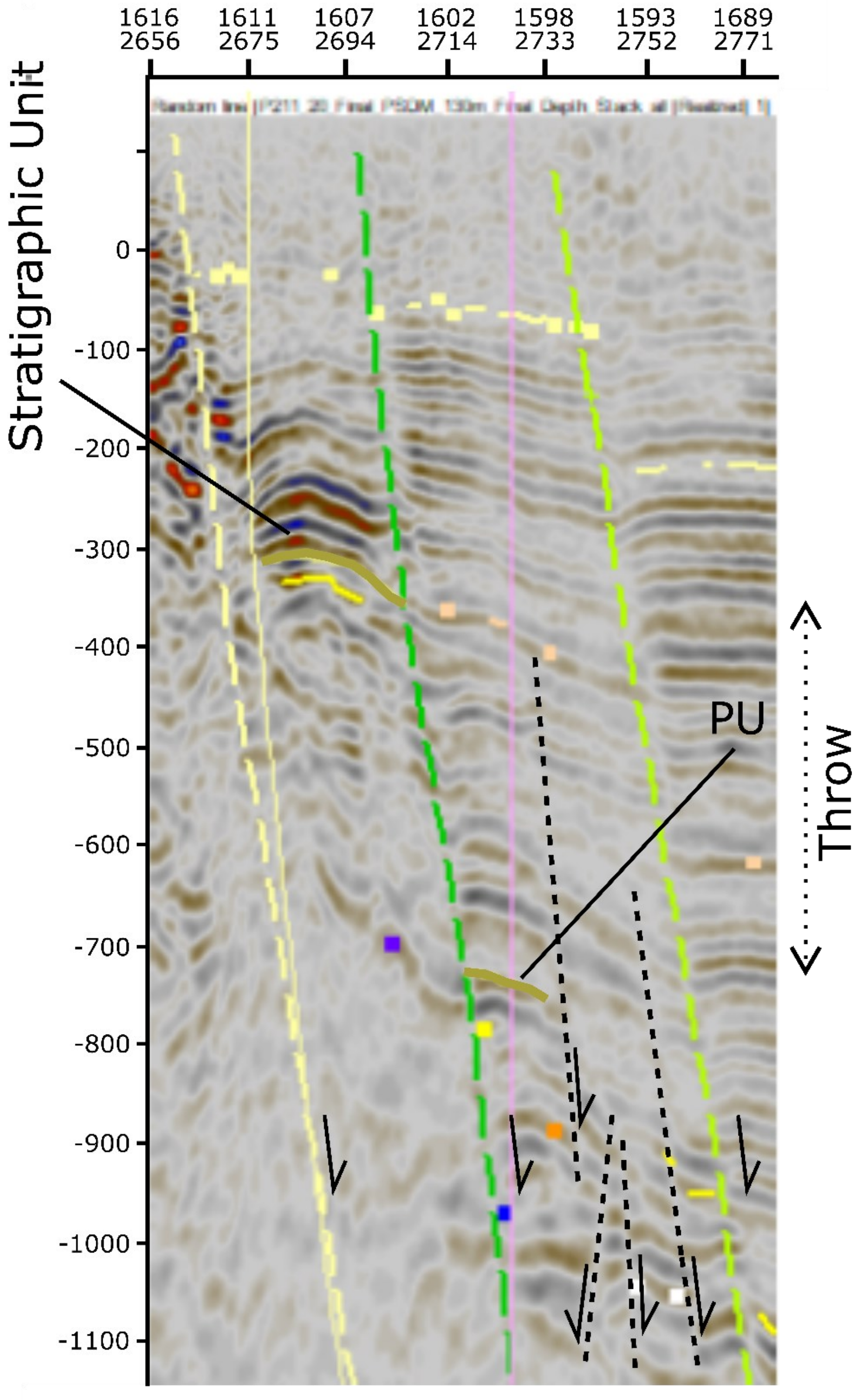

Figure 30: Calculating throw from profile 1. For location see Figure 29. Dotted black lines represent newly interpreted faults, which can be responsible for upward migration to the production unit (PU). Image without interpretation can be seen in appendix.

6.7 Helpdrill

The column was either added to determine the depth top borehole of the stratigraphic unit containing the production unit in case this information was missing in the deepest reaching borehole or to aid determining the throw. The throw for each production unit was calculated by the depth difference between the highest trap point of the reservoir (profile 2 in Figure 28) on the fault and the same stratigraphic unit at the other side of the fault. The column "Helpdrill" enabled to find the same unit on both sides of a fault. The latter procedure was only possible in the case, where the stratigraphic information was provided and also if there are boreholes on both sides of a fault.

6.8 Position

Under "Position" it is stated whether the hydrocarbon occurrence is in the hanging wall or footwall. It might seem easy to determine in which of the blocks it is located, however, when there are many parallel faults (or similar orientation) it might get more difficult. To illustrate this, we are going to have a look on Figure 31.

The easiest case is represented in Figure 31a-b. All production units east of the purple fault that have their structure being closed by the purple fault are going to be on the hanging wall, even when considering the red fault that is located further away. The same applies for the production units west of the red fault. In this case, however, the production units are going to be at the footwall.

The other cases (Figure 31c-h) are going to be more complex since the production unit is located between two parallel faults. In these cases, we will have to look where the structure goes to. In Figure 31c-d the structure goes to the red fault, therefore, the production unit is located on the hanging wall.

Similar happens in Figure 31e-f, however, here the structure goes to the purple fault. Therefore, the production unit is located on the footwall of the purple fault.

The more complicated case would be when we have two production units located between the two faults (Figure 31g-h). The production unit on the west, which has its structure going west to the red fault will be positioned on the hanging wall. The other production unit more to the east is going to be similarly located on the footwall of the purple fault.

6.9 Fault related Preview

The "Fault Related Preview" in Table 2 only considers if there is a fault in which the targeted sediment layer is intersected by a fault, without taking into consideration the vertical throw along the fault or the layer thickness.

6.10 Fault related calculations

To determine if production unit is fault related or not, we systematically addressed the three questions below.

i. Is there a fault?
ii. Does the structure reach until the fault?
iii. Is the throw larger than minimum thickness of the layer?

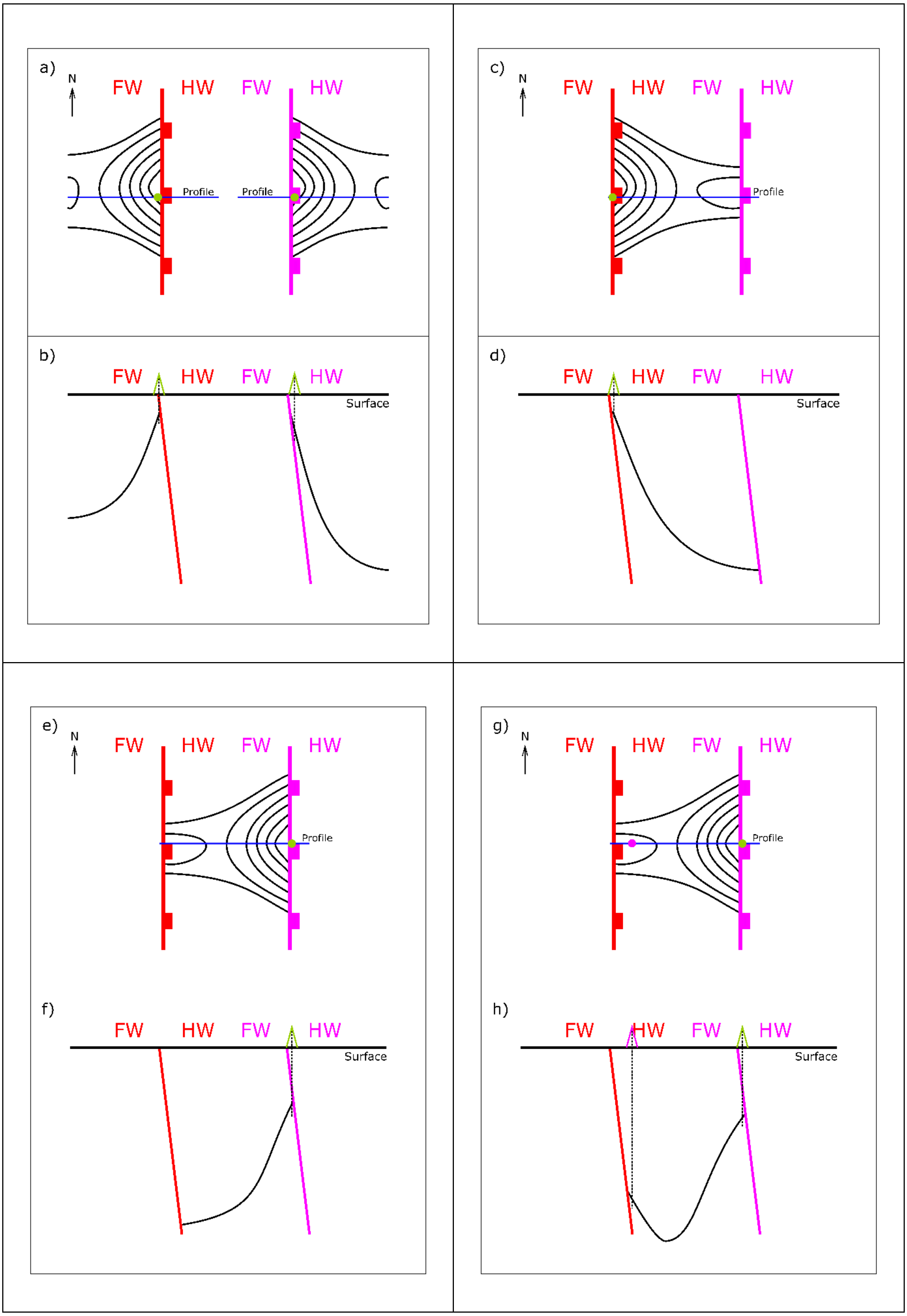

Figure 31: Location of Production unit.

6.11 Diagrams

The first goal was to analyze, which production units (PUs) that were producing in 2020, are fault related. The original data provided by OMV consisted of 270 production units. As mentioned before, some of them had to be removed for particular reasons and these are stated below.

- Some traps had not been drilled by the start of the thesis (3 PUs were removed).
- The depth value for the stratigraphic unit was not found in any table and could not be interpreted from the seismic through a nearby borehole (43 PUs).
- The production units within the Matzen Field were interpreted as not fault related (117 PUs). There are faults in the Matzen Field, however, the present throws are so small that layer would still be in self-juxtaposition or small SGR values allowing migration. It is interpreted that the Matzen Field is a big dome with only small faults cutting through.
- Not having the OWC values, either due to incomplete borehole information or due to the absence of boreholes on both sides, was the reason to put OWC depth values aside (after analysis) and not to use them in this study. Instead, it was decided to determine which production units are fault related by comparing parameters that were extracted from seismic and borehole data.

Once these production units have been removed, 106 production units remained. In the end, 40 production units (42 input values since two production units appear at the footwall of one fault and at the hanging wall of another fault - Figure 31) are interpreted as fault related production units. Importantly, throw and depth to the production unit could be determined in these boreholes. The position of the production units used in the study are shown in Figure 32. In Figure 32, for the cases where the production units are geographically very close position to each other or even overlapping, bigger circles were drawn and the number of production units in that region is also present. The faults represented in Figure 32 are only schematically shown in order to make a more punctual analysis of some of the segments of the fault. More detailed map showing connectivity and continuity of the faults in the Vienna Basin is shown in Figure 33.

Some other boreholes are fault related, but due to absence of a borehole on the other side of a fault or due to absent stratigraphic interpretation along the borehole it was not possible to determine the throw (these cases will be discussed later). Throw values derived only from seismic interpretation was left out, because they were often contradicting borehole data (Figure 34).

For example, the production unit shown in Figure 34a, occurs in the 11th Sarmatian, at the depth of 1397 m (TVDss) according to the well top data. Therefore, it would be expected that the 8th Sarmatian had to be above (in a shallower depth). However, as it is shown the interpreted seismic horizon 8th Sarmatian lies deeper than the 11th Sarmatian derived from well data. Similarly, the production unit in Figure 34b occurs, based on the well top data, in the 20th Sarmatian at 1704m depth (TVDss). Interpreted seismic horizon 8th Sarmatian corresponds actually to the 20th Sarmatian derived well top data. These two examples clearly demonstrate the issue of using purely seismic data to determine the throw. Consequently, in Figure 34a, the throw value would change around 300m and in Figure 34b around 600m.

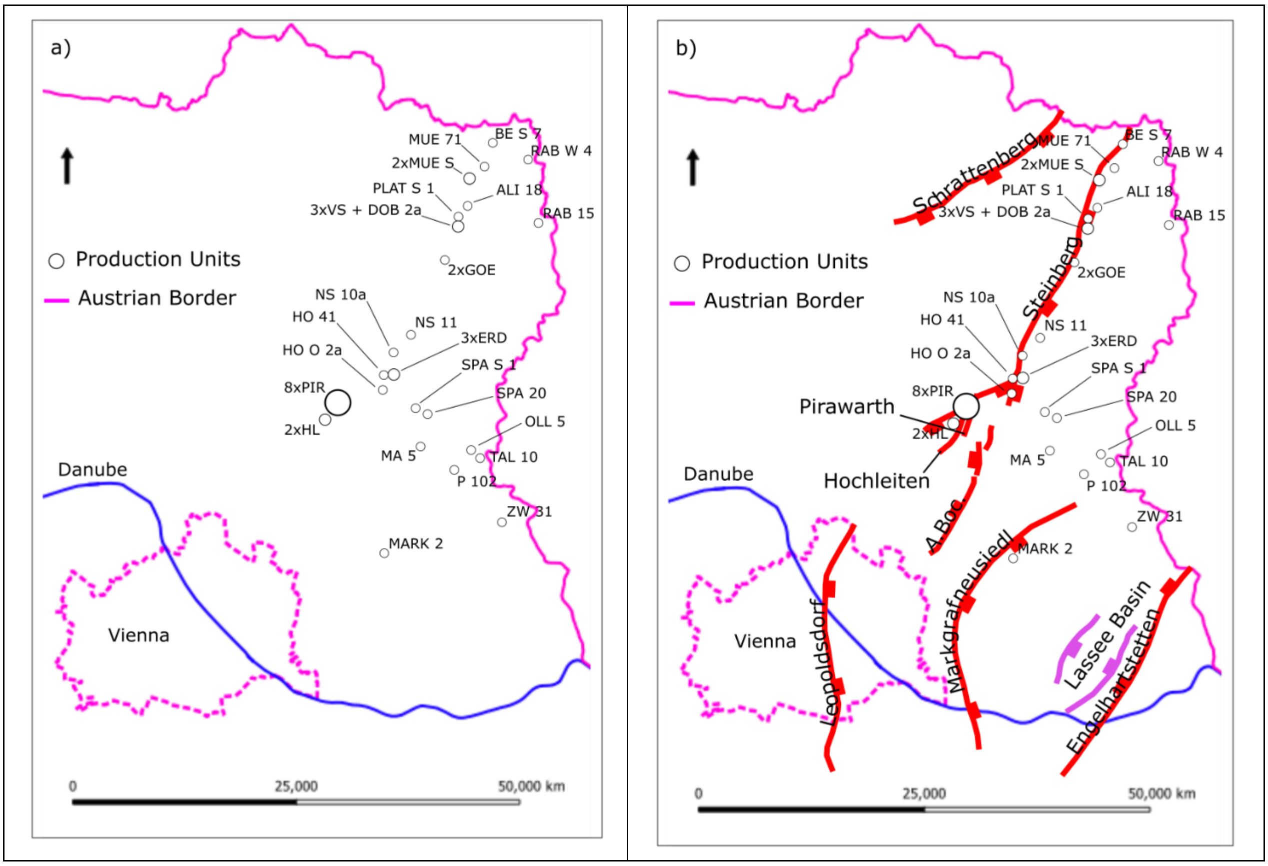

Figure 32: a) Production Units within the Vienna Basin at the locations that have documented throw and depth values, b) with added regional faults. The coordinates are not shown due to sensitivity of the data.

In case of the Steinberg Fault, we cannot determine the throw of the production units (19 production units), due to the fact that the production unit's stratigraphic layer present in the hanging wall is absent (already eroded or not deposited) at the footwall (Figure 35).The colored lines (i-pink, ii-blue, iii-green) in Figure 35 are some projections of how the horizon could behave in the already eroded footwall and there is no way to determine which of the coloured lines represent the continuation of the horizon. Therefore, in these cases, we determined the throw by only considering the depth below sea surface (TVDSS) and adding the borehole's elevation above the sea surface (Figure 35). It has to be emphasized, by doing this, that we only have part of the original throw since the counterpart of the stratigraphic horizon in the footwall would be above the current surface and is mostly eroded (Figure 35). Due to the missing stratigraphy in the footwall, with some exceptions, we come to the situation when plotting throw against depth (for the production units against Steinberg) that almost all points occur on one linear regression close to -1 (Figure 36-40). As previously explained, using these values (minimal throw) will lead us to misinterpretation. For this reason, it was plotted separately. Despite that, we will not be using them at the throw against depth plot (Figure 41-45), however, they will still be accounted for when determining where more production units occur (Figure 46).

Most of the production units that are not related to the Steinberg fault but to another fault within the Vienna Basin, have much smaller throw values (Figure 41-45). The throw values range from 0 to 400m and that they appear much shallower (600 to 1000m depth) than the production units at the Steinberg fault (Figure 36-40). Secondly, it is shown that the correlation number between throw and depth is farther away (-0.57) from -1 than the Steinberg fault values. This value points to the situation where a linear regression is not completely guaranteed.

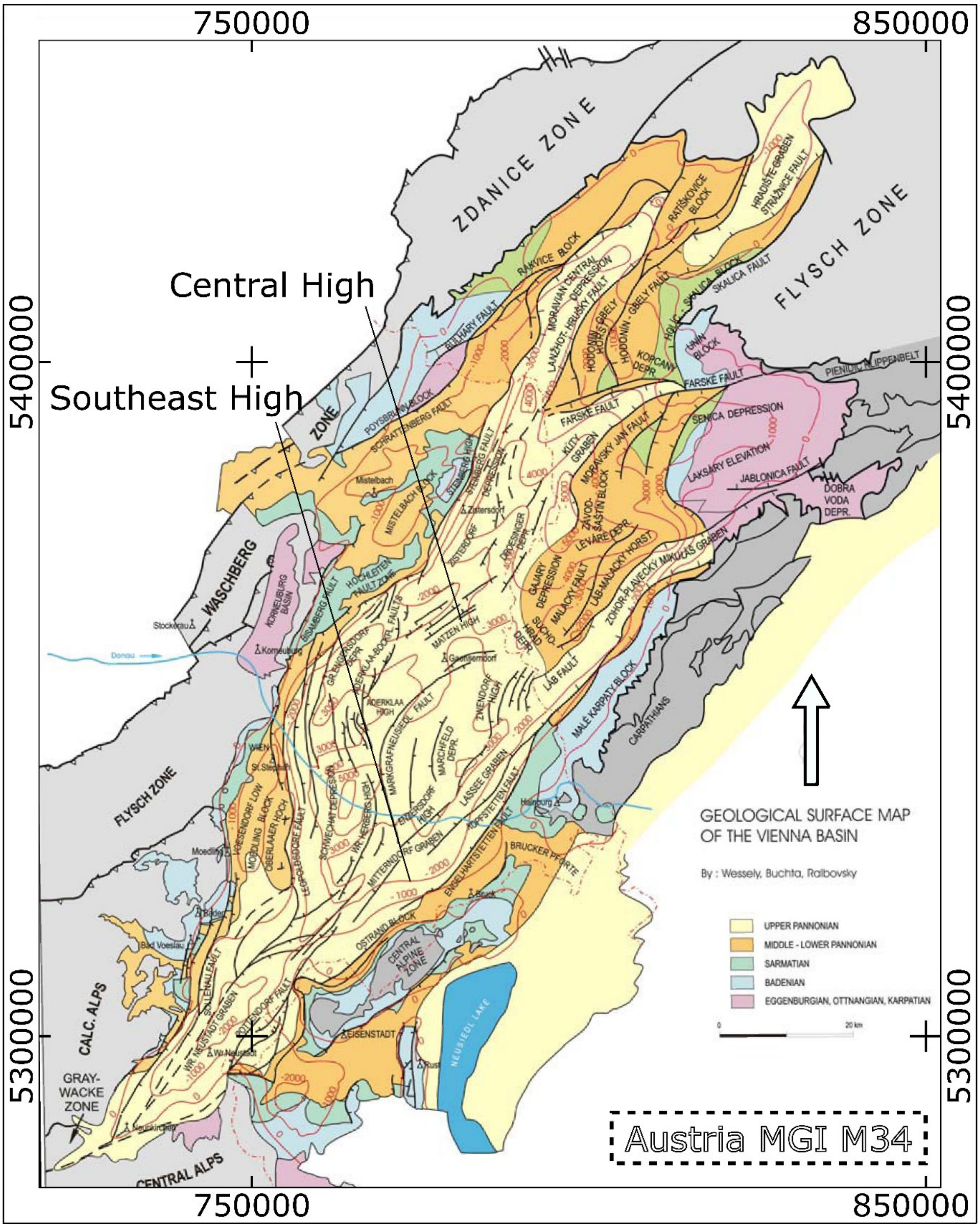

Figure 33: Map from Harzhauser and Piller (2005) showing continuity of faults and connectivity between different faults with interpreted stratigraphic units of the Neogene in the Vienna Basin. Central High and Southeast High (mentioned in Rupprecht et al., 2019) are also shown.

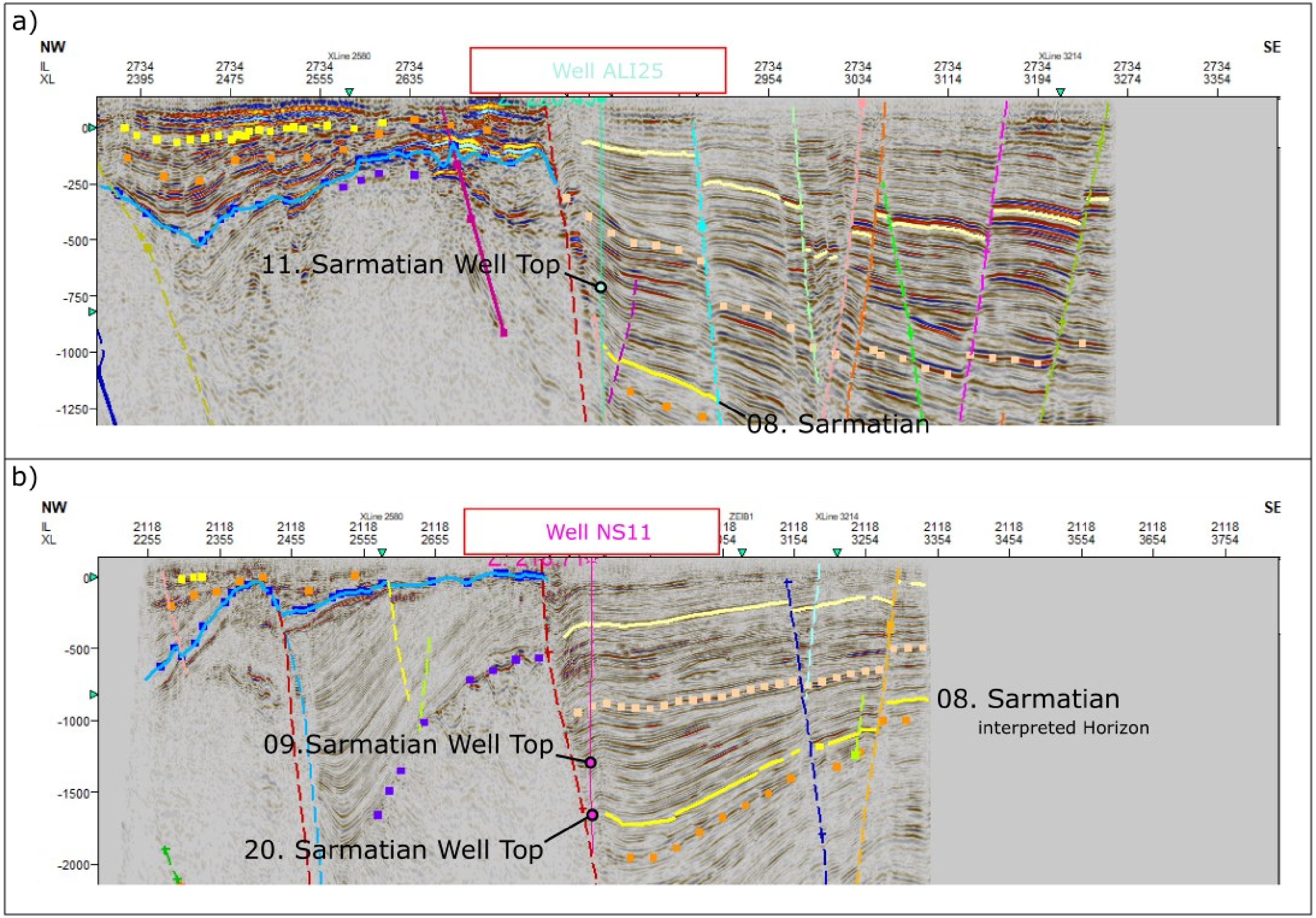

Figure 34: Examples of problem regarding matching interpreted seismic horizons with well tops. a) Pu in 11th Sarmatian, but 8th Sarmatian seismic horizon is interpreted deeper than 11th Sarmatian. b) Pu in 20th Sarmatian in well NS11 corresponds to 8th Sarmatian interpreted on seismic data.

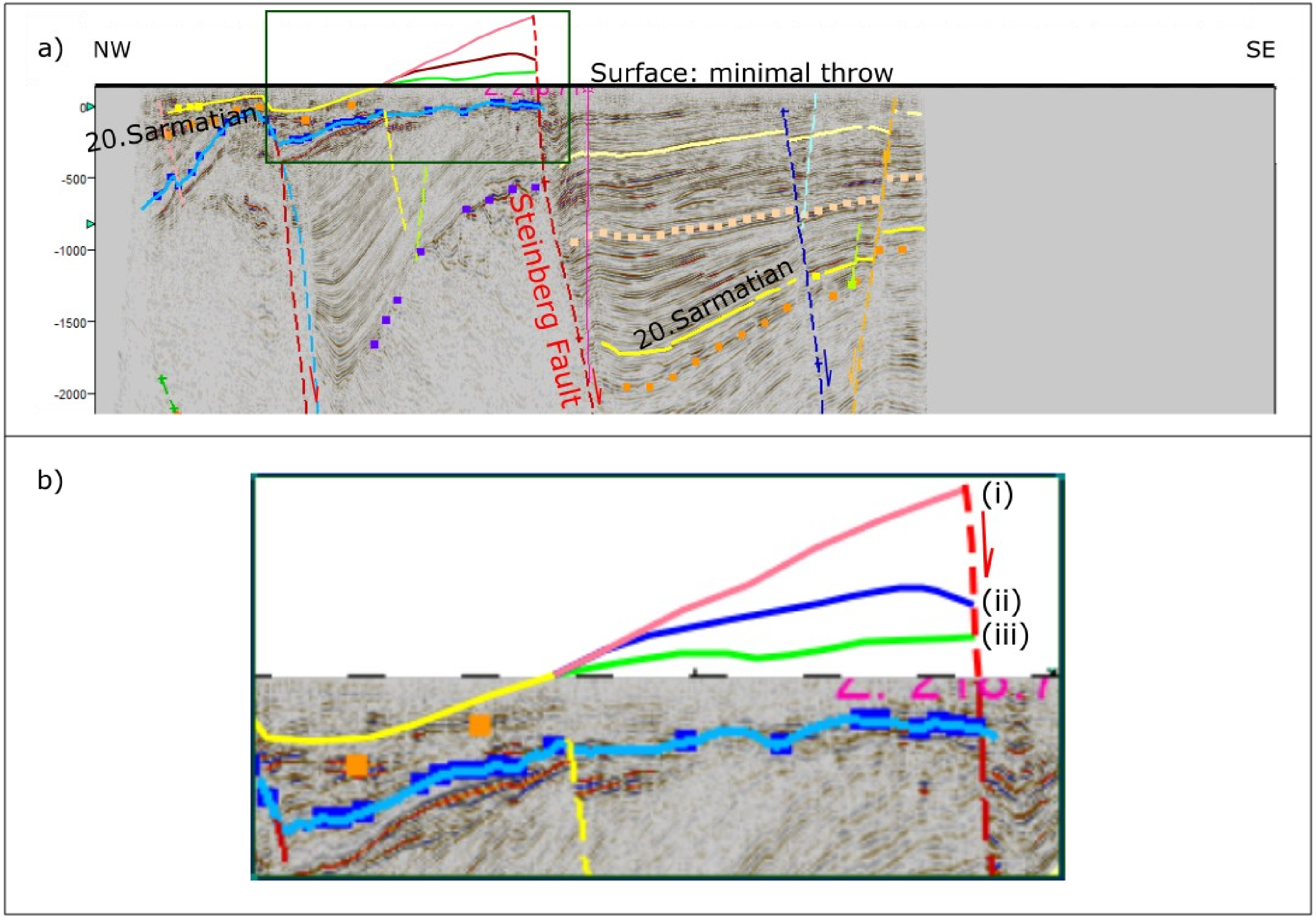

Figure 35: Projection of well top of the 20th. Sarmatian (see Figure 34) to the Steinberg Fault on the already eroded part of the footwall.

We can also conclude from Figure 41-42 that almost all production units that appear at the footwall, violet points, happen to be in the area represented by the red square (except for RAB15). The production units within this square show throw values with a maximum around 100m. Two of the production units, within this red square, happen to be on the hanging wall, PIR48 and PIR60, and are at the same stratigraphic unit (05 and 07 Sarmatian) of two production unit from the footwall, PIR17 and PIR18 respectively (Table 6).

From the analyzed production units, those at the Steinberg Fault are well distributed between the Sarmatian and Badenian packages having the depth of around 1200m and 1400m as threshold (Figure 40). The production units that are related to faults other than the Steinberg Fault, are located mostly in the Sarmatian package with only two exceptions. One of the production units is located in the Badenian and the other in the Karpatian package (Figure 45).

Table 6: Production units with a counterpart at the same stratigraphic on the other side of the fault

Hanging wall	Footwall	Stratigraphic Unit
PIR48	PIR17	05 Sarmatian
PIR60	PIR18	07 Sarmatian

At the production units that reach to faults other than Steinberg fault (Figure 41-42), a slight predomination of production units in the hanging wall is observed. However, after adding production units located along the Steinberg fault (Figure 36-40), the results tend to reinforce the idea that for the Vienna Basin more production units occur in the hanging wall (Figure 46). In numbers, from the 42 production units classified as fault related, 33 are in the hanging wall (78.5%) and only 9 are located in the footwall (21.5%).

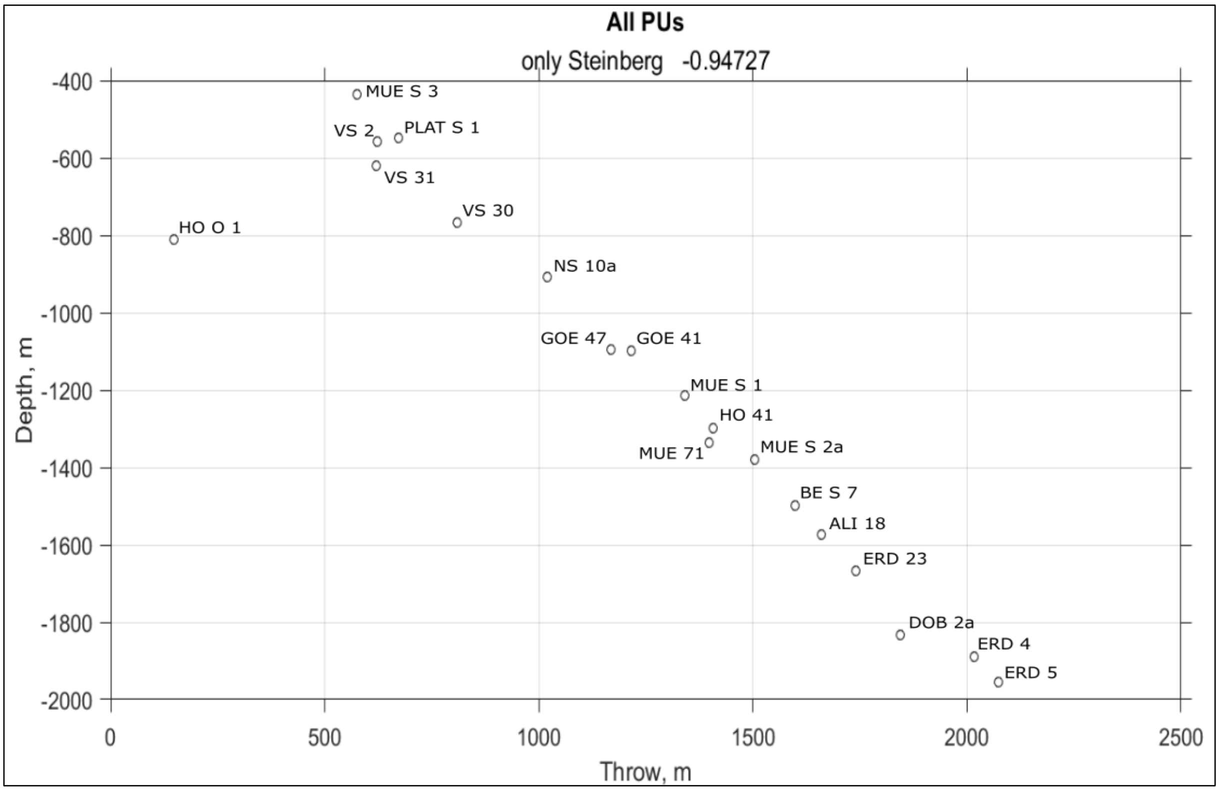

Figure 36: Fault throw plotted against depth for PUs against Steinberg fault.

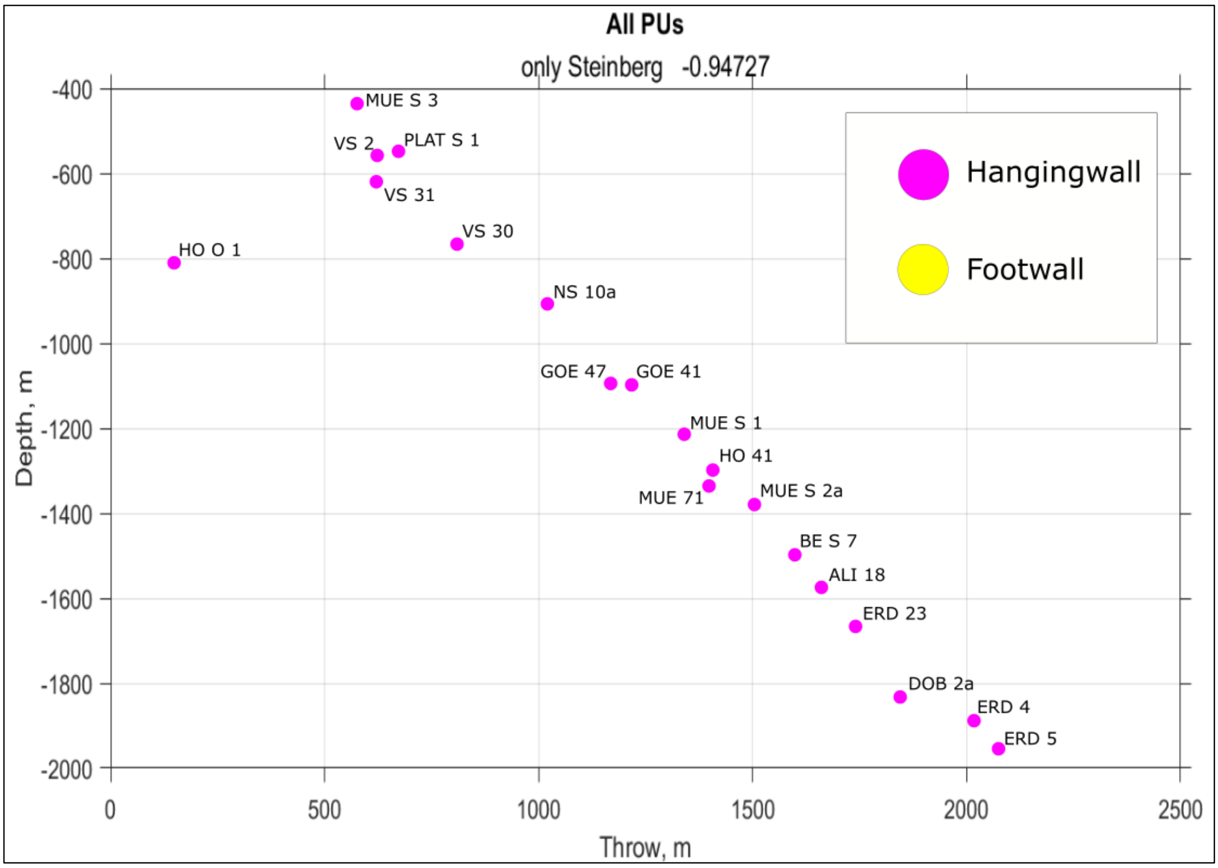

Figure 37: Production Units distribution along the Steinberg Fault.

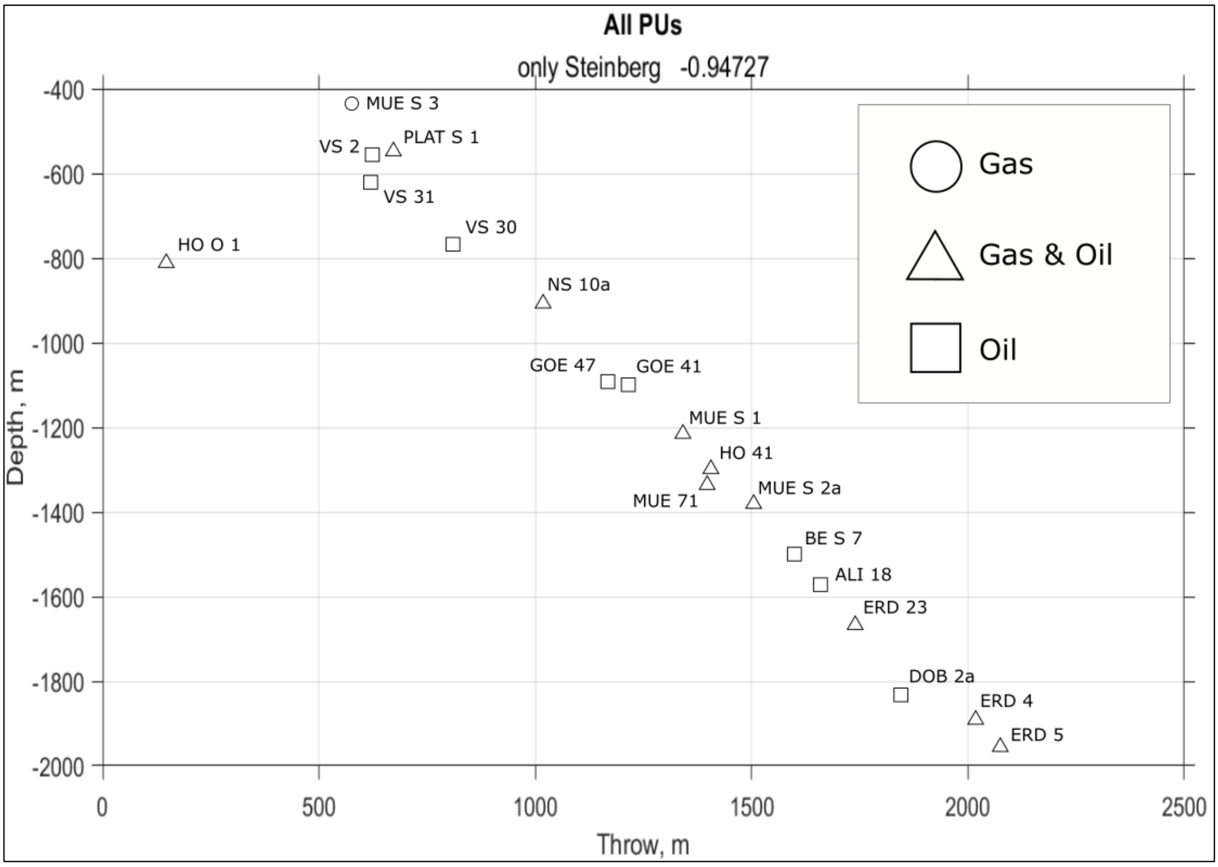

Figure 38: Hydrocarbon for each Production Unit along Steinberg Fault.

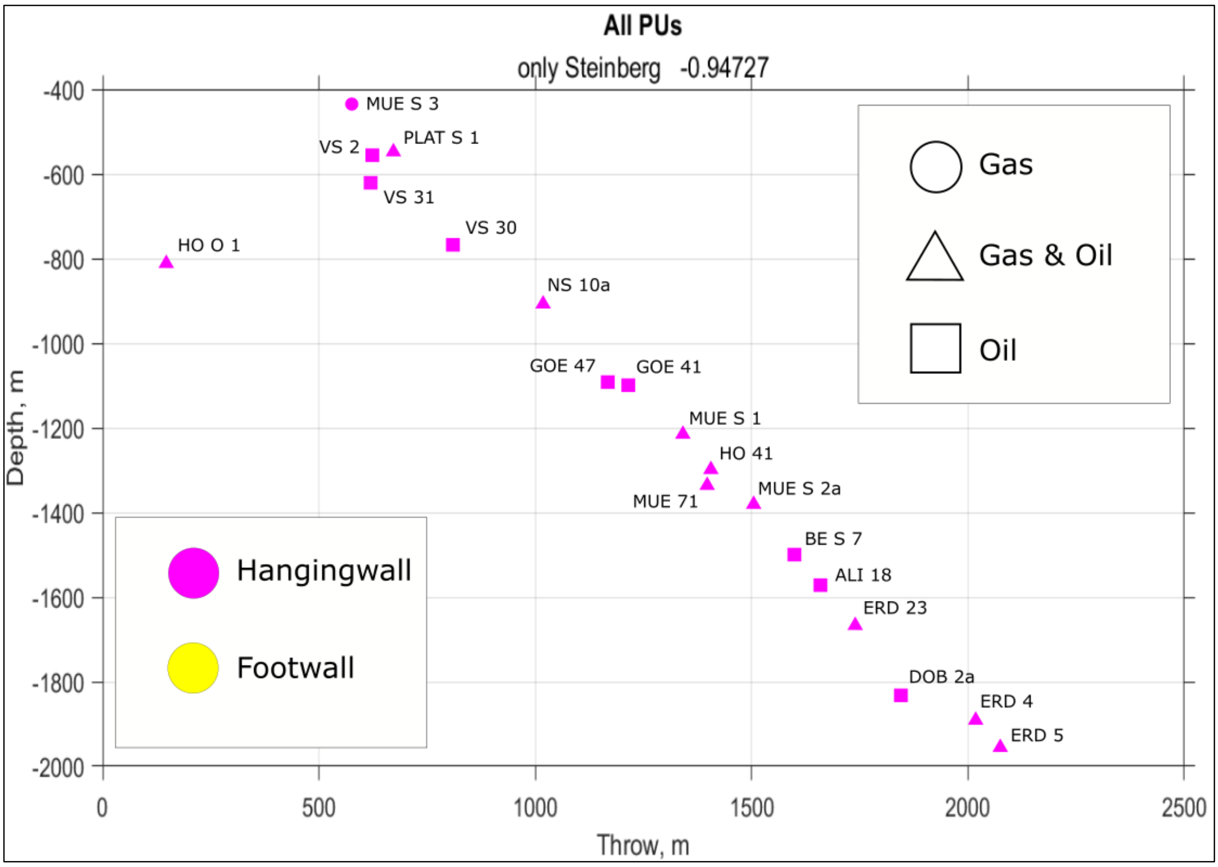

Figure 39: Hydrocarbon distribution along Steinberg Fault considering its position.

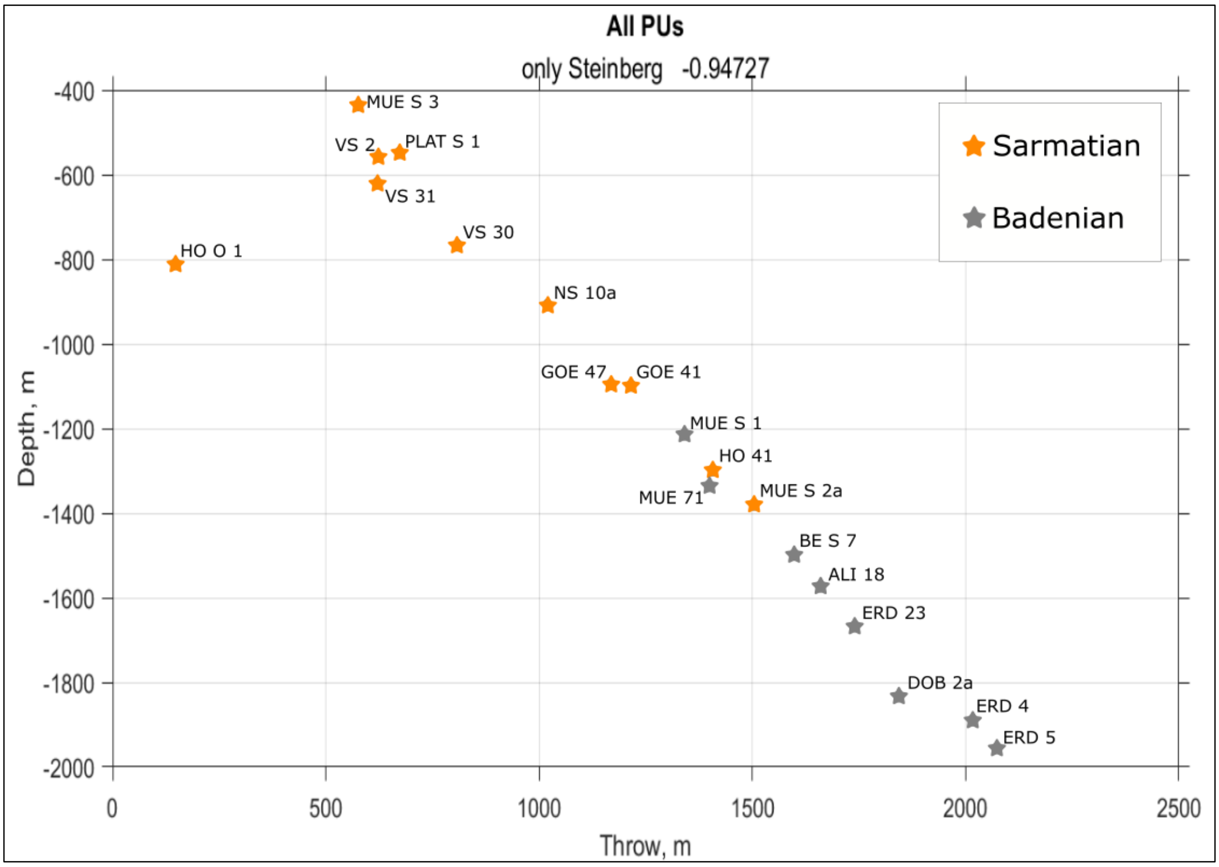

Figure 40: Stratigraphy of the Production along the Steinberg Fault.

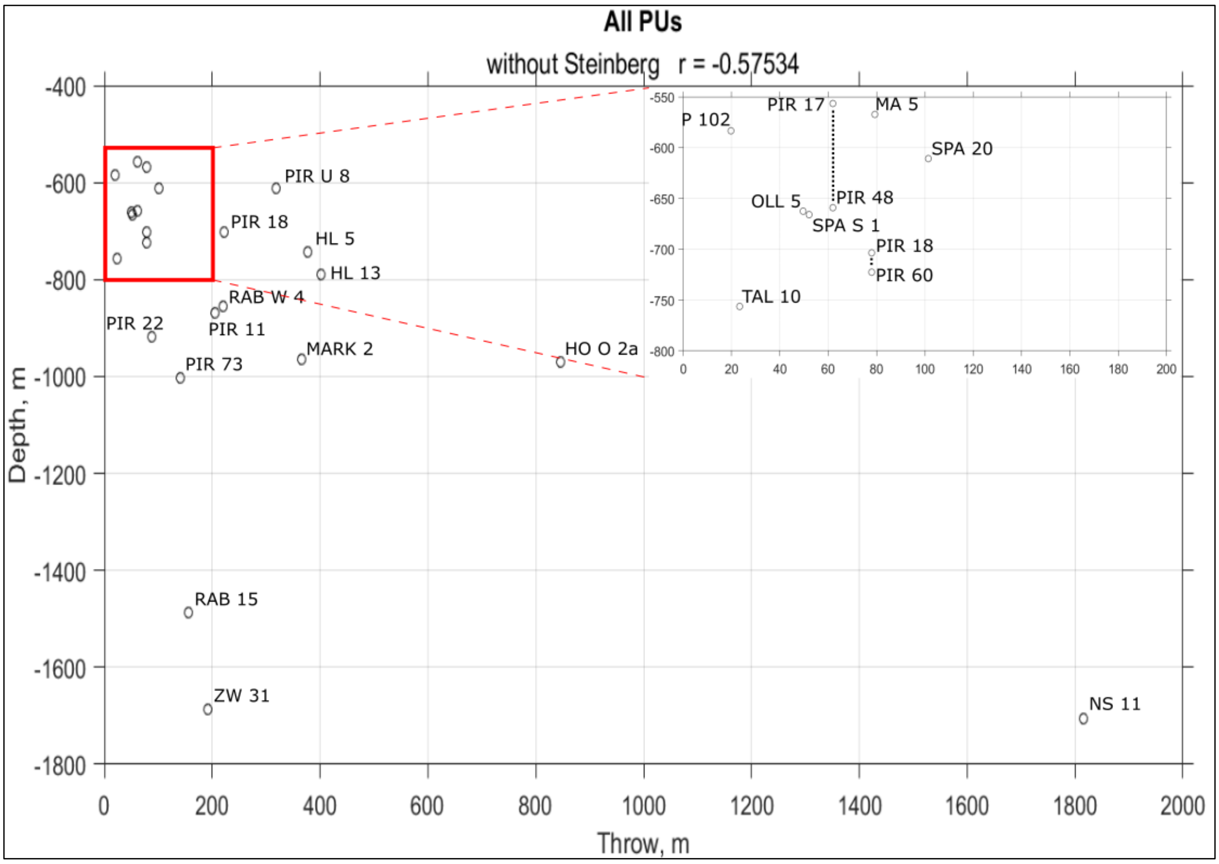

Figure 41: Production units without Steinberg.

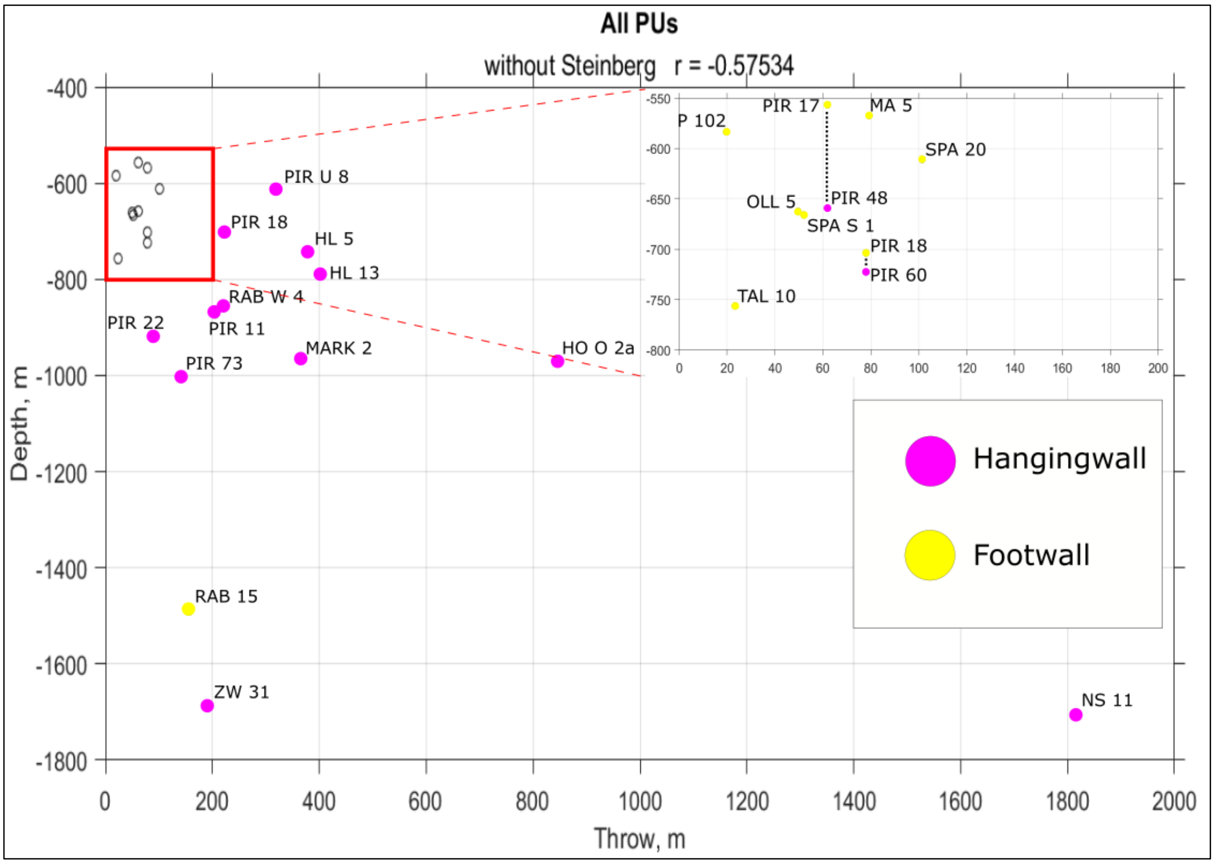

Figure 42: Production Units position relative to the fault.

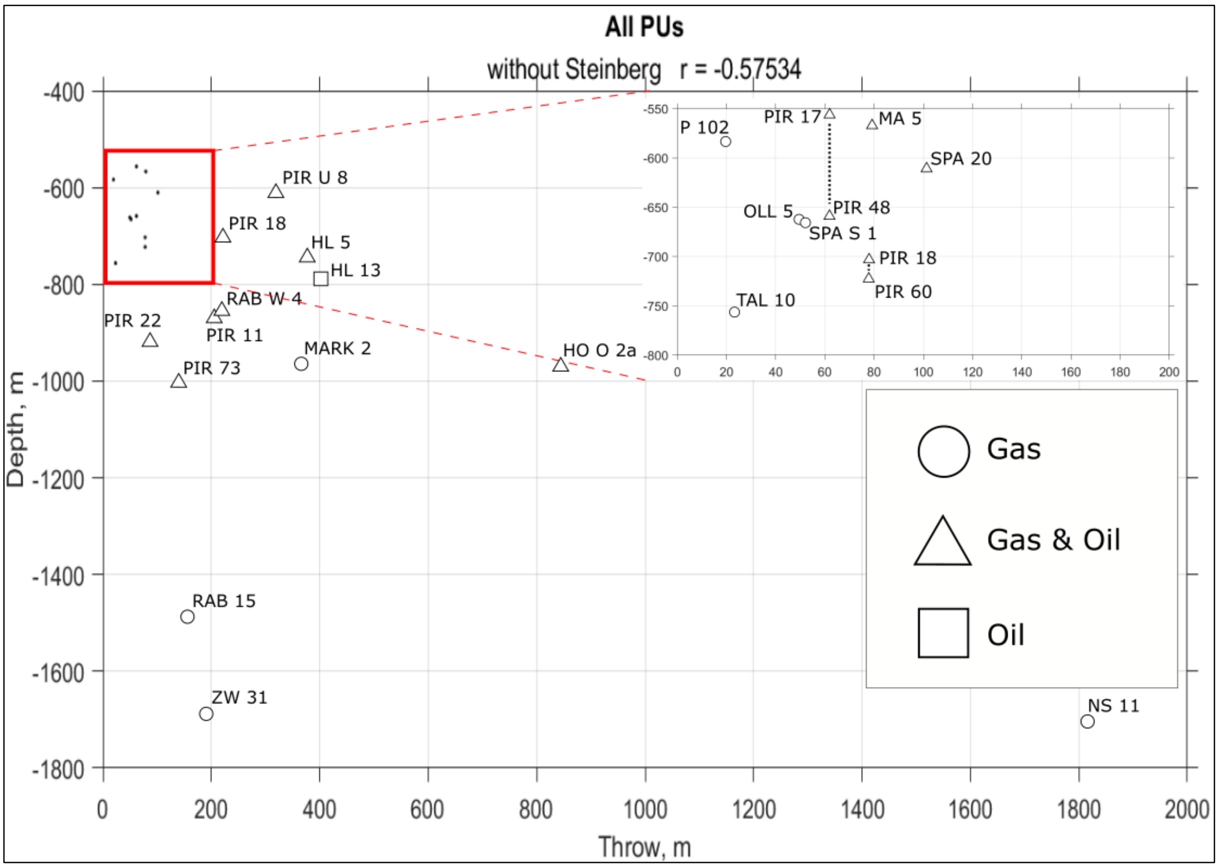

Figure 43: Hydrocarbon found at each Production Unit.

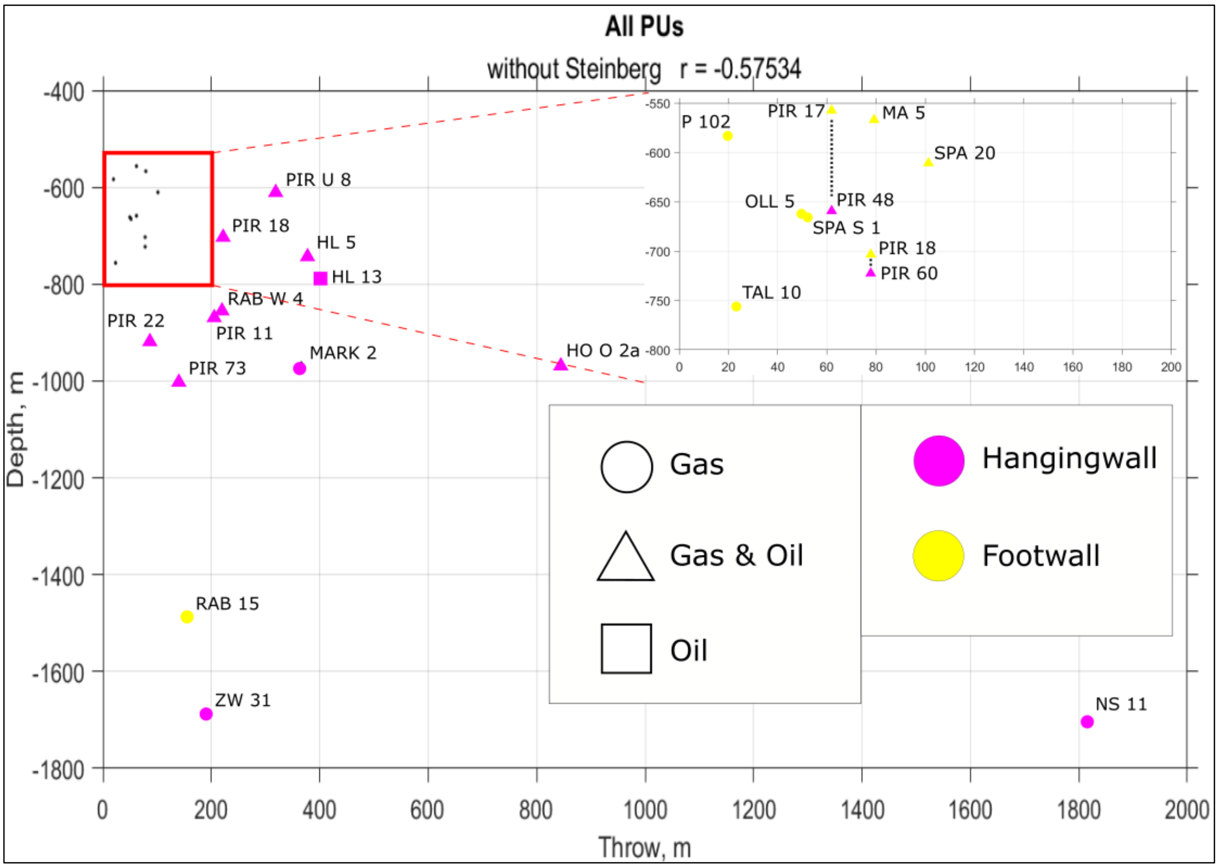

Figure 44: Combination of what hydrocarbon can be found at which side of the fault.

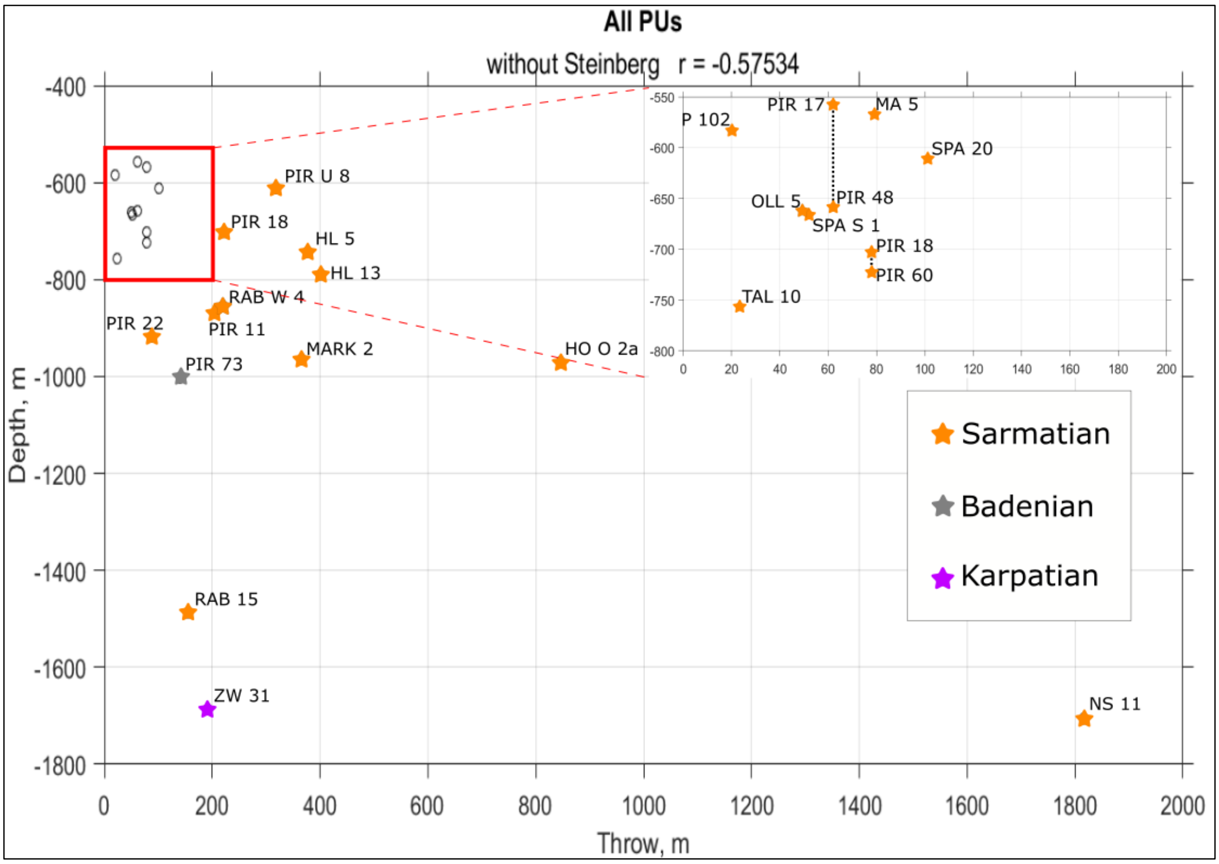

Figure 45: Stratigraphy of the production in the Vienna Basin, without production units along Steinberg Fault.

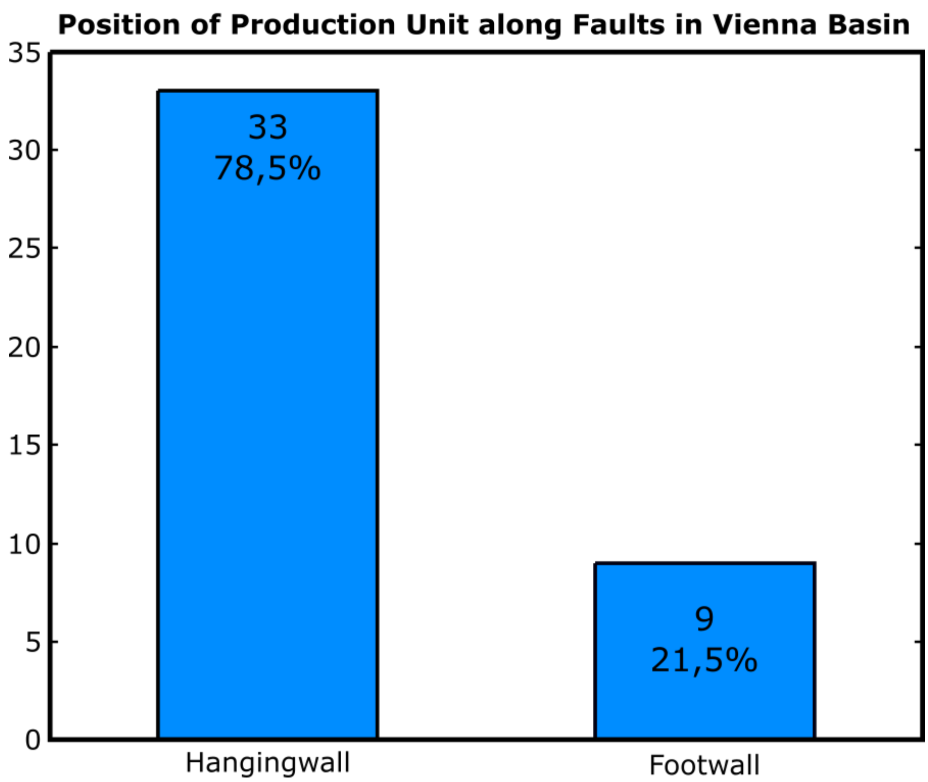

Figure 46: Distribution of the analyzed fault related production units (Steinberg + No Steinberg).

7. Discussion

In this chapter, the relationship between major faults located in the Vienna Basin and the analyzed production units is discussed. Large-scale faults include the Steinberg, the Pirawarth and the Markgrafneusiedl faults. Small-scale unnamed faults are also included. All basin faults were not active/existed at the same time and it resulted in variable sediment distribution and significant thickness differences in the basin. As shown earlier in Figure 6, the thickness of the layers has changed throughout the basin and also through time. Non-uniform, fault-controlled sediment accommodation through time led to variably thick stratigraphic unit. In general, active faults generate accommodation, where depocenters can be temporarily formed. Hölzel et al. (2008) analyzed the regional subsidence history in the Vienna Basin by taking 50 boreholes and dividing them in thirteen groups (Figure 47a-b), mostly based on their geographical position. They also considered, when defining the groups, boreholes in the same fault block (delimited by major faults) or location in depocenters that reached the same depth. Critical for this work, is a good understanding of the basin subsidence history.

7.1 Faults

7.1.1 Steinberg Fault

The Steinberg Fault (SSW-NNE orientated) is one of the largest faults in the Vienna Basin, considering both, its extension and its throw. In some areas the vertical throw can be over 6km (Rupprecht et al., 2019). This process, however, did not happen in one sudden movement and was in reality a continuous process, which lasted millions of years (Figure 47b). The subsidence rate was not constant, including faster and slower movement periods (Hölzel et al., 2008). The activity of one fault can be reconstructed from the deposition history along a fault.

Group G13 in Hölzel et al. (2008) is located mostly in the southern part of the Steinberg Fault (Figure 47a), close to the area, where the Pirawarth faults with NE-SW strike orientation are located (Rupprecht et al., 2019). There could be an argument that considering the subsidence of the entire Steinberg fault from this group is not ideal, since it may only reflect subsidence of the southern part of the fault and not the subsidence history of the whole Steinberg Fault. This is, however, a good approach to see when the fault was active.

The subsidence curve in Figure 47b shows that the steepest parts of the curve occurs in the Bulimina Rotalia Zone (Upper Badenian) and in the Upper Sarmatian. The overall curve documents activity of the Steinberg Fault from the Lower Lagenid Zone (Lower Badenian) to Upper Pannonian with highest subsidence rates during the two periods - Upper Badenian and Upper Sarmatian. The achieved subsidence rate peak was 1000m/Ma in the Upper Badenian and 500m/Ma in the Upper Sarmatian (Hölzel et al., 2008).

The stratigraphic distribution of HC-reservoirs in Vienna Basin sediments (Figure 47c) show that along the Steinberg fault the oil and gas reservoirs were found in sediments of the Upper Badenian, whereas in the Southeast High the reservoirs are found in older Badenian sediments, and the oil and gas discoveries in the Central High (including Spannberg and Matzen) were found in the older Bockfliess Formation with sediments of Ottnangian and Karpatian age. For locations see Figure 33.

The base of the Upper Badenian succession shows an unconformity (Kováč et al., 2007), which most likely also marks the initiation of syn-sedimentary activity of the Steinberg Fault (OMV Report). There might be a relation between this unconformity, the syn-sedimentary deposition in the Upper Badenian and that the subsidence rate of the Steinberg Fault was the highest during this period.

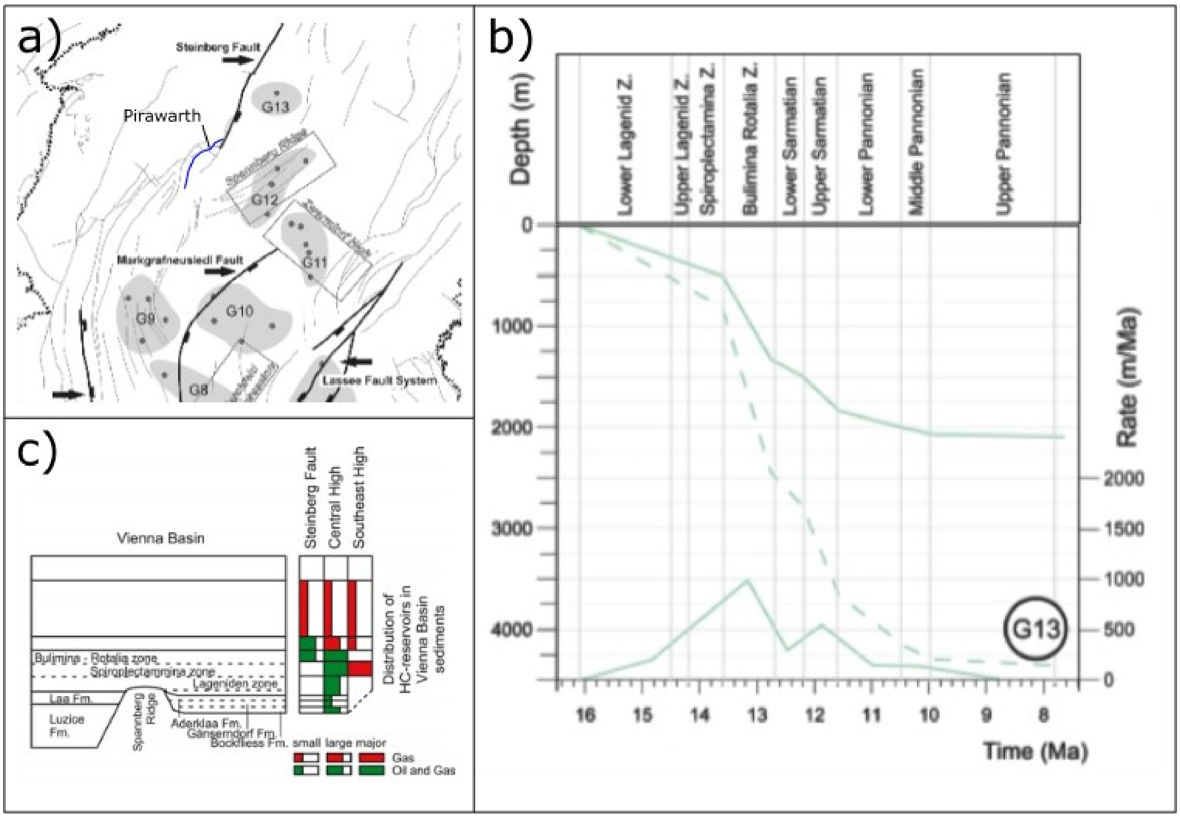

Figure 47: a) Boreholes divided into groups in order to analyze quantitative subsidence in Vienna Basin (Hölzel et al., 2008), b) Subsidence analysis for group 13, along Steinberg Fault, showing highest subsidence rate (1000m/Ma) in Bulimina Rotalia Zone and second peek (500m/Ma) at Upper Sarmatian (Hölzel et al., 2008), c) Distribution of Hydrocarbons in the Vienna Basin, first encounters of hydrocarbons along Steinberg Fault at Bulimina Rotalia Zone (Rupprecht et al., 2019).

Another structures along the fault that can, in general, contribute to hydrocarbon migration inside the fault zone are the so-called fault lenses (Lindanger et al., 2007). Within the fault zone, fault lenses may facilitate communication within the reservoirs and help vertical migration through sediment layers especially for sedimentary rocks with depositional alternation between high permeable rocks and low-permeable rocks (Childs et al., 1997; Fredman et al., 2007; Lindanger et al., 2007). Although this thesis does not deal in detail with structures that are responsible for vertical migration, it is important to note that fault lenses are also found in the Vienna Basin, were identified in this study and should be studied closer (Figure 48).

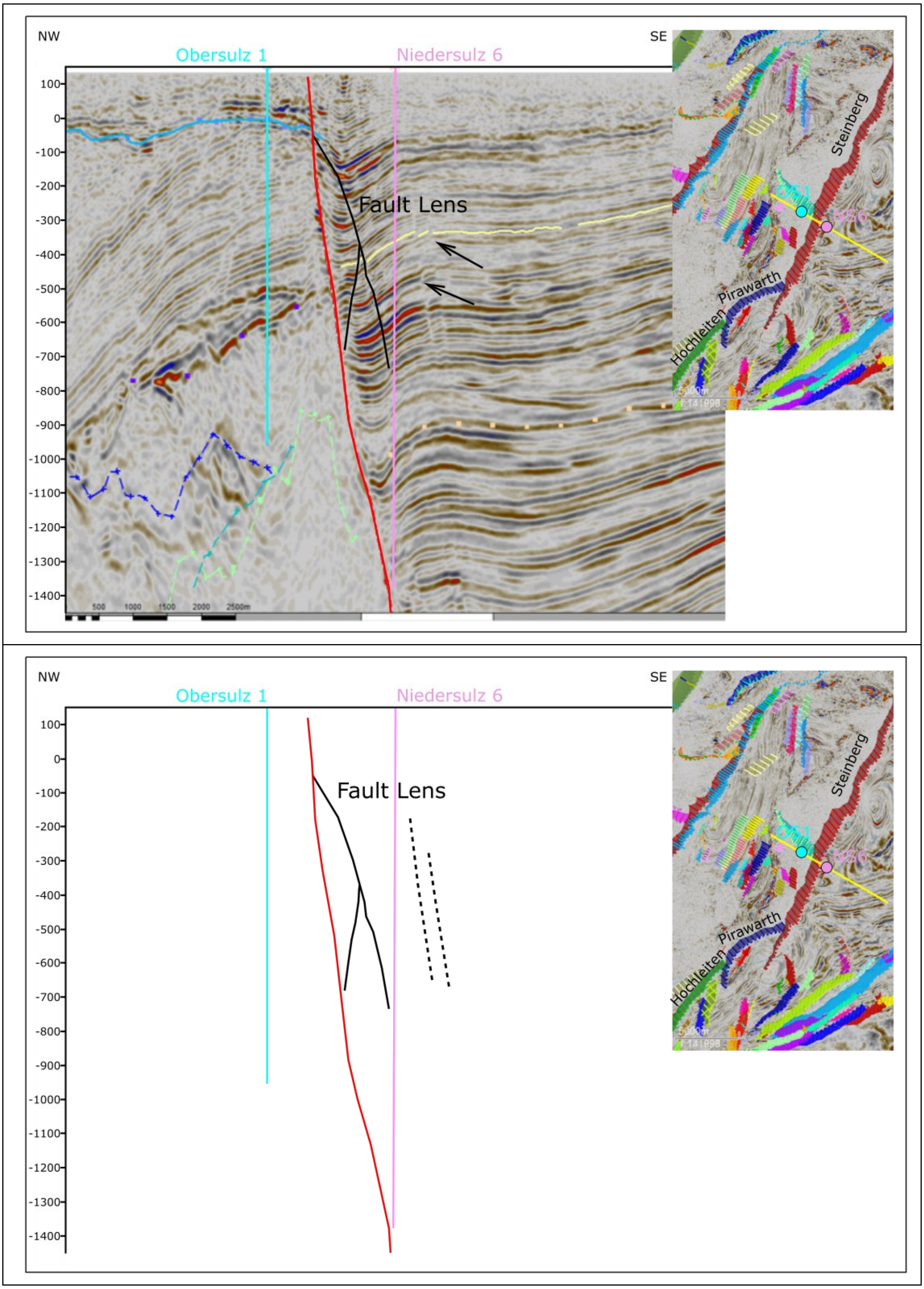

Figure 48: Fault Lens in Fault Zone from the Steinberg fault. Black arrows and dotted line showing undocumented and newly interpreted faults.

7.1.2 Pirawarth/Hochleiten faults

SW-NE oriented faults that belong to the Pirawarth group (Figure 47a) are truncated in the northeast by the Steinberg Fault and they interact or are truncated by the Leopoldsdorf Fault in the southwest (Figure 33).

The geometry of right stepping en enchelon faults in the Pirawarth area might have been caused by the sinistral movement on the Steinberg Fault (OMV report). Besides this, the geometry of the faults also facilitates the origin of relay ramps, where oil and gas can be found. The relay ramps occur between the continuation of the Steinberg Fault and the Pirawarth Fault and were also mapped between the Pirawarth and Hochleiten faults. Especially in the area, where the Pirawarth Fault exhibits more N-S orientation and is truncated by the Hochleiten Fault (orange square), hydrocarbons can accumulate in these areas (Figure 49-51).

As outlined in the introduction, oils and gas can be trapped in relay ramps, if the main faults (in this case the Steinberg and the Pirawarth) do not allow the flow of hydrocarbons, but faults with smaller throw values could be acting as migration paths for hydrocarbons to these stratigraphic traps (examples is given in Section 7.1.4).

Many of these en echelon faults occurring in the Pirawarth/Hochleiten area (Figure 49-51). The faults, that delimit the production units and are shown in Figure 49-51, have similar SW-NE orientation with dip direction to the SE, but throw of each fault is different. The fault's throw decreases northwards as shown on the seismic lines in the Profiles 1 and 2 (Figure 49 and 50) and the throw value are taken from OMV interpreted horizon.

There are some production units in the region presented by profiles 2 (figure 50) and profile 3 (figure 51). However, two of these production units represented by PIR11 (13. Sarmatian) and PIR45 (12. Sarmatian) show no or very small fault throw. Consequently, these two production units were not plotted and removed from the final analysis. However, even not having high throw values, for unspecified reason, there is no hydrocarbon flow between them (and they are thus considered by OMV as two different production units).

Two possible reasons for this could be either (i) secondary cementation or (ii) lateral displacement on the fault. Due to compaction of sedimentary rocks, some minerals and even sediments themselves can partially dissolve and the newly formed fluids that migrate and crystalize elsewhere, e.g. in pores between grains. This process would not only diminish the volume of the pores, but also decrease the permeability of the rock, thus impeding the fluid flow through the rock (Girnun et al., 2020).

The strike slip fault regime (Figure 12) also contribute to rock fracturing. However, this process does not lead to concentration of shale material in the fault zone. On the other hand, a combination of these two factors - lateral displacement and incorporation of the shale into the fault is commonly observed along the oblique faults. As outlined in the chapter Introduction, the Vienna Basin has a complex fault pattern. There are duplexes along sinistral strike slip systems and normal faulting formed during Middle to Upper Miocene (Hölzel et al., 2008). Literature documents that many of the faults in the Vienna Basin have also a lateral movement component, sinistral transfer faults (Peresson and Decker, 1997; Kováč et al., 2007; Hölzel et al., 2008). It would be important to analyze which faults in the Vienna Basin are exclusively normal faults, and which faults also have lateral displacement (oblique faults). Assuming that there is no lateral displacement without proper investigation, would most likely cause loss of relevant information about fluid flow.

The area between the two main faults (for location see Figure 48), the Pirawarth and the Hochleiten, represented by an orange square in Figure 49-51) is interpreted to represent a relay ramp delimited by these two large scale faults. As shown in Figure 13 in section 3.3, the relay ramp classification

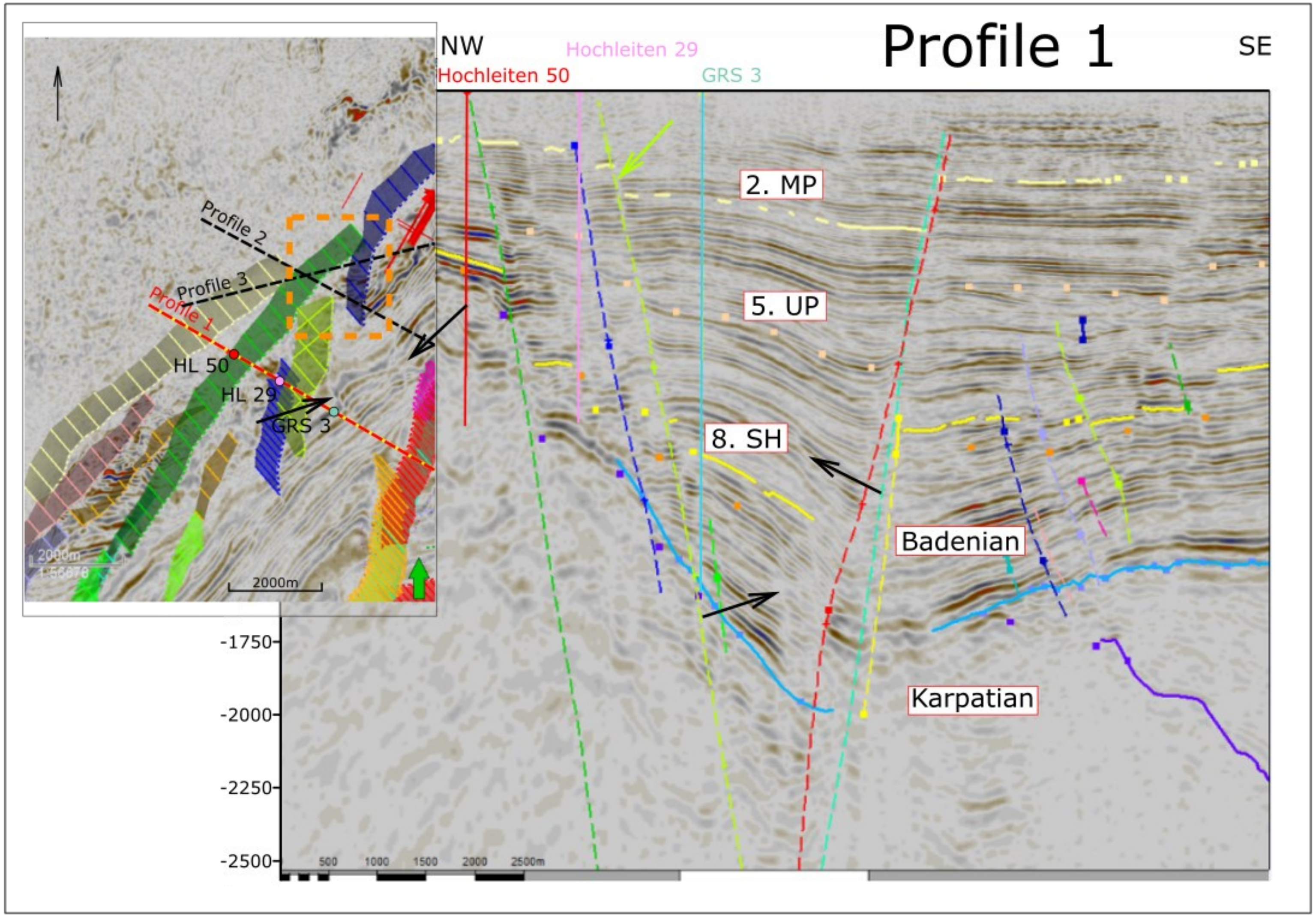

Figure 49: Map showing Pirawarth area and the southernmost profile (Profile 1). Black arrows showing undocumented faults. Green arrow showing light green fault mentioned in section 7.1.2.

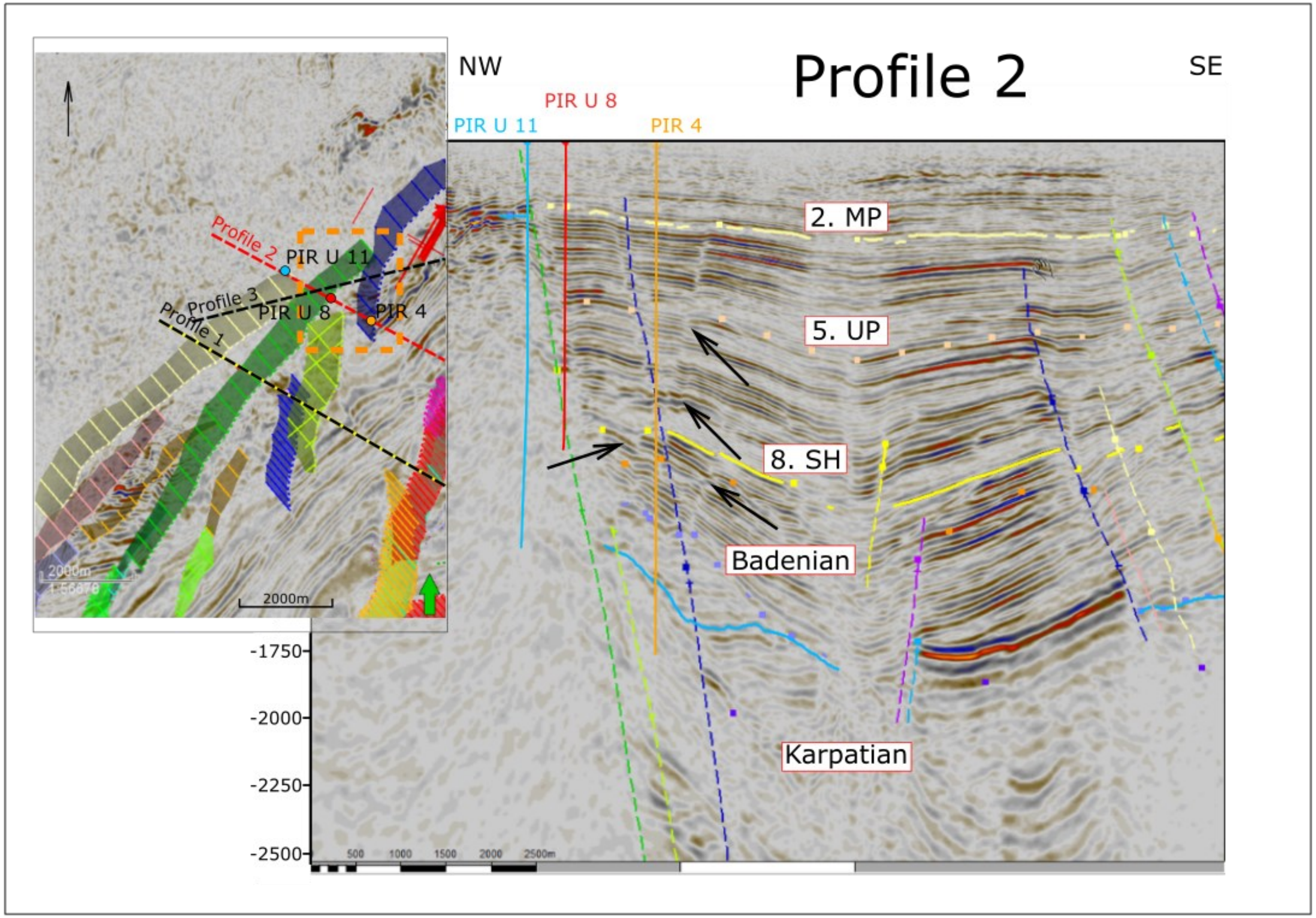

Figure 50: Map showing Pirawarth area and the northernmost profile (Profile 2). Black arrows showing undocumented faults.

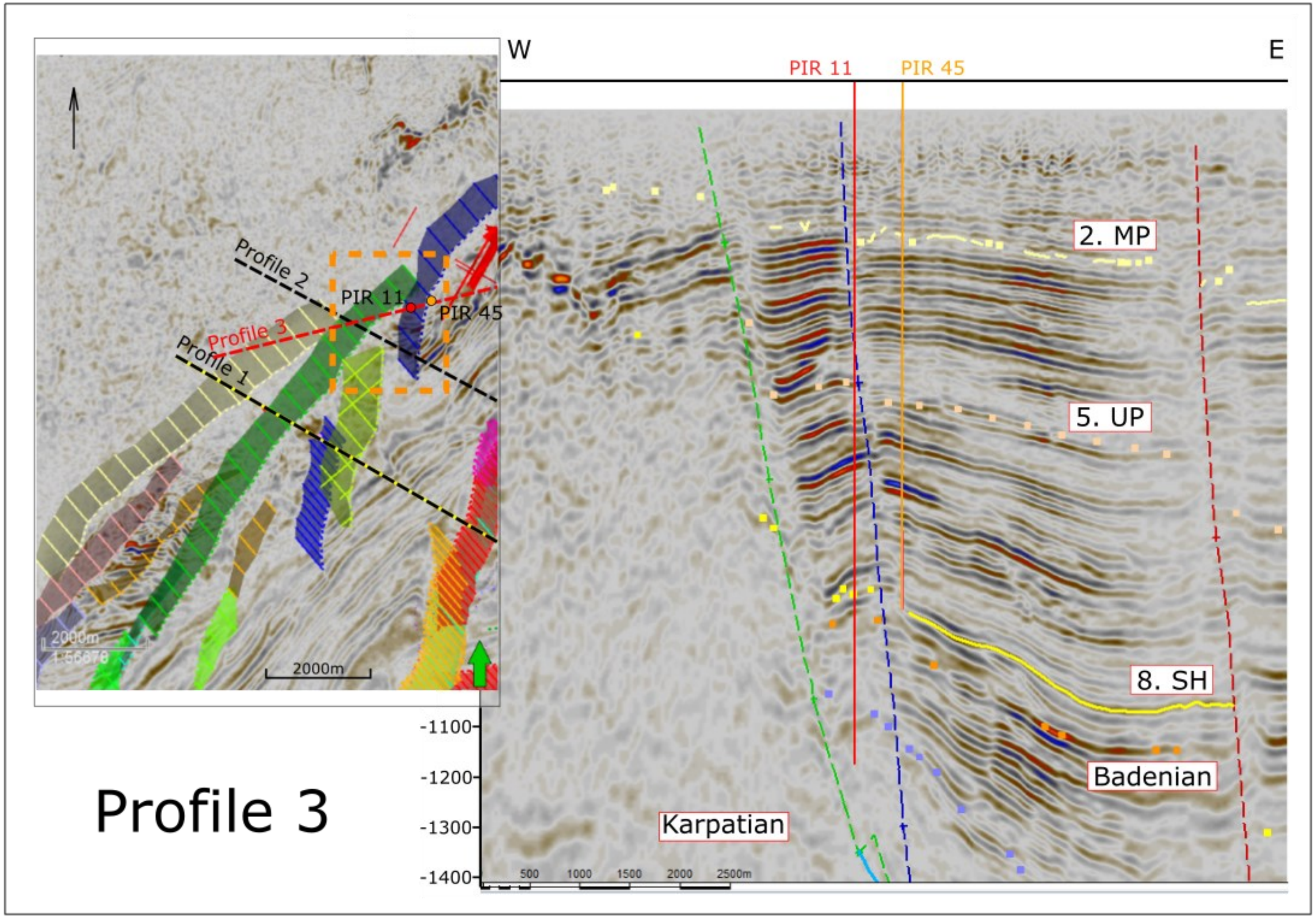

Figure 51: Map showing Pirawarth area southwest – northeast oriented profile (Profile 3), showing small displacement between two production units (PIR11 and PIR45).

comprises four stages of relay ramp development (Peacock and Sanders, 1994). Based on the large throw of the Hochleiten Fault (c. 400 m, Figure 30) and higher SGR values that impede flow, we estimate that the relay ramp is in the fourth stage of development with cut off only in the footwall side (footwall cut-off).

In the relay ramp we can also see an N-S oriented light green fault (Figure 49), which seems to be normal faults formed during transtension in the pull apart phase in the Vienna basin. If this is the case, the light green fault and other faults with similar orientation would have more vertical displacement and the NE-SW Pirawarth and Hochleiten faults, more lateral displacement than the N-S trending faults.

7.1.3 Markgrafneusiedl Fault

The 16km long Markgrafneusiedl Fault is located in the central part of the Vienna Basin (Spahić et al., 2013) southeast of the Steinberg Fault and east of the Leopoldsdorf Fault (Figure 32b, 33 and 52a).

The Markgrafneusiedl Fault was most likely formed by the linkage of older smaller fault segments with younger small fault segments that were created as a response to ongoing and increasing stress field (Spahić et al., 2013). The fault that served as connection between the smaller two faults impeded further lateral propagation of these smaller faults (see Figure 3 and faults F1 and F2 in Spahić et al., 2013). Consequently, nowadays this fault segment shows the biggest displacement (Ackermann et al., 2001). The studied section of the Markgrafneusiedl Fault dates from the Lower Sarmatian to almost the Middle Pannonian (Spahić et al., 2013) and the maximum vertical offset occurred after the small fault segments had been linked into one large-scale fault (Ackermann et al., 2001; Spahić et al., 2013).

According to the analysis done by Hölzel et al. (2008), the Markgrafneusiedl Fault is a young feature, since the groups G8-10 (Figure 52) show a similar subsidence evolution (Hölzel et al., 2008). Therefore, it is believed that the faulting happened in Upper Pannonian times, after the sedimentation had taken place in the basin (Hölzel et al., 2008). Interestingly, the two periods the Lower Sarmatian and the Middle Pannonian exhibit the highest subsidence rates in groups G8-G10 (Figure 52). During these periods, the Markgrafneusiedl Fault probably started to form (Spahić et al., 2013) and it further reinforces the fact, that the Markgrafneusiedl Fault formed after the deposition of Middle Pannonian strata in the basin. In case that the Markgrafneusiedl Fault existed and was active prior to Upper Pannonian times, the boreholes groups G8-G10 would have different subsidence evolution since they are not located on the same blocks (hanging wall or footwall).

7.1.4 Undocumented small faults and development sequence

Many small faults, which are shown in Figure 48-50, are not defined and interpreted on the seismic data. Since the main faults are considered to be impermeable, besides the migration paths that are mentioned in chapter 4 (i.e., vertical migration through membrane seal or hydraulic seal), these smaller faults can act as migration paths from deeper reservoirs to shallower ones. To document, study and analyse how the small faults developed relative to the main faults (the Steinberg, Pirawarth, Hochleiten, Markgrafneusiedl) is essential to have a better understanding of hydrocarbon migration in the Vienna Basin.

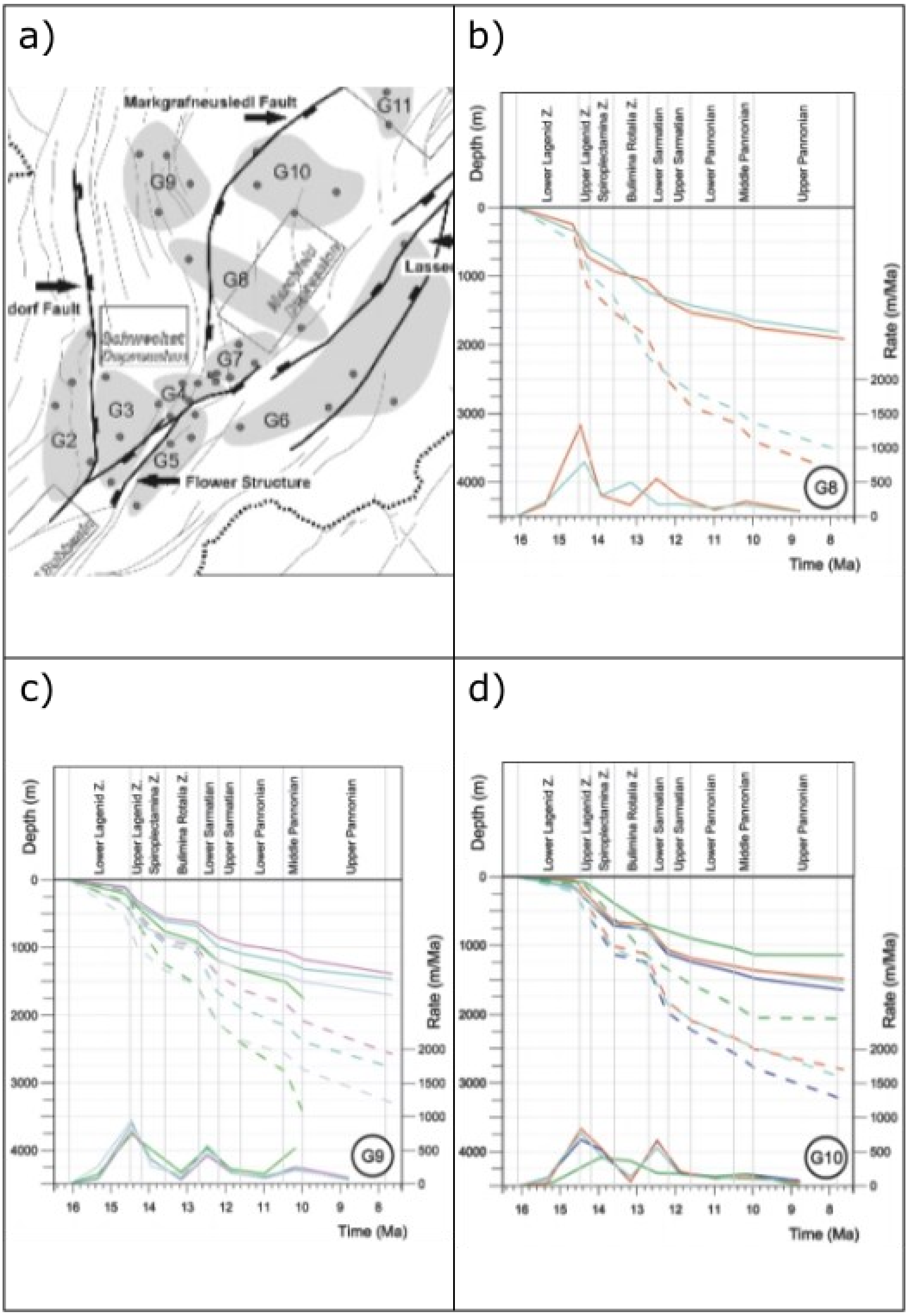

Figure 52: Division of the boreholes into groups G8-10. a) Location of the boreholes in each group. b-d) Subsidence of each borehole divided in the respective group (extracted from Hölzel et al., 2008).

Figure 48-50 illustrate some of these previously mentioned undocumented small faults. The new interpretation of these small faults, done during this study, can be seen in Figure 53-55. Fault 1 shown in dashed line in Figure 53 corresponds to the light green fault on the seismic profile in Figure 49-51. Faults 2 and 3 are not documented in Figure 49-51. We can see that smaller unmapped antithetic faults branch off the large scale Pirawarth fault (in blue) on Profile in Figure 50. One of these faults is newly interpreted, roughly N-S oriented Fault 2 depicted in Figure 53 and it extends in a map view towards the orange fault located to the southeast of it. These individual branches can show different geometries and offsets along the length of a main fault. At one place one branch shows larger offset while at another place, another branch is more developed.

A better understanding of the relation between faults of same hierarchic level (main faults vs. main faults or small fault vs. small fault) but also at different hierarchic level (main fault vs. small fault) should be studied in closer detail. For this reason, the approach of such study (Reeve 2015) is shown as an example in Figure 56. The author studied specifically the fault tips located in the North Sea (Figure 56a-b), in order to see what the relation between them are. He concluded that the faults G1, G2 and G3 (Figure 56c), due to their proximity and a bell-shaped profile of summed throws might represent a kinematically linked system and link in deeper level (Reeve et al., 2015). The same process he applies for the smaller fault population (Figure 56d), where the author could distinguish one fault from the other and conclude that these faults have different initial nucleation and were linked together at another fault development stage (Reeve et al., 2015).

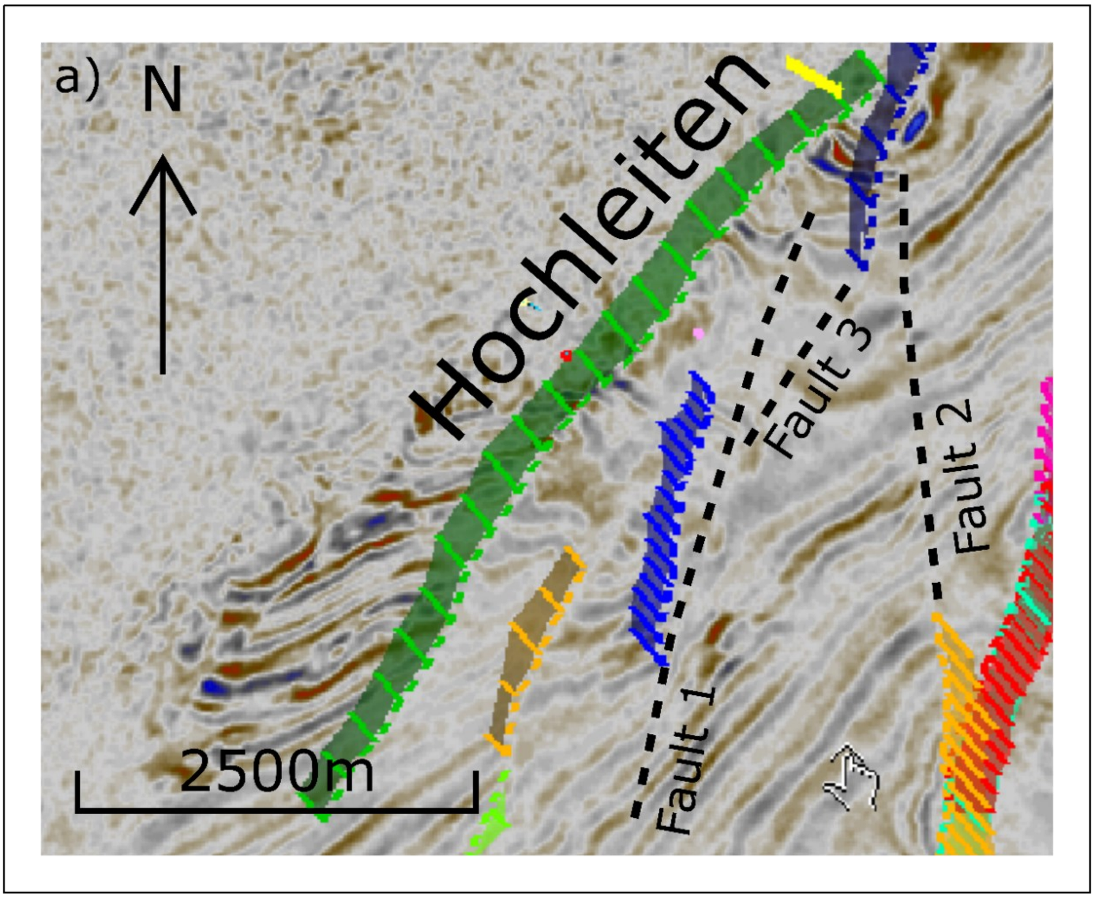

Figure 53: Small faults that are not mapped.

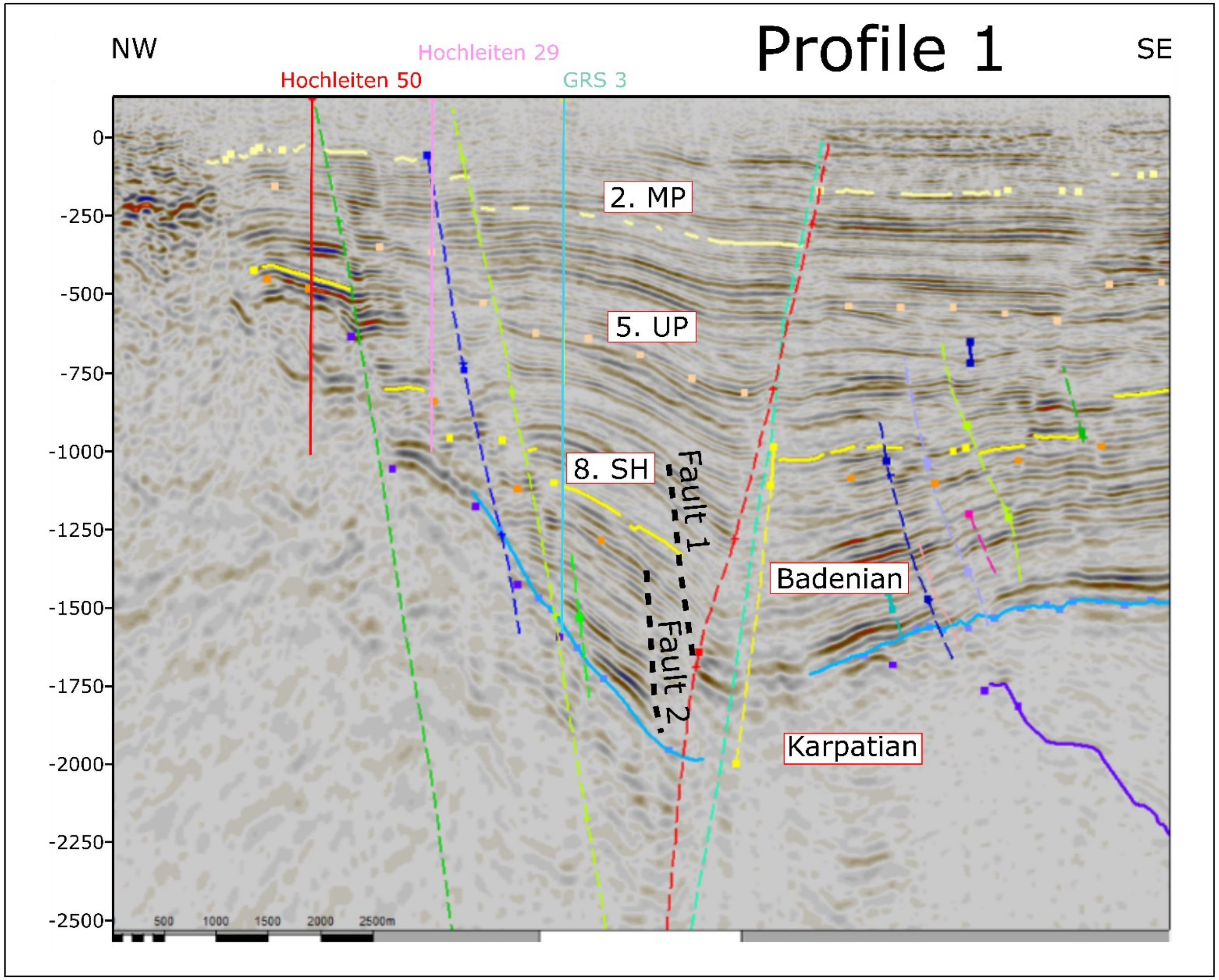

Figure 54: Small undocumented faults branching of the red fault. For location see Figure 49.

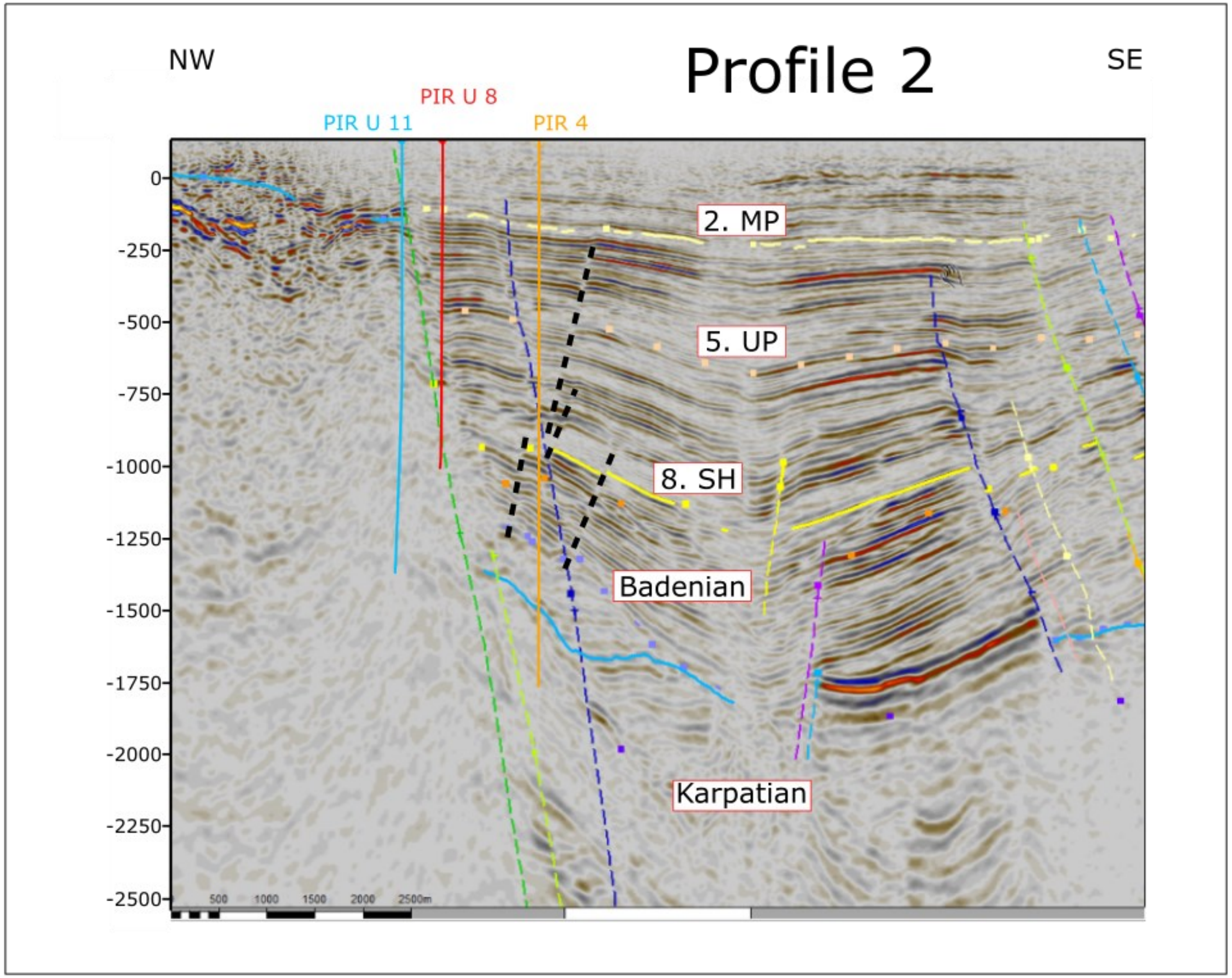

Figure 55: Undocumented small faults branching of the Pirawarth and Hochleiten Fault. For location see Figure 50.

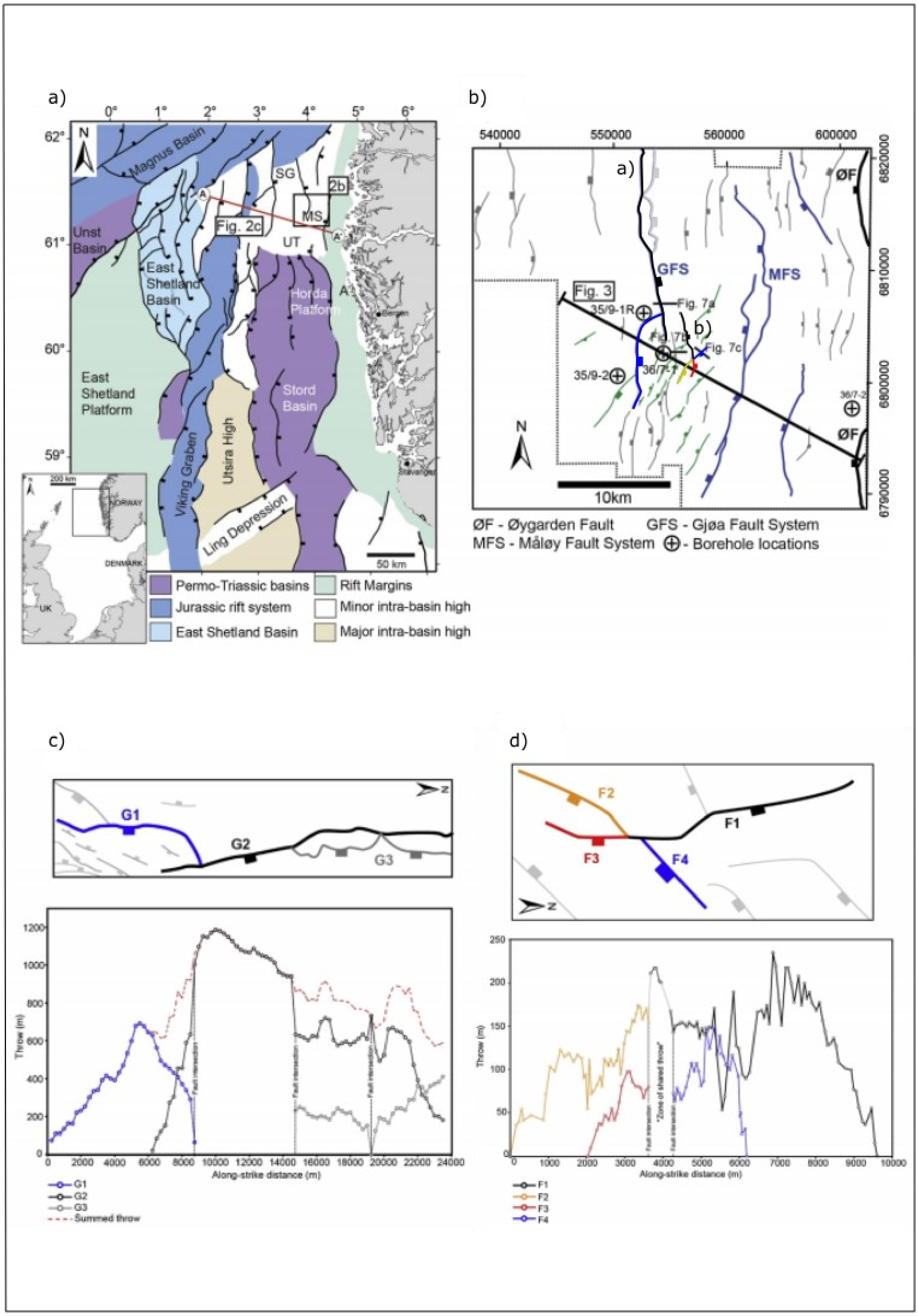

Figure 56: Analysis of fault evolution in the rift zone in the North Sea (modified from Reeve et al., 2015). a) North Sea region with stratigraphic units. b) Study area. c) Analyzing major faults. d) Analyzing smaller fault populations.

7.1.5 SGR Diagrams in the Vienna Basin

Shale gouge ratio (SGR) were already briefly mentioned in subchapter 3.5 to define the SGR diagrams (from internal OMV report). Since the Vienna Basin is a large basin and has a complex tectono-stratigraphic evolution, we included seven additional SGR diagrams located elsewhere in the Vienna Basin in Appendix B. Location of the boreholes with SGR are shown in Figure 57a). From the obtained throw values we have achieved the threshold of 20% and this would tend to impede flow through the faults (cf. Harris et al., 2002; Yielding et al., 2010).

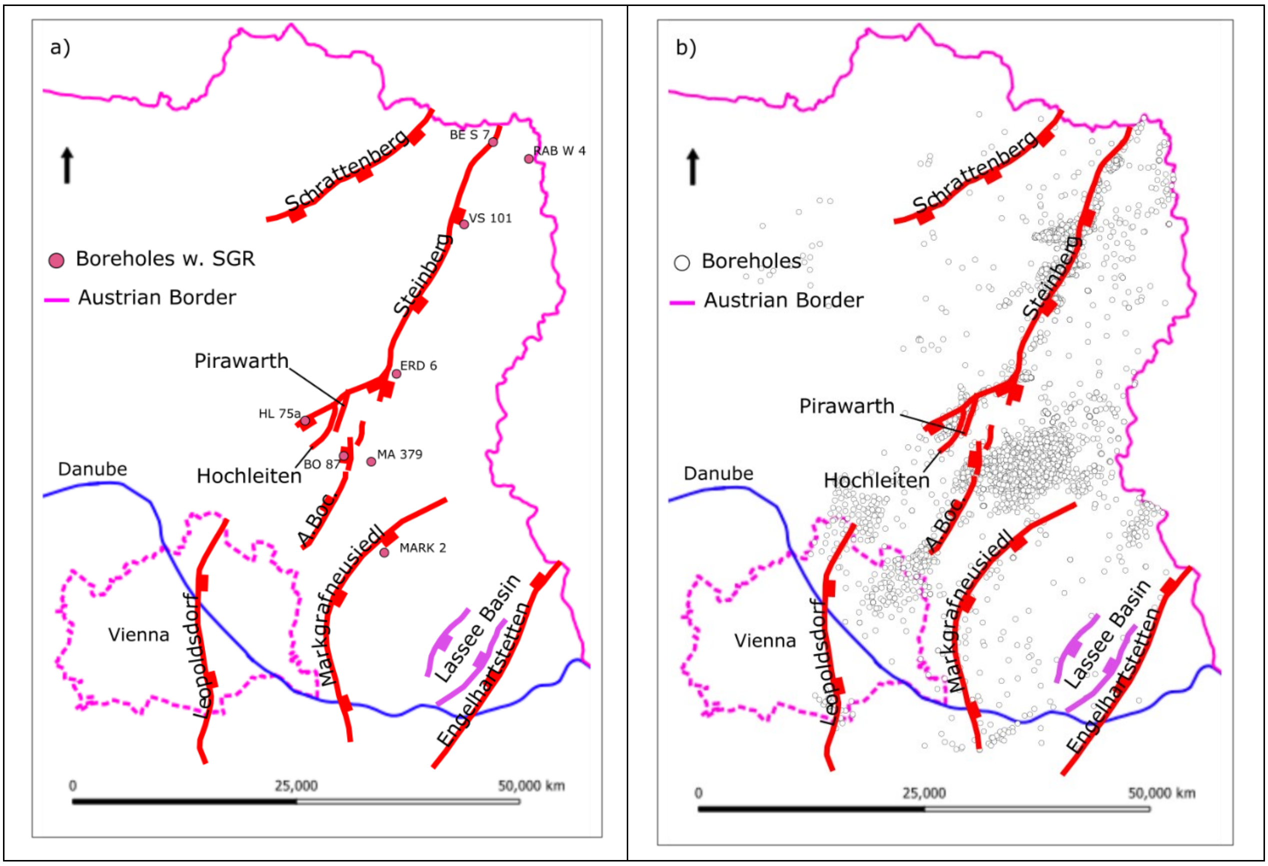

Figure 57: Distribution of boreholes in the Vienna Basin. a) Boreholes with provided SGR Diagrams. b) Boreholes in the Vienna Basin. The coordinates are not shown due to sensitivity of the data.

7.2 Production units and boreholes

7.2.1 Selected boreholes within the Vienna Basin

First it has to be recalled that the provided dataset contained only production units that were active in the year of 2020. According to OMV, there are 1043 former production units (not active anymore by 2020). These inactive production units were not analyzed due to time constraints and it is possible that further, more detailed investigation of these depleted units would reveal different trends.

According to the results presented in this study, there are more production units located in the hanging wall than in the footwall (Figure 46). When looking at the geographical distribution and number of wells, we see evenly distributed well locations, both in the footwall and the hanging wall (Figure 57b). In addition, clusters of well locations distort the well count in the footwall versus the hanging wall areas. Disregarding the clusters of boreholes due to field development (Figure 57b), i.e., many of the boreholes in these areas of borehole clusters were drilled after there was a hydrocarbon discovery to extract or to delimit the trap, we see an equal distribution of the boreholes in the hanging wall and in the footwall.

The predominance of production units in the hanging wall could also be due to the selection of production units in the study area (northern part of the Vienna Basin, north of Danube). Next point would be analyzing, as mentioned above, the selection of production unit and checking if the results would be the same if inactive production units were considered. This is, however, beyond the scope of this thesis and could be addressed in future studies.

Another point to be discussed is, if there are as many traps in the footwall as in the hanging wall. Due to the high throw value in the Steinberg Fault and partially erosion of the Neogene strata on the footwall of the Steinberg Fault, there is actually no point in comparing the presence of structures in the Neogene between hanging wall and footwall. However, we can compare the traps between the Neogene for the hanging wall with the production units on older stratigraphic layers in the footwall (e.g., Palaeogene).

7.2.2 Pattern and algorithm

As mentioned previously, two secondary objectives within the scope of the thesis was (i) to try to find a pattern among the data and (ii) to develop an algorithm in order to try to predict the chances of finding some new fields.

After careful analysis of the provided data, these two objectives prove impossible due to low number of input (42) that was left after eliminating many from the original dataset (270). As mentioned in the previous subchapter, production units that were not active in 2020 were not in the database, which could also influence directly in the “model training” inside machine learning (Verbraeken et al., 2021). Another important point would be to analyze boreholes that despite their high potential of finding oil or/and gas were found empty and also put these in the database with the same parameters as for the production units. This approach would provide much better results when training the model since it would not only have data from production units, but also for “traps” that were empty. Besides including dry boreholes into the analysis, other data (parameters) like OWC (GWC or OGC), buoyancy pressure and column high would be extremely beneficial for this thesis and should be included in future studies. For example, study conducted by Bretan et al. (2020) used besides throw and depth also buoyancy pressure, column high and type of seal (juxtaposition seal or hydraulic seal).

8 Conclusion

1 From original 270 production units active in 2020 and provided by OMV, 42 production units were found suitable for the analysis carried out in this study.

2 It is concluded that between the analyzed wells in the Vienna Basin there is a predomination of production units in the hanging wall, when comparing in absolute numbers.

3 The current spatial distribution and depth of hydrocarbon wells does not reflect the hanging wall versus footwall trap problem statement. Wells were drilled based on hydrocarbon indicators dependent on the technology available at the time of drilling (e.g. gravimetry, nearby hydrocarbon founds, 3D seismic). Thus, a statistical and equally distributed sampling of hanging wall and footwall traps is not guaranteed.

4 All faults should have been in place before the start of migration in order to identify the fault as a key factor responsible for the presence of hydrocarbon in the trap.

5 Depth versus throw assessment and diagrams, length vs. throw, (Reeve et al., 2015) prove to be a valuable tool for fault characterization and for fault segment delineation. This method was not used widely in the Vienna Basin up to now.

6 In the case of large-scale fault lenses, one production unit can be situated in the hanging wall or in the footwall position, depending on the point of view. An example is well PIR 18.

7 Algorithm, which could predict the chances of finding new oil/gas fields was not developed due to low number of production units with good parameters.

References

Ackermann, R.V., Schlische, R.W., Withjack, M.O., 2001. The geometric and statistical evolution of normal fault systems: an experimental study of the effects of mechanical layer thickness on scaling laws. J. Struct. Geol. 23, 1803–1819. https://doi.org/10.1016/S0191-8141(01)00028-1

Arzmüller, G., Buchta, Š., Ralbovský, E., Wessely, G., 2006. The Vienna Basin, in: The Carpathians and Their Foreland<subtitle>Geology and Hydrocarbon Resources</Subtitle>. American Association of Petroleum Geologists. https://doi.org/10.1306/985608M843068

Axaopoulos, P., Tzanes, G., 2021. Wind Energy Potential (Measurements, Evaluation, Forecasting), in: Reference Module in Earth Systems and Environmental Sciences. https://doi.org/10.1016/B978-0-12-819727-1.00151-5

Beidinger, A., Decker, K., 2011. 3D geometry and kinematics of the Lassee flower structure: Implications for segmentation and seismotectonics of the Vienna Basin strike–slip fault, Austria. Tectonophysics 499, 22–40. https://doi.org/10.1016/j.tecto.2010.11.006

Chen, J., Wang, W., Chen, L., 2023. A Strain Hardening and Softening Constitutive Model for Hard Brittle Rocks. Appl. Sci. 13, 2764. https://doi.org/10.3390/app13052764

Childs, C., Manzocchi, T., Walsh, J.J., Bonson, C.G., Nicol, A., Schöpfer, M.P.J., 2009. A geometric model of fault zone and fault rock thickness variations. J. Struct. Geol. 31, 117–127. https://doi.org/10.1016/j.jsg.2008.08.009

Childs, C., Walsh, J.J., Watterson, J., 1997. Complexity in fault zone structure and implications for fault seal prediction, in: Norwegian Petroleum Society Special Publications. Elsevier, pp. 61–72. https://doi.org/10.1016/S0928-8937(97)80007-0

Cong, F., Zhang, H., Hao, F., Xu, S., 2020. Direct control of normal fault in hydrocarbon migration and accumulation in northwestern Bozhong subbasin, Bohai Bay Basin, China. Mar. Pet. Geol. 120, 104555. https://doi.org/10.1016/j.marpetgeo.2020.104555

Decker, K., 1996. Miocene tectonics at the Alpine-Carpathian junction and the evolution of the Vienna basin.

Decker, K., Peresson, H., Hinsch, R., 2005. Active tectonics and Quaternary basin formation along the Vienna Basin Transform fault. Quat. Sci. Rev. 24, 305–320. https://doi.org/10.1016/j.quascirev.2004.04.012

Dembicki Jr, H., 2017. Chapter 8 - Basin Modeling, in: Practical Petroleum Geochemistry for Exploration and Production. Elsevier, pp. 273–308. https://doi.org/10.1016/B978-0-12-803350-0.00008-8

Fitzpatrick, R., 2017. Theoretical Fluid Mechanics, 2053-2563. IOP Publishing. https://doi.org/10.1088/978-0-7503-1554-8

Fossen, 2016. Structural Geology.

Fredman, N., Tveranger, J., Semshaug, S., Braathen, A., Sverdrup, E., 2007. Sensitivity of fluid flow to fault core architecture and petrophysical properties of fault rocks in siliciclastic reservoirs: a synthetic fault model study. Pet. Geosci. 13, 305–320. https://doi.org/10.1144/1354-079306-721

Girnun, J., Emmanuel, S., Levenson, Y., Anovitz, L.M., 2020. Quantification of mechanical compaction and cementation during contact metamorphism of sandstone. J. Struct. Geol. 136, 104062. https://doi.org/10.1016/j.jsg.2020.104062

Grotzinger, J., Jordan, T., 2017. Press/Siever Allgemeine Geologie. Springer Berlin Heidelberg, Berlin, Heidelberg. https://doi.org/10.1007/978-3-662-48342-8

Hamilton, Wagner, L., Wessely, G., 2000. Oil and Gas in Austria. Austrian journal of earth sciences 235–262.

Hardman, R.F.P., Booth, J.E., 1991. The significance of normal faults in the exploration and production of North Sea hydrocarbons. Geol. Soc. Lond. Spec. Publ. 56, 1–13. https://doi.org/10.1144/GSL.SP.1991.056.01.01

Harris, D., Yielding, G., Levine, P., Maxwell, G., Rose, P.T., Nell, P., 2002. Using Shale Gouge Ratio (SGR) to model faults as transmissibility barriers in reservoirs: an example from the Strathspey Field, North Sea. Pet. Geosci. 8, 167–176. https://doi.org/10.1144/petgeo.8.2.167

Harzhauser, M., Piller, W.E., 2005. Neogen des Wiener Beckens. 75 Jahrestag. Paläontol. Ges. 42.

Hinsch, R., Decker, K., Peresson, H., 2005a. 3-D seismic interpretation and structural modeling in the Vienna Basin: implications for Miocene to recent kinematics.

Hinsch, R., Decker, K., Wagreich, M., 2005b. 3-D mapping of segmented active faults in the southern Vienna Basin. Quat. Sci. Rev. 24, 321–336. https://doi.org/10.1016/j.quascirev.2004.04.011

Holleman-Wiberg, 1976. Lehrbuch der Anorganichen Chemie, 81st–90th ed. De Gruyter, Berlin.

Hölzel, M., Wagreich, M., Faber, R., Strauss, P., 2008. Regional subsidence analysis in the Vienna Basin (Austria) 11.

Kováč, M., Andreyeva-Grigorovich, A., Bajraktarević, Z., Brzobohatý, R., Filipescu, S., Fodor, L., Harzhauser, M., Nagymarosy, A., Oszczypko, N., Pavelić, D., Rögl, F., Saftić, B., Sliva, U., Studencka, B., 2007. Badenian evolution of the Central Paratethys Sea: paleogeography, climate and eustatic sea-level changes.

Kularathna, E.K.C.W., Pitawala, H.M.T.G.A., Senaratne, A., Ratnayake, A.S., 2020. Play distribution and the hydrocarbon potential of the Mannar Basin, Sri Lanka. J. Pet. Explor. Prod. Technol. 10, 2225–2243. https://doi.org/10.1007/s13202-020-00902-8

Lankreijer, A., Kováč, M., Cloetingh, S., Pitoňák, P., Hlôška, M., Biermann, C., 1995. Quantitative subsidence analysis and forward modelling of the Vienna and Danube basins: thin-skinned versus thick-skinned extension. Tectonophysics 252, 433–451. https://doi.org/10.1016/0040-1951(95)00099-2

Lee, E.Y., Wagreich, M., 2017. Polyphase tectonic subsidence evolution of the Vienna Basin inferred from quantitative subsidence analysis of the northern and central parts. Int. J. Earth Sci. 106, 687–705. https://doi.org/10.1007/s00531-016-1329-9

Lindanger, M., Gabrielsen, R.H., Braathen, A., 2007. Analysis of rock lenses in extensional faults. Nor. J. Geol.

Misch, D., Guo, S., F. Sachsenhofer, R., Zhu, Y., Xin, T., Bai, W., 2022. A New Image Processing Workflow for the Detection of Quartz Types in Shales: Implications for Shale Gas Reservoir Quality Prediction. Minerals. https://doi.org/10.3390/min12081027

Morton, R.A., Bernier, J.C., Buster, N.A., 2009. Simple methods for evaluating accommodation space formation in coastal wetlands. Wetlands 29, 997–1003. https://doi.org/10.1672/09-025D.1

Peacock, Sanders, 1994. Geometry and Development of Relay Ramps in Normal Fault Systems. AAPG Bull. 78. https://doi.org/10.1306/BDFF9046-1718-11D7-8645000102C1865D

Peresson, H., Decker, K., 1997. Far-field effects of Late Miocene subduction in the Eastern Carpathians: E-W compression and inversion of structures in the Alpine-Carpathian-Pannonian region. Tectonics 16, 38–56. https://doi.org/10.1029/96TC02730

Reeve, M.T., Bell, R.E., Duffy, O.B., Jackson, C.A.-L., Sansom, E., 2015. The growth of non-colinear normal fault systems; What can we learn from 3D seismic reflection data? J. Struct. Geol. 70, 141–155. https://doi.org/10.1016/j.jsg.2014.11.007

Rögl, Spezzafari, Coric, 2002. Micropaleontology and biostratigraphy of the Karpatian-Badenian transition (Early-Middle Miocene boundary) in Austria (Central Paratethys). CFS Courier Forschungsinstitut Senckenberg 47–67.

Royden, L.H., 1985. The Vienna Basin: a thin-skinned pull-apart basin, in Biddle, K. T., and Christie-Blick, N., eds., Strike-slip deformation, basin formation and sedimentation, Volume 37: Tulsa, OK, Society of Economic Paleontologists and Mineralogists Special Publication. Society of Economic Paleontologists and Mineralogists Special Publication 37, 319–338.

Rupprecht, B.J., Sachsenhofer, R.F., Gawlick, H.-J., Kallanxhi, M.-E., Kucher, F., 2017. Jurassic source rocks in the Vienna Basin (Austria): Assessment of conventional and unconventional petroleum potential. Mar. Pet. Geol. 86, 1327–1356. https://doi.org/10.1016/j.marpetgeo.2017.07.026

Rupprecht, B.J., Sachsenhofer, R.F., Zach, C., Bechtel, A., Gratzer, R., Kucher, F., 2019. Oil and gas in the Vienna Basin: hydrocarbon generation and alteration in a classical hydrocarbon province. Pet. Geosci. 25, 3–29. https://doi.org/10.1144/petgeo2017-056

Singh, D., Kumar, P.C., Sain, K., 2016. Interpretation of gas chimney from seismic data using artificial neural network: A study from Maari 3D prospect in the Taranaki basin, New Zealand. J. Nat. Gas Sci. Eng. 36, 339–357. https://doi.org/10.1016/j.jngse.2016.10.039

Spahić, D., Exner, U., Behm, M., Grasemann, B., Haring, A., Pretsch, H., 2011. Listric versus planar normal fault geometry: an example from the Eisenstadt-Sopron Basin (E Austria). Int. J. Earth Sci. 100, 1685–1695. https://doi.org/10.1007/s00531-010-0583-5

Spahić, D., Grasemann, B., Exner, U., 2013. Identifying fault segments from 3D fault drag analysis (Vienna Basin, Austria). J. Struct. Geol. 55, 182–195. https://doi.org/10.1016/j.jsg.2013.07.016

Strauss, P., Harzhauser, M., Hinsch, R., Wagreich, M., 2006. Sequence stratigraphy in a classic pull-apart basin (Neogene, Vienna Basin). A 3D seismic based integrated approach 13.

Sverdrup, H., Ragnarsdóttir, K.V., 2014. Natural Resources in a Planetary Perspective. Geochem. Perspect. 129–341. https://doi.org/10.7185/geochempersp.3.2

Vandenbroucke, M., Largeau, C., 2007. Kerogen origin, evolution and structure. Org. Geochem. 38, 719–833. https://doi.org/10.1016/j.orggeochem.2007.01.001

Verbraeken, J., Wolting, M., Katzy, J., Kloppenburg, J., Verbelen, T., Rellermeyer, J.S., 2021. A Survey on Distributed Machine Learning. ACM Comput. Surv. 53, 1–33. https://doi.org/10.1145/3377454

Villamil, T., 1999. Campanian–Miocene tectonostratigraphy, depocenter evolution and basin development of Colombia and western Venezuela. Palaeogeogr. Palaeoclimatol. Palaeoecol. 153, 239–275. https://doi.org/10.1016/S0031-0182(99)00075-9

Vitale, S., Mazzoli, S., 2008. Heterogeneous shear zone evolution: The role of shear strain hardening/softening. J. Struct. Geol. 30, 1383–1395. https://doi.org/10.1016/j.jsg.2008.07.006

Vrolijk, P.J., Urai, J.L., Kettermann, M., 2016. Clay smear: Review of mechanisms and applications. J. Struct. Geol. 86, 95–152. https://doi.org/10.1016/j.jsg.2015.09.006

Wagreich, M., Schmid, H.P., 2002. Backstripping dip-slip fault histories: apparent slip rates for the Miocene of the Vienna Basin. Terra Nova 14, 163–168. https://doi.org/10.1046/j.1365-3121.2002.00404.x

Watts, N.L., 1987. Theoretical aspects of cap-rock and fault seals for single- and two-phase hydrocarbon columns. Mar. Pet. Geol. 4, 274–307. https://doi.org/10.1016/0264-8172(87)90008-0

Wessely, G., 2006. Geologie der Österreichischen Bundesländer - Niederösterreich, Verlag d. Geologischen Bundesanstalt. ed.

Yielding, G., Bretan, P., Freeman, B., 2010. Fault seal calibration: a brief review. Geol. Soc. Lond. Spec. Publ. 347, 243–255. https://doi.org/10.1144/SP347.14

Yielding, G., Freeman, B., Needham, D.T., 1997. Quantitative Fault Seal Prediction. AAPG Bull. 81, 897–917. https://doi.org/10.1306/522B498D-1727-11D7-8645000102C1865D

Table of Figures

Appendix A

The pink borehole (HL5) is presented in the figure below in the hanging wall of the Hochleiten Fault. The next step would be to construct a cross section containing this borehole and at the same time cutting the Hochleiten fault (green surface) orthogonally (yellow line).

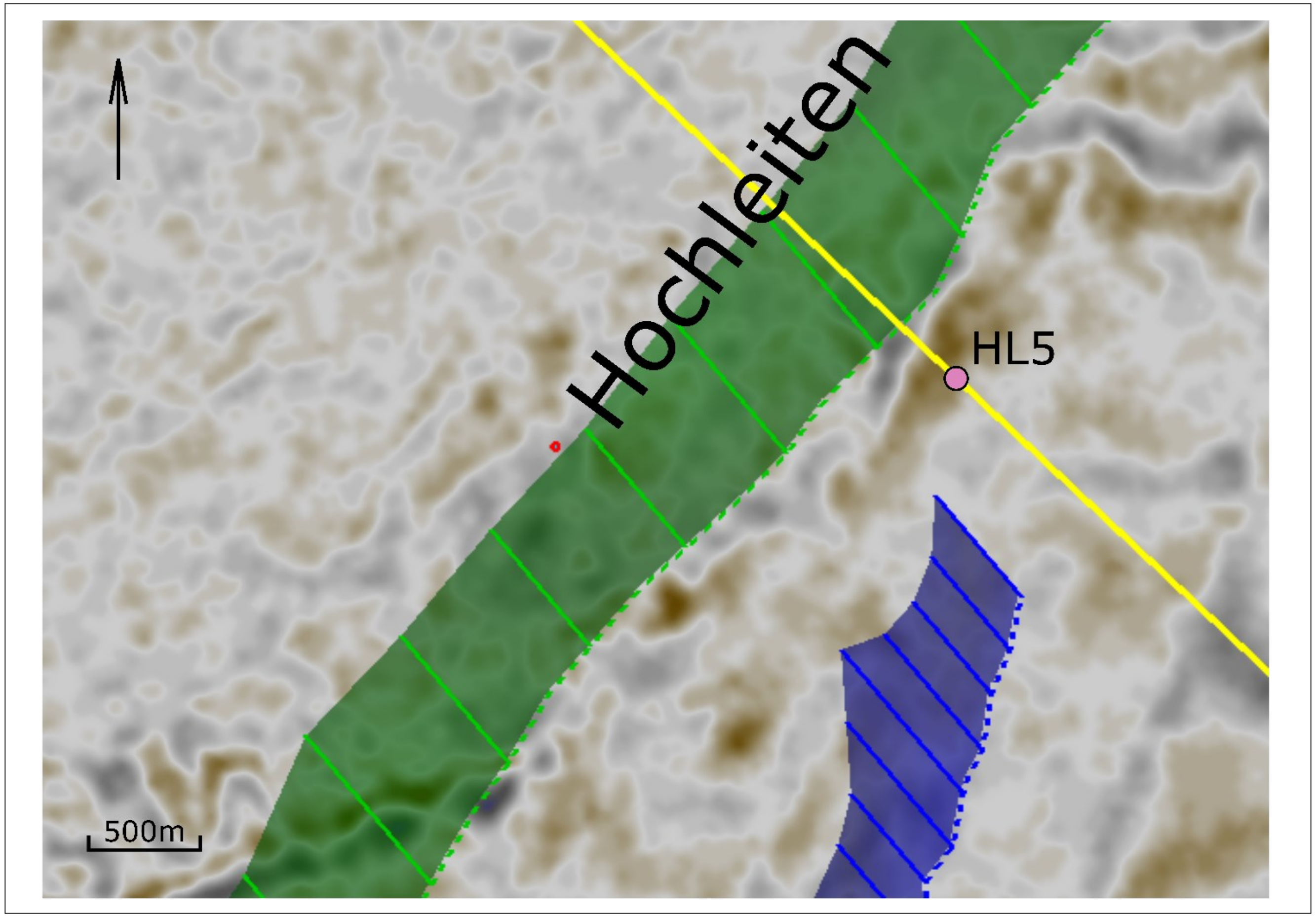

Figure 58: Borehole (HL5) for production unit (located in the 10th Sarmatian) along the Hochleiten Fault (green) and profile orthogonal to the Hochleiten Fault.

Secondly, we had to move this NW-SE cross section to the NE and SW in order to determine the highest trap point for the production unit. In this case, the yellow line represented by profile 1.

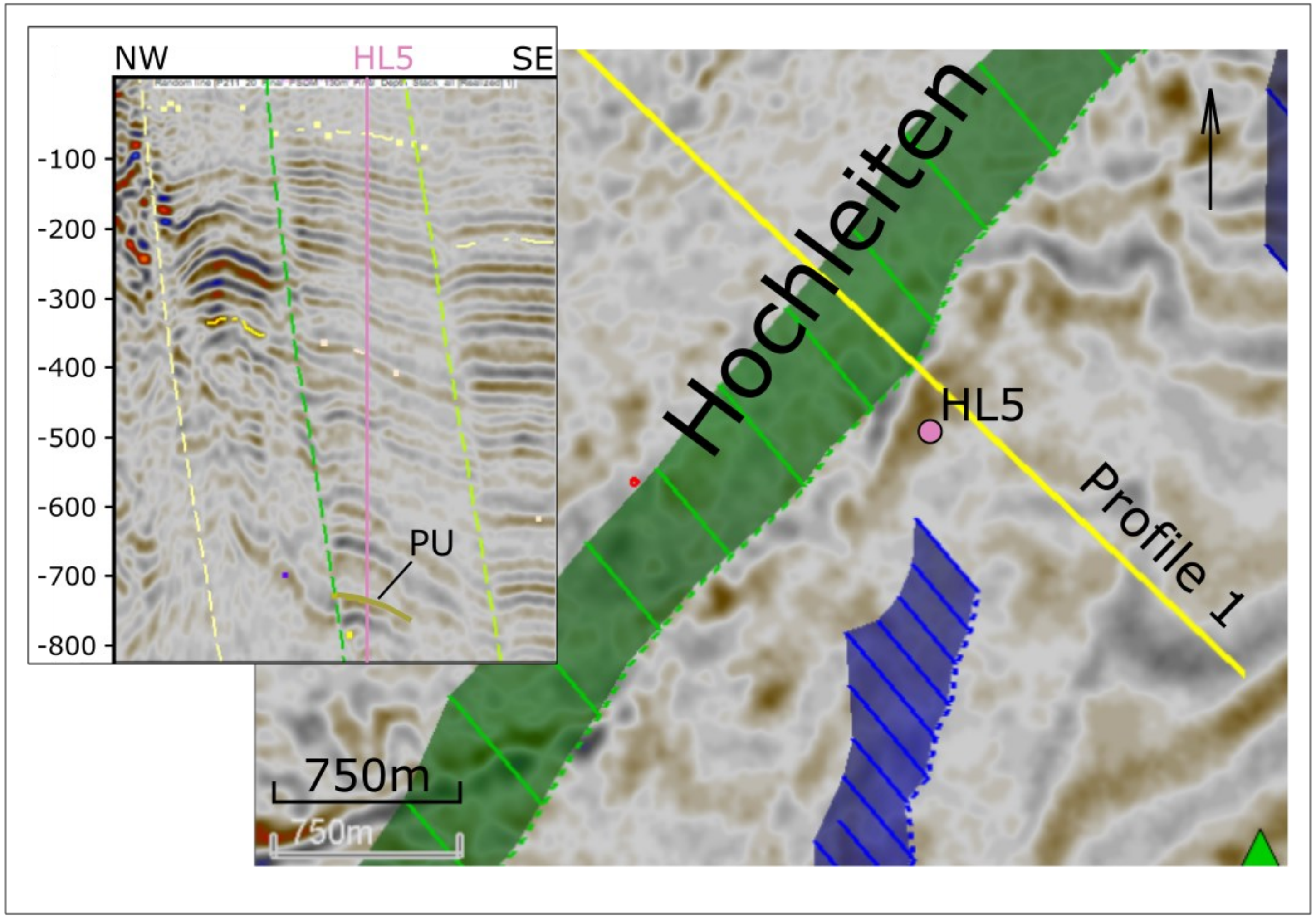

Figure 59: Finding highest trap point on the profile orthogonal to the Hochleiten Fault and on map view the production unit at around 740m depth.

We found one borehole containing the 10th Sarmatian on the footwall (HL50, red point). We followed the reflector corresponding to this stratigraphic unit to another borehole (HL74, yellow point) and traced a line connecting between the two boreholes (profile 2).

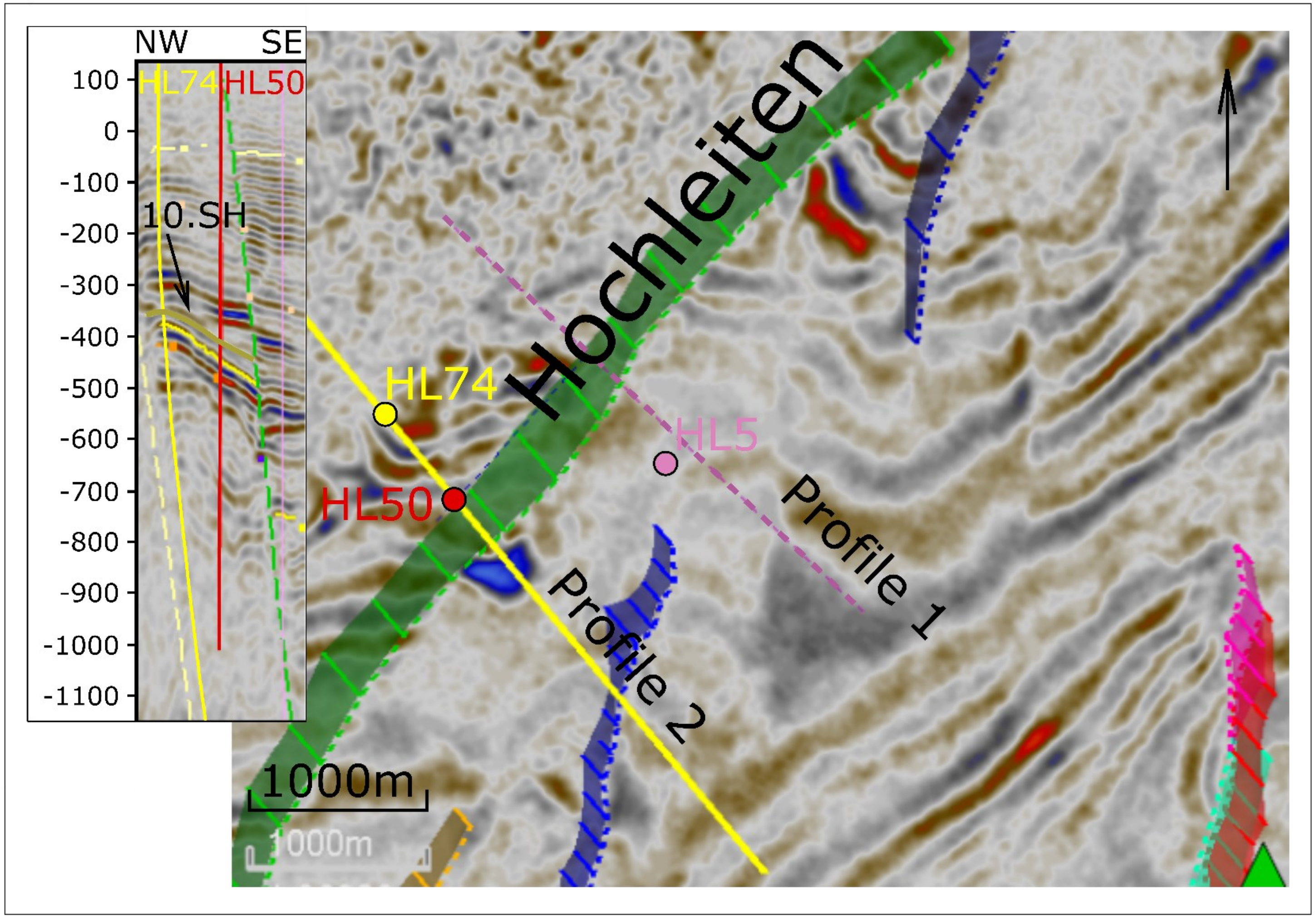

Figure 60: Finding and drawing the stratigraphic unit (10th Sarmatian) on the hanging wall of the Hochleiten fault at boreholes Hochleiten 50 and Hochleiten 74.

Than the interpreted stratigraphic unit along profile 2 had to be traced to the profile in which we are going to measure the throw (profile 1). For this, the stratigraphic unit was interpreted (by following the correct seismic reflector) along profile 3.

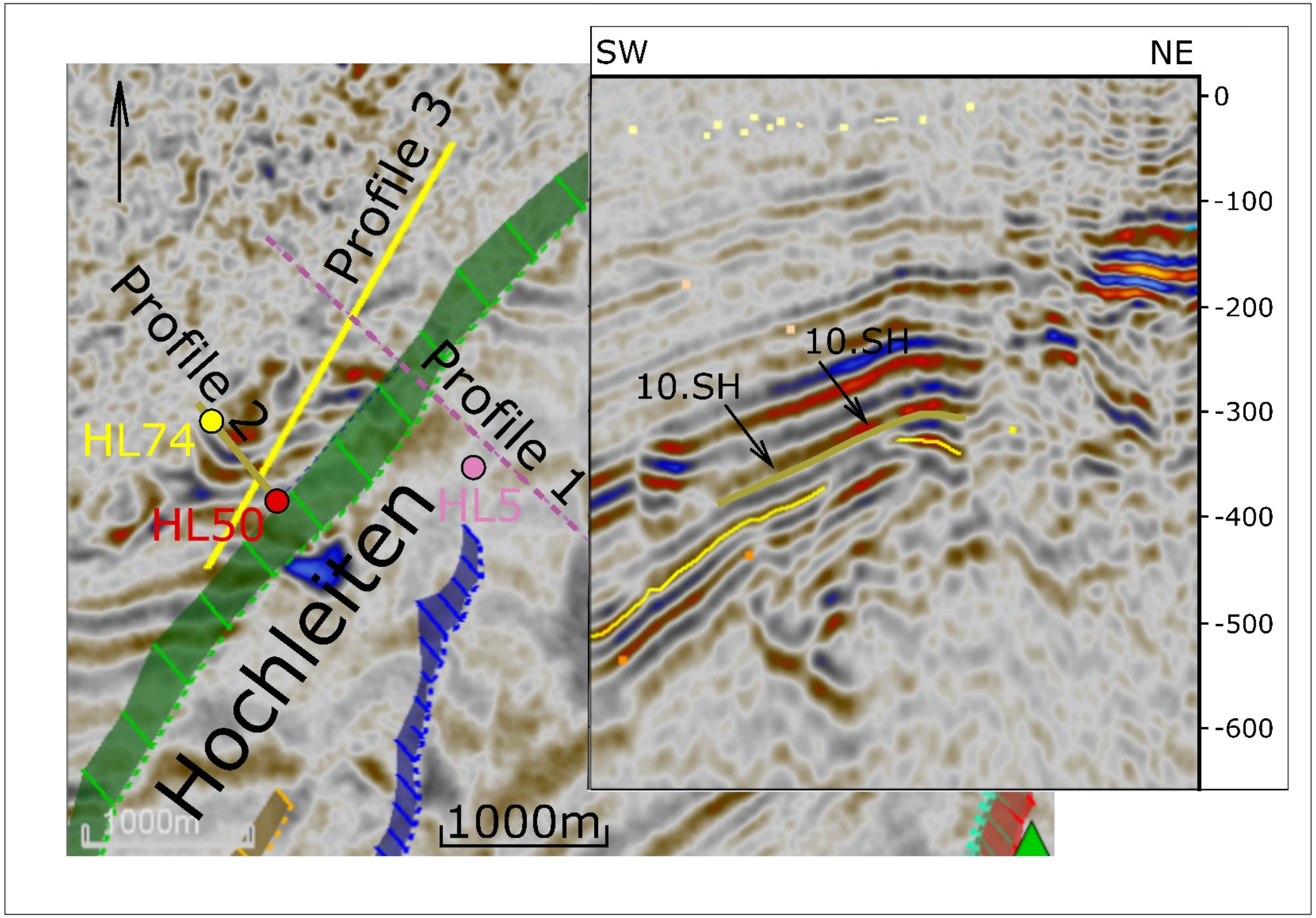

Figure 61: The 10th Sarmatian is interpreted along profile 3.

Back to profile 1, now the production unit is mapped at the hanging wall and the equivalent stratigraphy unit on the footwall. The last step is to calculate the (throw) along profile 1 (Figure 30).

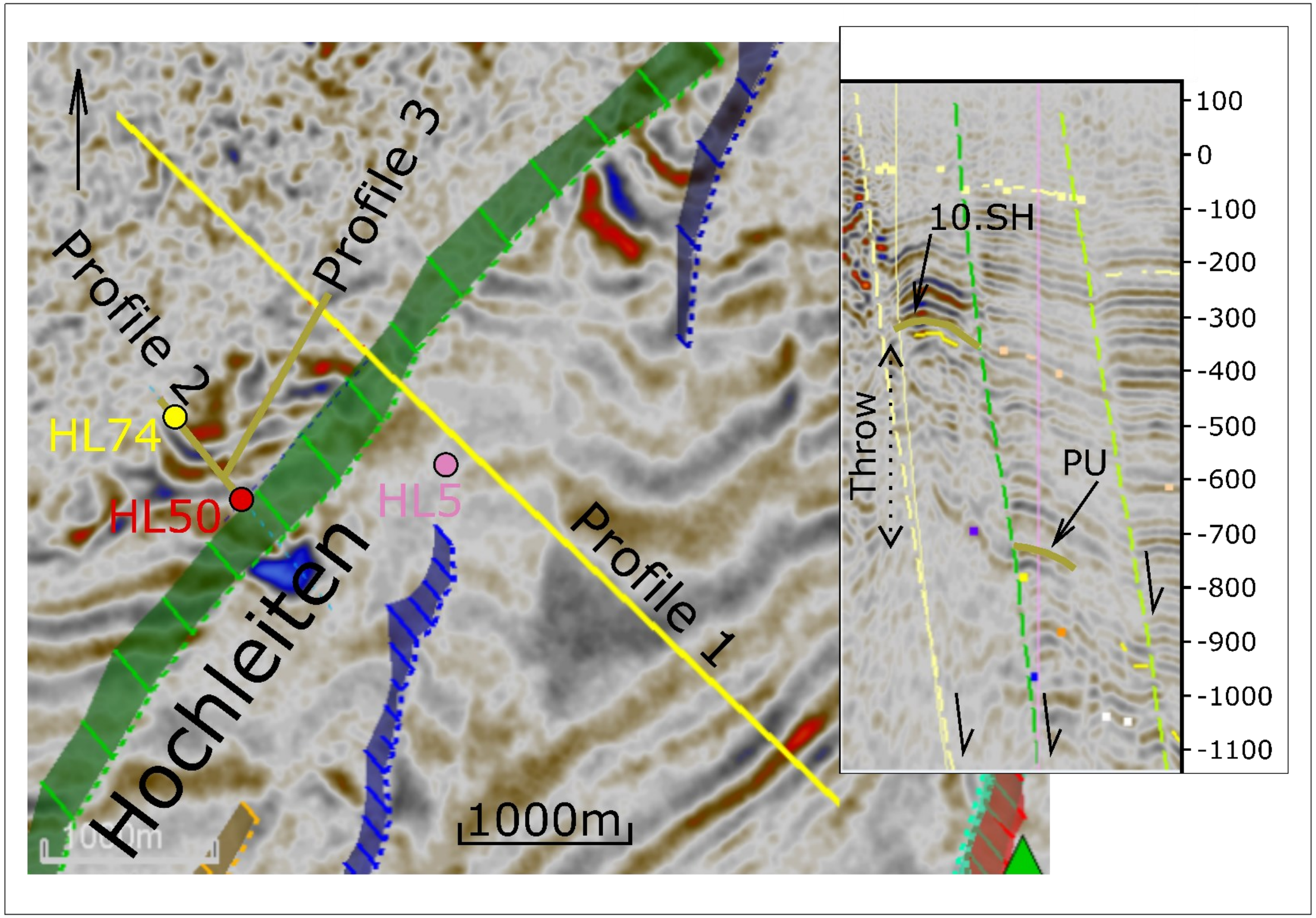

Figure 62: Establishing throw value of around 400m for the production unit along profile 1.

Appendix B

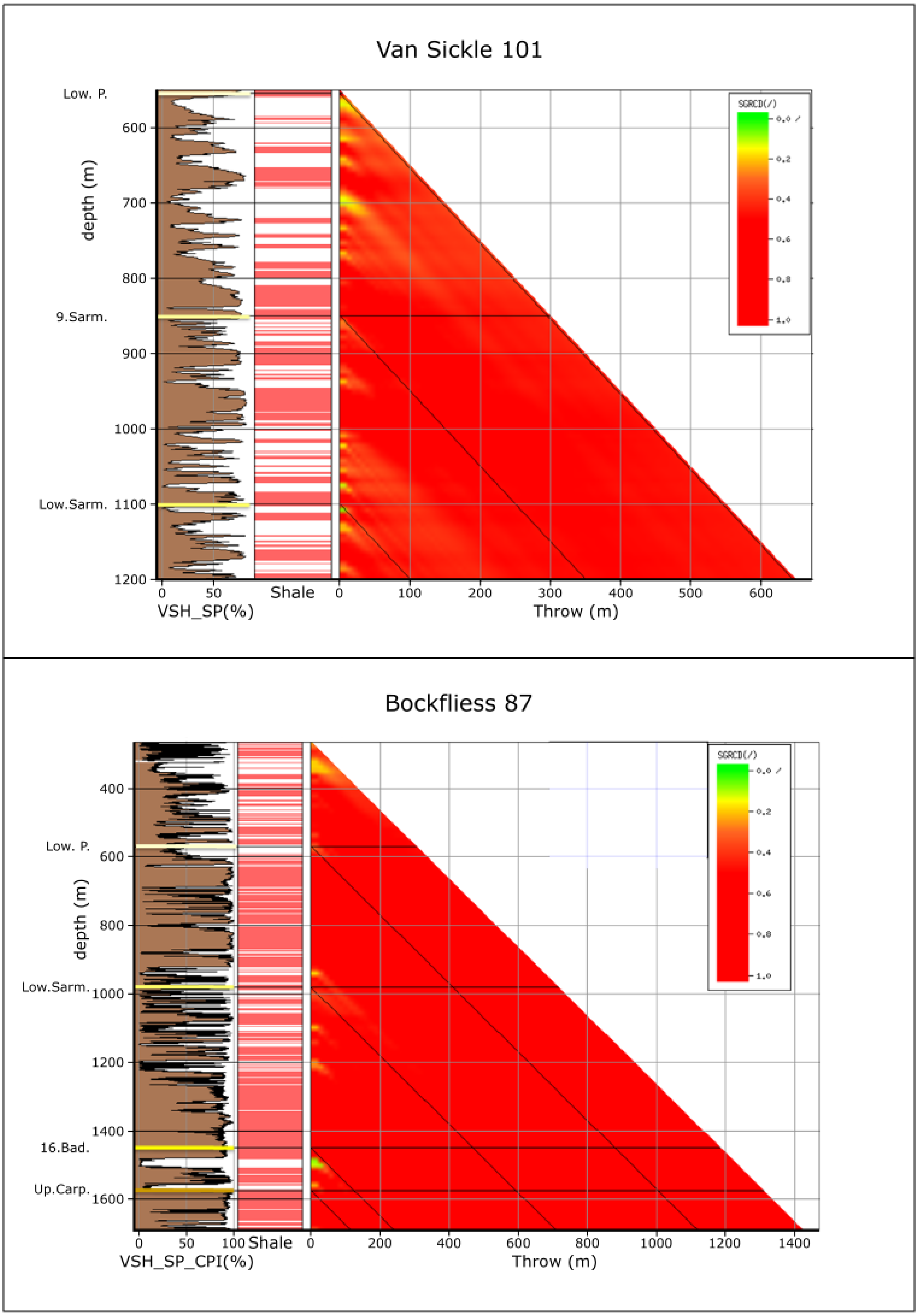

Figure 63: SGR Diagrams for Van Sickle 101 and Bockfliess 87.

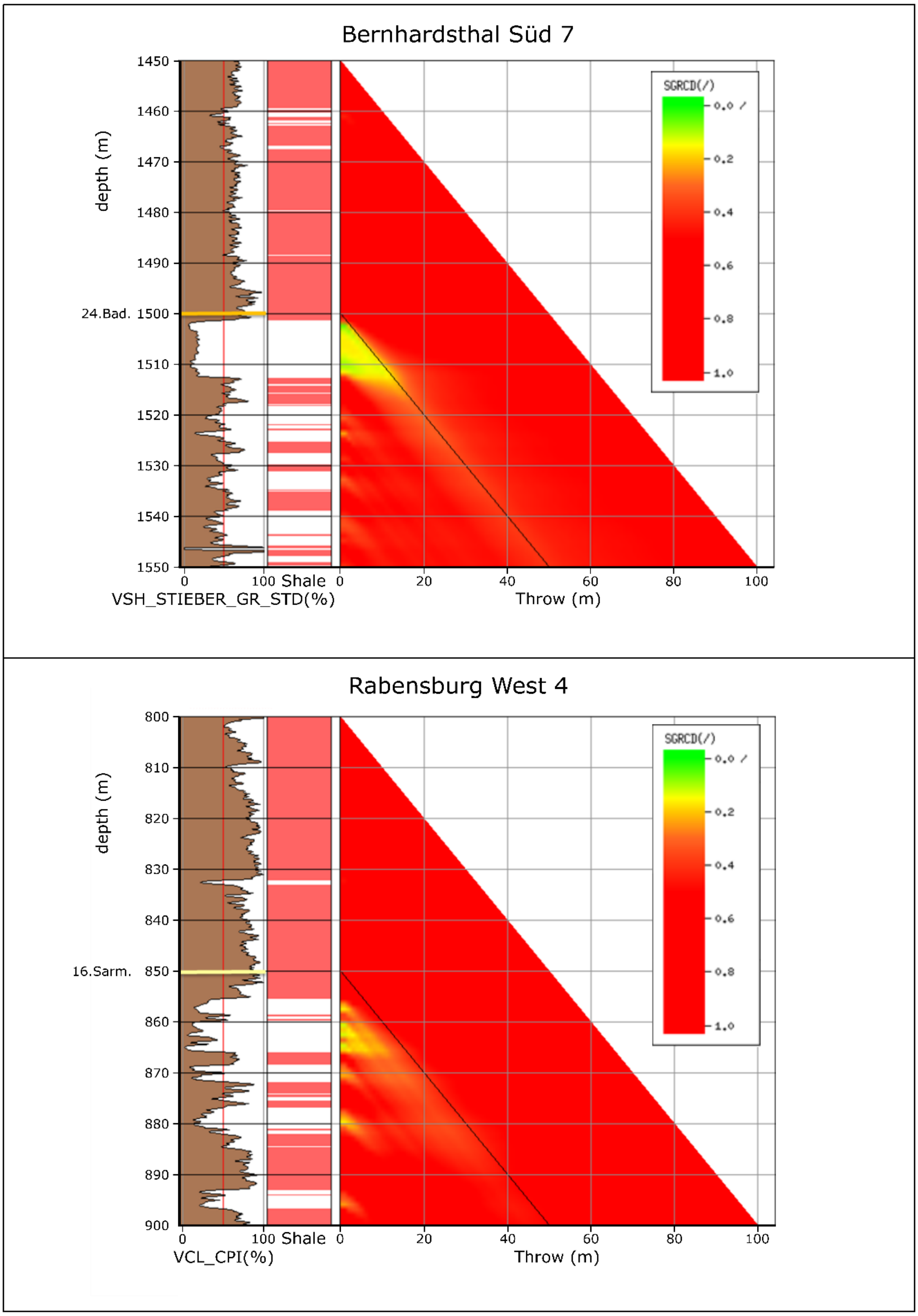

Figure 64: SGR Diagrams for Bernhardsthal Süd 7 and Rabensburg West 4.

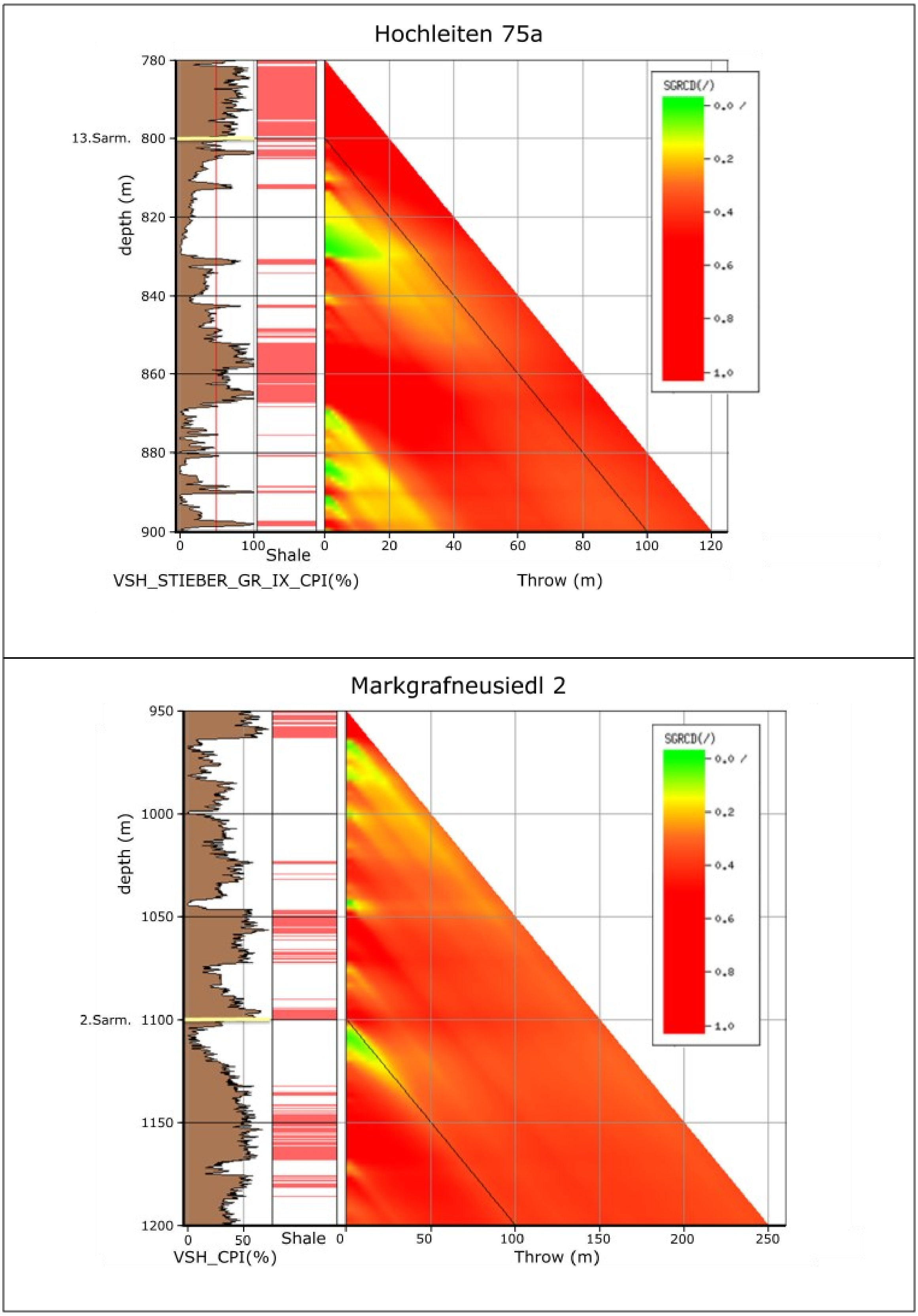

Figure 65: SGR Diagrams for Hochleiten 75a and Markgrafneusiedl 2.

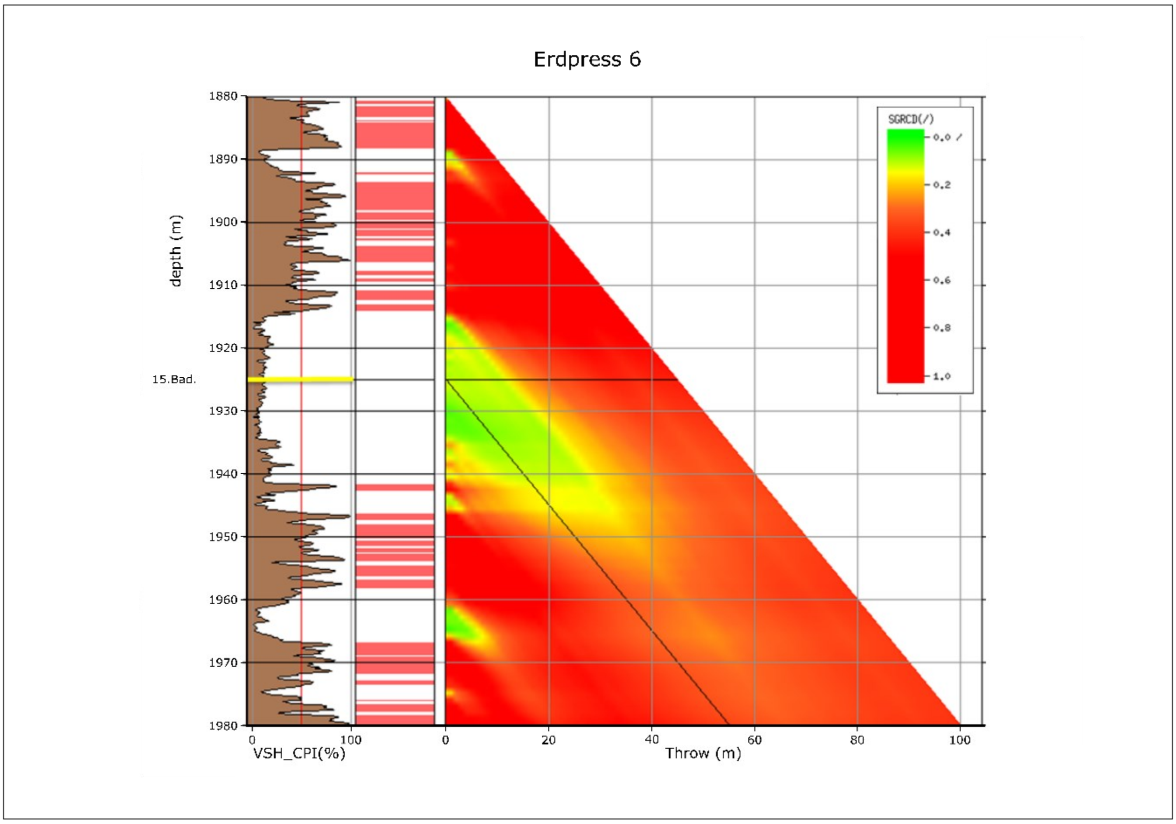

Figure 66: SGR Diagrams for Erdpress 6.